

A LABORATORY STUDY OF HETEROGENEOUS REACTIONS RELEVANT TO THE ATMOSPHERIC BOUNDARY LAYER: SOOT AS A REACTIVE SUBSTRATE

THÈSE N° 2258 (2000)

PRÉSENTÉE AU DÉPARTEMENT DE GÉNIE RURAL

ÉCOLE POLYTECHNIQUE FÉDÉRALE DE LAUSANNE

POUR L'OBTENTION DU GRADE DE DOCTEUR ÈS SCIENCES

PAR

Dominik STADLER

Ingénieur en sciences naturelles diplômé EPF
de nationalité suisse et originaire de Birrwil (AG)

acceptée sur proposition du jury:

Dr M. Rossi, directeur de thèse
Prof. H. Brune, rapporteur
Dr L. Forro, rapporteur
Dr M. Larichev, rapporteur
Dr P. Wiesen, rapporteur

Lausanne, EPFL
2000

ABSTRACT	5
ZUSAMMENFASSUNG	7
<u>PART A</u>	9
1 INTRODUCTION	11
1.1 THE BIRTH OF HETEROGENEOUS ATMOSPHERIC CHEMISTRY.	11
1.2 THE RESEARCH IN ATMOSPHERIC CHEMISTRY.	12
2 NO₂, HONO AND SOOT PARTICLES.	14
2.1 NITROGEN DIOXIDE (NO ₂)	14
2.2 THE IMPORTANCE OF NITROUS ACID (HONO) IN ATMOSPHERIC CHEMISTRY.	16
2.3 SOOT PARTICLES IN THE ATMOSPHERE.	23
3 EXPERIMENTAL SET-UP.	31
3.1 THE KNUDSEN FLOW REACTOR.	31
3.2 GENERAL DESCRIPTION OF THE EXPERIMENT.	32
3.3 GAS FLOW CALIBRATION TECHNIQUE.	39
3.4 ERRORS AND UNCERTAINTIES.	39
4 REACTANT PREPARATION.	41
4.1 PREPARATION OF SOOT SAMPLES FROM HEXANE AND DECANE.	41
4.2 PREPARATION OF SOOT SAMPLES FROM ACETYLENE GAS.	43
4.3 PRODUCTION/PURIFICATION OF GAS PHASE REACTANTS.	43
4.4 SOXHLET EXTRACTION OF 'GREY' DECANE SOOT.	44
4.5 DEPOSITION OF 1,2,10-TRIHYDROXYANTHRACENE FILMS.	45
5 CHARACTERIZATION OF THE SOOT SAMPLES.	46
5.1 BET SURFACE AREAS.	46
5.2 ELEMENTAL ANALYSIS.	49
6 INTERACTION OF NO₂, NO AND HONO WITH SOOT PARTICLES GENERATED IN THE LABORATORY.	52
6.1 THE REPRODUCIBILITY OF THE GENERATION OF SOOT SAMPLES.	52
6.2 INTERACTION OF NO ₂ AND HONO WITH DECANE SOOT FROM A RICH FLAME ('GREY' DECANESOOT).	54
6.3 INTERACTION OF NO ₂ AND HONO WITH DECANE SOOT FROM A LEAN FLAME ('BLACK' DECANESOOT')	60
6.4 'GREY' VS. 'BLACK' DECANE SOOT. – WHAT ARE THE DIFFERENCES?	65
6.5 MULTIPLE EXPOSURE EXPERIMENTS.	68
6.6 NO ₂ /DECANE SOOT INTERACTION WITH A CONCOMITANT FLOW OF H ₂ O.	72
6.7 UPTAKE KINETICS OF NO ₂ ON 'GREY' AND 'BLACK' DECANE SOOT.	73
6.8 UPTAKE KINETICS OF HONO ON 'BLACK' DECANE SOOT.	77
6.9 HEATING OF SOOT SAMPLES.	79
6.10 AGING OF 'GREY' DECANE SOOT IN DRY SYNTHETIC AIR.	83
7 THE REACTIVITY OF NO₂ WITH HEXANE SOOT.	85
7.1 PRODUCTS AND MECHANISM.	85

8 THE REACTIVITY OF NO₂ AND HONO WITH ACETYLENE SOOT.	87
8.1 THE INTERACTION OF NO ₂ ON ACETYLENE SOOT.	87
8.2 THE INTERACTION OF HONO ON ACETYLENE SOOT.	88
8.3 QUANTITATIVE ASPECTS OF NO ₂ UPTAKE AND PRODUCT FORMATION ON ACETYLENE SOOT.	91
8.4 UPTAKE KINETICS OF NO ₂ AND HONO ON ACETYLENE SOOT.	93
8.5 HEATING OF ACETYLENE SOOT SAMPLES.	96
8.6 AGING OF ACETYLENE SOOT	98
9 SOXHLET EXTRACTION OF 'GREY' DECANE SOOT.	99
10 A MODEL COMPOUND: 1,2,10-TRIHYDROXYANTHRACENE.	103
10.1 1,2,10-TRIHYDROXYANTHRACENE CONDENSED ON THINLAYER CHROMATOGRAPHY PLATES.	103
10.2 1,2,10-TRIHYDROXYANTHRACENE CONDENSED ON SOOT SAMPLES.	106
11 SUMMARY AND OUTLOOK.	109
11.1 SUMMARY OF MAIN RESULTS.	109
11.2 CONCLUSIONS AND OUTLOOK.	111
REFERENCES	114
<u>PART B</u>	119
12 THE OH RADICAL IN THE TROPOSPHERE.	121
12.1 SOURCES AND CONCENTRATIONS OF THE OH RADICAL IN THE TROPOSPHERE.	121
12.2 THE ROLE OF THE OH RADICAL IN THE O ₃ PRODUCING PHOTOOXIDATION CYCLE.	122
12.3 REACTION MECHANISMS OF THE HYDROCARBON DEGRADATION INITIATED BY THE OH RADICAL.	125
12.4 LABORATORY TECHNIQUES MEASURING THE KINETICS OF OH RADICAL REACTIONS.	127
12.5 KINETIC DATA FOR OH RADICAL REACTIONS OBTAINED IN LABORATORY STUDIES.	129
12.6 ESTIMATION OF OH RADICAL RATE CONSTANTS.	131
12.7 THE DEGRADATION OF COMPOUNDS OF LOW VOLATILITY IN THE GAS PHASE AND ADSORBED ON SOLID PARTICLES.	132
13 EXPERIMENTAL SET-UP.	134
13.1 REACTION CELL FOR THE MEASUREMENT OF THE GAS PHASE KINETICS OF THE OH RADICAL WITH ORGANIC COMPOUNDS.	134
14 RESULTS OF THE PHOTOOXIDATION EXPERIMENTS.	144
14.1 VALIDATION OF THE SYSTEM USING CYCLOHEXANE AND TOLUENE.	144
14.2 1,3,5-TRIMETHYLBENZENE (MESITYLENE).	150
14.3 BIPHENYL.	152
14.4 SEMIVOLATILE AND POLAR COMPOUNDS.	155
15 CONCLUSIONS AND OUTLOOK.	157
REFERENCES	159
CURRICULUM VITAE	163

Abstract

The present work deals with two subjects. The interaction of NO_2 and HONO with different types of soot are examined in the first part whereas in the second part an experimental set-up is presented which has been built in order to measure the kinetics of the degradation of organic compounds by OH radicals.

Both soot particles as well as NO_2 are mainly produced by fossil fuel and biomass burning. The two species are therefore ubiquitous in the atmospheric boundary layer where they may react with each other. It has been shown that one possible product of this heterogeneous interaction is nitrous acid (HONO). HONO is an important trace gas in atmospheric chemistry because it is easily photolysed resulting in OH radical and NO. Thus, the photolysis of HONO significantly enhances photooxidation processes early in the morning.

In the present study two different types of decane soot have been produced. It has been shown that the air/fuel ratio of the diffusion flame is a key parameter influencing the reactivity of soot towards NO_2 . Whereas soot from a rich flame ('grey' decane soot) leads to HONO with yields up to 100% upon interaction with NO_2 , only small amounts of HONO, but significant amounts of NO are formed in the presence of soot originating from a lean flame ('black' decane soot). A reaction mechanism has been developed showing that NO_2 is initially converted to HONO by a redox reaction. HONO produced in this way is subsequently either quantitatively desorbed into the gas phase on 'grey' decane soot or it decomposes to a large extent in a disproportionation reaction on 'black' decane soot. The products of disproportionation are NO, which is instantaneously desorbed into the gas phase and NO_2 , which undergoes secondary reactions. In addition to the HONO producing pathway there is a reaction channel that leads to adsorption of NO_2 for both types of soot which is irreversible on the time scale of our standard experiments.

Saturation effects that are occurring on the time scale of our experiments are primarily caused by saturation of adsorption sites and not by the depletion of the reducing agent. It seems that the fraction of NO_2 that is irreversibly adsorbed is blocking part of the surface sites where NO_2 is initially adsorbed.

Uptake coefficients γ take initial values of up to 0.1 for both types of soot. However, with increasing uptake of NO_2 γ is decreasing. After a NO_2 consumption of approximately 8×10^{13} molecule cm^{-2} , which corresponds to 13% of a formal monolayer, γ drops to values of 3×10^{-7} for 'grey' decane soot and 6×10^{-7} for 'black' decane soot, respectively. Furthermore, our results show that the rate of initial uptake is the rate limiting step of the NO_2 /soot interaction mechanism.

Experiments where 'black' decane soot has been exposed to a flow of HONO revealed that it readily decomposes into NO and NO_2 . For HONO concentrations above 3.3×10^{11}

molecule cm^{-3} a total product yield of 50%, whereof 40% NO and 10% NO_2 , has been observed.

The initial uptake coefficient (γ_0) for HONO on 'black' decane soot did not show clear saturation effects but varied randomly in the concentration range from 1.2×10^{12} to 5.9×10^{12} molecule cm^{-3} . The average value measured at these concentrations was equal to 0.027. The strong interaction of HONO with 'black' decane soot shows that soot is not only a potential source, but also a potential sink of HONO. On the other hand, no significant uptake could be observed when 'grey' decane soot was exposed to HONO. This is consistent with the observation that NO_2 is converted to HONO at yields of up to 100%.

Acetylene soot is an additional type of soot that has been examined. The results for the initial uptake coefficients were basically the same as for 'grey' and 'black' decane soot, that is maximum values of γ_0 of 0.1 for NO_2 uptake decreasing with increasing concentrations of NO_2 . This similarity holds only for the first few seconds of interaction because acetylene soot saturates much faster than 'grey' and 'black' decane soot with continuous exposure. The acetylene samples are generally almost completely saturated after only three minutes of exposure to NO_2 .

Soxhlet extractions of 'grey' decane soot which have been performed using tetrahydrofuran as a solvent also produced HONO upon interaction with NO_2 . This shows that the active reactants are not part of the graphitic soot backbone but are extractable, rather polar compounds of the organic fraction of soot. This assumption is supported by the observation that the corresponding benzene extraction is not reactive in relation to NO_2 uptake and HONO formation.

In the second part of the present work an experimental set-up is described which has been built in order to measure the rate constants of the reaction of organic compounds with the OH radical in the gas phase using a relative rate technique at atmospheric pressure. The system may be called a 'mini smog chamber' as the reaction cell has a volume of only 480 cm^3 .

The system was validated by measuring the relative rate constants of the reactant pair cyclohexane/toluene. These measurements have been performed for temperatures ranging from 300 to 360 K and led to results which are in excellent agreement with literature data.

However, the experimental set-up also had some important limitations. Biphenyl which has a boiling point of 529 K was the compound with the lowest volatility that could be examined in our reaction cell. Compounds with lower vapor pressures or compounds with polar groups adsorbed to a large extent onto the glass walls of the reaction cell even at temperatures of up to 373 K. Additional problems occurred in the closed ion source of the mass spectrometer leading to non linear and/or unstable MS signals. These phenomena were most probably caused by secondary ion-molecule reactions in the closed ion source.

Zusammenfassung

Die vorliegende Arbeit behandelt zwei Gebiete. Im ersten Teil wird die Wechselwirkung von NO_2 und HONO mit verschiedenen Arten von Russ untersucht, wohingegen im zweiten Teil eine experimentelle Apparatur präsentiert wird, welche gebaut wurde, um die Kinetik des Abbaus organischer Verbindungen durch OH Radikale zu messen.

Sowohl Russpartikel als auch NO_2 werden hauptsächlich durch die Verbrennung fossiler Brennstoffe und von Biomasse gebildet. Beide Spezies sind deshalb allgegenwärtig in der atmosphärischen Grenzschicht, wo sie miteinander reagieren können. Es wurde gezeigt, dass salpetrige Säure (HONO) ein mögliches Produkt dieser heterogenen Wechselwirkung ist. HONO stellt eine wichtige Spurenverbindung der Atmosphärenchemie dar, weil sie leicht zu NO und OH Radikalen photolytisch wird. Folglich beschleunigt die Photolyse von HONO am frühen Morgen in beträchtlichem Ausmass Photooxidations-Prozesse.

In der vorliegenden Arbeit wurden zwei verschiedene Dekan-Russe hergestellt. Es wurde gezeigt, dass das Luft/Brennstoff-Verhältnis ein Schlüsselparameter der Diffusionsflamme ist, welcher die Reaktivität des Russes gegenüber NO_2 beeinflusst. Während Russ einer fetten Flamme („grauer“ Dekan-Russ) NO_2 mit Ausbeuten von bis zu 100% in HONO umsetzt, setzt Russ einer mageren Flamme („schwarzer“ Dekan-Russ) nur geringe Mengen von HONO, aber beträchtliche Mengen von NO frei. Es wurde ein Reaktionsmechanismus hergeleitet, welcher zeigt, dass NO_2 in einer Redox-Reaktion in HONO umgesetzt wird. Das so produzierte HONO desorbiert im Falle des ‚grauen‘ Dekan-Russes vollumfänglich in die Gasphase, wohingegen es auf dem ‚schwarzen‘ Dekan-Russ grösstenteils in einem Disproportionierungsprozess zersetzt wird. Die Produkte dieser Disproportionierung sind NO, welches sofort in die Gasphase desorbiert und NO_2 welches Folgereaktionen eingeht. Zusätzlich zum HONO produzierenden Reaktionspfad gibt es noch einen Reaktionszweig, welcher NO_2 - bezüglich der Zeitskala unserer Experimente – irreversibel adsorbiert.

Sättigungseffekte, die in der Zeitskala unserer Versuche auftreten, sind primär verursacht durch Sättigung der Adsorptionsplätze nicht jedoch durch eine Verarmung des reduzierenden Agens. Es scheint, dass derjenige Teil des NO_2 welcher irreversibel adsorbiert wird, einen Teil der Adsorptionsplätze blockiert.

Der Adsorptionskoeffizient γ weist für beide Russarten Anfangswerte von bis zu 0.1 auf. Mit zunehmender Aufnahme von NO_2 nimmt γ jedoch schnell ab. Nach einer Aufnahme von ungefähr 8×10^{13} Moleküle cm^{-2} , welches 13% eines formalen Monolayers entspricht, beträgt γ nur noch 3×10^7 für „grauen“ Dekan-Russ, respektive 6×10^7 für „schwarzen“ Dekan-Russ. Desweiteren zeigen unsere Resultate, dass die initiale Adsorption der geschwindigkeitsbestimmende Schritt der NO_2 /Russ-Wechselwirkung ist.

Versuche, in welchen „schwarzer“ Dekan-Russ einem Fluss von HONO ausgesetzt wurde, zeigten, dass sich dieses prompt zu NO und NO_2 zersetzt. Bei HONO Konzentrationen

grösser als 3.3×10^{11} Moleküle cm^{-3} wurden 50% des adsorbierten HONO in der Gasphase wiedergefunden, wovon 40% als NO und 10% als NO_2 .

Der Koeffizient der initialen Adsorption (γ_0) von HONO auf „schwarzem“ Dekan-Russ zeigte für HONO Konzentrationen zwischen 1.2×10^{12} und 5.9×10^{12} Moleküle cm^{-3} keine Sättigungseffekte sondern variierte zufällig. Der Durchschnittswert für diese Konzentrationen betrug 0.027. Die starke Wechselwirkung von HONO mit „schwarzem“ Dekan-Russ zeigt, dass Russ nicht nur eine potentielle Quelle sondern auch eine potentielle Senke für HONO ist. Andererseits konnte keine messbare Wechselwirkung beobachtet werden, wenn „grauer“ Dekan-Russ einem Fluss von HONO ausgesetzt wurde. Dies ist folgerichtig, da wir gesehen haben, dass dieser Russ NO_2 mit Ausbeuten von bis zu 100% zu HONO umsetzt.

Eine weitere Russart, die untersucht wurde, ist Acetylen-Russ. Die Resultate bezüglich der Koeffizienten der initialen Adsorption von NO_2 sind grundsätzlich dieselben wie für „grauen“ und „schwarzen“ Dekan-Russ, das heisst, Maximalwerte für γ_0 von etwa 0.1. Diese Aehnlichkeit hält nur für die ersten, wenigen Sekunden eines Experimentes an, da Acetylen-Russ bei fortlaufender Exposition viel schneller sättigt als „grauer“ und „schwarzer“ Dekan-Russ. Acetylen-Russ ist im Allgemeinen schon nach dreiminütiger Exposition gegenüber NO_2 nahezu vollständig gesättigt.

Soxhlet-Extrakte von „grauem“ Dekan-Russ, die in Tetrahydrofuran ausgeführt wurden, produzierten ebenfalls HONO, wenn sie NO_2 ausgesetzt wurden. Dies zeigt, dass die reaktiven Verbindungen nicht Teil des graphitartigen „Russ-Skeletts“ sind, sondern extrahierbare, eher polare Verbindungen der organischen Fraktion des Russes. Diese Annahme wird durch die Beobachtung bestätigt, dass entsprechende Benzolextrakte kein HONO bilden, wenn sie NO_2 ausgesetzt werden.

Im zweiten Teil der vorliegenden Arbeit, wird eine experimentelle Apparatur vorgestellt, die gebaut wurde, um die Kinetik des Abbaus organischer Verbindungen durch OH Radikale in der Gasphase zu messen und zwar mittels Messung relativer Geschwindigkeitsraten bei Atmosphärendruck. Wegen des kleinen Volumens der Reaktionszelle von nur 480 cm^3 könnte das System als „Mini-Smogkammer“ bezeichnet werden.

Das System wurde validiert durch die Messung der relativen Geschwindigkeitskonstanten des Verbindungspaares Cyclohexan/Toluol. Diese Messungen wurden bei Temperaturen zwischen 300 und 360 K ausgeführt und führten zu Resultaten, die in ausgezeichneter Uebereinstimmung mit Literaturwerten sind.

Die Apparatur weist allerdings auch erhebliche Limitationen auf. Biphenyl mit einem Siedepunkt von 529 K war die schwerflüchtigste Verbindung die untersucht werden konnte. Schwerflüchtigere Verbindungen oder solche mit polaren Gruppen adsorbierten in hohem Ausmass auf den Wänden des Reaktors sogar bei Temperaturen von 373 K. Zusätzliche Probleme tauchten in der geschlossenen Ionenquelle des Massenspektrometers auf, was zu nicht linearen und/oder instabilen Signalen führte. Diese Phänomene wurden sehrwahrscheinlich durch sekundäre Ionen-Molekül Reaktionen verursacht.

Part A

Heterogeneous reactions of NO₂ and HONO on different types of laboratory generated soot.

1 Introduction

1.1 The birth of heterogeneous atmospheric chemistry.

Our knowledge of the environment has greatly increased in the last few decades. This is mainly due to the scientific progress made in many fields and to the fact that Man has become aware that the results of many of his activities may create important prejudice to the environment. This is particularly true for the atmosphere, where human activity may have damaging effects on its chemical balance, and may even lead to significant global climate change. Combustion of fossil fuels, biomass burning, use of fertilizer and agricultural practice add to the burden of anthropogenic compounds in the atmosphere.

The increase of the carbon dioxide concentration in the atmosphere, mostly due to fossil fuel burning, is only one example of the harmful impact that human activities may bear. The atmospheric concentration of the carbon dioxide concentration now corresponds to approximately 360 parts per million by volume (ppmv) compared to an estimated 280 ppmv before the start of widespread industrialization around 1850. This rate of increase even accelerated during the last 50 years. The CO₂-levels in the atmosphere are important because carbon dioxide is a “greenhouse” gas which absorbs infrared radiation and contributes to the warming of the lower atmosphere. Increased CO₂-levels are thus expected to lead to higher global average temperatures, the so-called global warming effect.

An other dramatic demonstration of Man’s influence on the atmosphere is the so-called “ozone hole” phenomenon. In 1974, Molina and Rowland realized that the chemically inert chlorofluorocarbons (CFC) could gradually be transported up to the stratospheric ozone layer by diffusion and convection, there to be met by such intense ultra-violet light that they would be dissociated into atomic and molecular fragments, notably chlorine atoms [Rowland and Molina, 1994]. They calculated that if human use of CFC gases was to continue at an unaltered rate the ozone layer would be depleted by many percentage points after some decades. A depletion of the ozone layer and the incident increase of ultra-violet radiation on Earth’s surface would cause increased skin cancer, weakening of the immune system of humans and animals and damage to plants, crops in particular, with famine as it worst consequence. The actual shock came in 1985 when Farman and coworkers noted a depletion of the Antarctic ozone layer that was much greater than expected from the calculations of the CFC effect [Farman et al., 1985]. This fast depletion of the ozone layer could not be explained by transport processes or by gas phase chemical reactions. Scientists realized that an alternative mechanism had to exist which would accelerate the decomposition of ozone. Crutzen, among other colleagues identified the missing part of the mechanism as chemical reactions on the surface of atmospheric particles in the stratosphere. Thus, the Antarctic ozone depletion appears to be connected with the extremely low prevailing temperatures, which lead

to condensation of water and nitric acid to form “polar stratospheric clouds” (PSCs). The ozone-decomposing chemical reactions are greatly accelerated in the presence of atmospheric particles. This insight has led to an exciting new branch of atmospheric chemistry, namely “heterogeneous” chemical reactions on particle surfaces.

While the collision frequency of a gas molecule with an average particle is only about 10^{-5} s^{-1} in the stratosphere, there are considerably more such collisions in the troposphere. The collision frequency in a highly polluted urban environment is about 1 s^{-1} , and loss processes with efficiencies of even 10^{-4} can compete with homogeneous gas phase processes. Thus, heterogeneous chemistry is not only important in stratospheric ozone depletion but also in the troposphere where atmospheric particulates are abundant near the ground.

1.2 The research in atmospheric chemistry.

The research in atmospheric chemistry may be classified into three main groups which interact with each other: Atmospheric modeling, field measurements of trace gases and laboratory studies of chemical reactions relevant to atmospheric chemistry.

The atmosphere is a very complex physicochemical system, including hundreds of physical and chemical processes. The only way of making quantitative predictions for such a complex system is to develop a quantitative computer model that takes into account the different processes occurring in the atmosphere. Models require a good understanding of all individual atmospheric processes. The “perfect” model which would simulate all physical and chemical processes taking place in the atmosphere does not yet exist, and probably never will. Such a model would allow to make accurate scientific predictions which are essential in reaching political decisions or legislation for the purpose of reducing the effects of the pollution. The atmospheric model is therefore the final tool which atmospheric research may produce.

The field measurements include the identification of the substances present in the atmosphere, the measurement of their concentration and the determination of their sources and sinks. The data obtained in the field studies are used in models as initial or boundary conditions, or for comparing model predictions to the real atmosphere. Field measurements may also point to situations that cannot be explained by the actual knowledge of the atmosphere. In these case they suggest new processes which have to be included in the models in order to describe the system.

The third research element to which this thesis is related corresponds to laboratory studies which are aimed at discovering which physical or chemical processes may occur in the atmosphere. In the case of atmospheric chemistry, the laboratory studies help to determine which reactions may occur, the products of these reactions, how fast and under which

conditions these reactions occur. Again, the results of the laboratory studies are used as input for the models. Field measurements are related to laboratory studies as well: if a reaction has been demonstrated to be relevant or to generate an important species, the field measurements will be directed towards the conditions indicated by the laboratory results. In our simplified scheme of the organization of research in the field of atmospheric chemistry, the results obtained in the laboratory are used to obtain parameters that are critical to the modeling runs.

The interplay of the three subdivisions of atmospheric research may be illustrated by role played by nitrous acid (HONO) in the troposphere. HONO is an important species because it is influencing the oxidative capacity of the troposphere. It has been detected in field measurements for the first time in the seventies [Nash, 1974]. Of course, the scientists wanted to know the sources of such an important species and they therefore asked questions of the modelers. The modelers put the rate constants of all known HONO producing reactions into their calculations but the results never led to the relatively high concentrations of HONO that have been measured in the field. The conclusion was that some as yet unknown reactions must have been responsible for the high levels of HONO. That is the point where the laboratory studies come into play. Candidates for HONO producing reactions are postulated based on the observations of field measurements and tested in the controlled environment of the laboratory. As the homogeneous gas phase chemistry is considered to be well known, the unknown HONO source is situated – akin to the “ozone hole case” – most likely in the field of heterogeneous atmospheric chemistry.

The aim of the present laboratory study in this context is to clarify whether the heterogeneous system that is represented by the interaction of solid soot particles and gaseous NO_2 may significantly contribute to the formation of HONO concentration levels that are observed in field studies. The next chapters will give therefore a more detailed description of the “leading actors” NO_2 , HONO and soot particles.

2 NO₂, HONO and soot particles.

2.1 Nitrogen dioxide (NO₂)

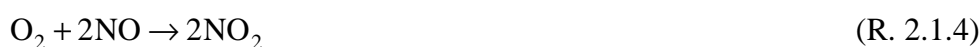
In almost all cases NO₂ is formed *via* its precursor nitric oxide (NO). The species are therefore generally considered together and summarized in the term NO_x (NO + NO₂ = NO_x). A special feature of both molecules is that they represent relatively stable molecules although they are radicals. The reason is that they are stabilized by resonance. The structure of NO₂ is displayed in Figure 2.1.1.

The most important source of NO_x is the combustion of fossil fuels. It has been estimated that its contribution amounts to approximately 46% of the total global emission of 53 Tg(N) per year [IPCC, 1995]. The basic mechanism has been established by Zeldovitch [1947]. It describes the oxidation of molecular nitrogen in combustion processes at temperatures above 850°C:



The equilibrium of (R. 2.1.2) and (R. 2.1.3) strongly depends on the temperature.

NO that is formed by the Zeldovitch mechanism may then be oxidized by molecular oxygen to form NO₂ which is at ambient temperature and pressure thermodynamically more stable than NO ($\Delta H_f^\circ(\text{NO}_2) = 33.8 \text{ kJ/mol}$; $\Delta H_f^\circ(\text{NO}) = 90.4 \text{ kJ/mol}$).



This reaction may be significant in the exhaust pipe of a vehicle where NO concentrations can reach up to 1000 ppm. At NO_x concentrations of 10-1000 ppb which are typical for urban areas [National Research Council, 1991] (R. 2.1.4) is rather slow because its kinetics is termolecular. Under those conditions it is mainly O₃ that is responsible for the conversion of NO into NO₂ (see R.2.1.7). Together with reactions (R. 2.1.5 and R. 2.1.6) this reaction describes the inter-conversion of NO and NO₂:



Under the assumption of steady state conditions one can derive the so called Leighton ratio from these reactions (E. 2.1) (Leighton, 1961):

$$\frac{[\text{O}_3][\text{NO}]}{[\text{NO}_2]} = \frac{k_{\text{R.2.1.5}}}{k_{\text{R.2.1.7}}} \quad (\text{E.2.1})$$

According to this relationship, the concentration of O₃, NO and NO₂ at any time *t* in an air mass should be constant and given by ratio of rate constants for photolysis of NO₂ and for the reaction of NO with O₃. Since *k*_{R.2.1.5} changes with the Zenith angle of the sun, this ratio of concentrations is also expected to change during the day. However (E. 2.1) does not hold when loss processes other than (R. 2.1.7) become significant so that O₃ is no longer in a steady state. This is the case if higher concentrations of alkenes, NO₂, HO₂ or OH are present. Deviations from (E. 2.1) are also expected at sunrise and sunset because the rate of photolysis of NO₂ is sufficiently low that the steady state assumption on oxygen atoms and O₃ is not valid (Calvert and Stockwell, 1983). Finally, photolysis of O₃ to produce electronically excited oxygen atoms, O(¹D), which further react with water vapor to produce OH can also contribute to the deviation from (E. 2.1).

In general, the Leighton ratio is expected to hold when sufficient NO is present such that reaction (R. 2.1.7) is the major loss for O₃, for example, at relatively low hydrocarbon to NO ratio.

Even if forest fires, anaerobic processes in soil, oxidation of biogenic NH₃ and lightning are natural sources of NO_x, the anthropogenic NO_x burden principally caused by fossil fuel combustion is predominant.

The implication of NO_x in the photochemical cycle which determines the oxidative capacity will be discussed in the next Section.

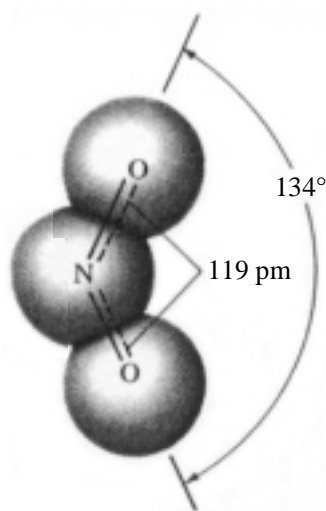


Figure 2.1.1: The structure of the NO₂ molecule.

2.2 The importance of nitrous acid (HONO) in atmospheric chemistry.

2.2.1 The oxidizing capacity of the atmosphere.

The oxidizing capacity of the troposphere mostly depends on the concentration of the principal oxidants, the OH-radical, NO₃, O₃ and H₂O₂. These oxidants interact with each other and with the trace gases emitted at the earth's surface and determine the atmospheric lifetime of chemical substances. The atmospheric lifetime is a key parameter for evaluating the impact of natural and anthropogenic emissions on the composition and on the radiative properties of our atmosphere.

In recent years it has been demonstrated that a change in the oxidizing potential of the troposphere may have important consequences on its chemical balance and therefore for air pollution. Acidification, the concentration of photooxidants, and in particular the increase of tropospheric ozone, the concentration of greenhouse gases and of substances that deplete the ozone layer are all linked to the chemistry in relation to the oxidizing capacity of the troposphere.

Hydroxyl radicals, OH, dominate the day-time chemistry of the troposphere. The high reactivity of the OH-radical with respect to a wide variety of species leads to oxidation and chemical conversion of most constituents that have an appreciable lifetime in the troposphere. The major source of OH in the troposphere is produced by ozone photolysis [Finlayson-Pitts and Pitts, 1986]:



Because H₂O is present in the lower troposphere at mixing ratios up to 10⁴ ppm (1%) and because (R. 2.2.2) has a rate constant about a factor of ten larger than the quenching reaction (R.2.2.1b) with M = N₂ or O₂ as much as 10% of the O(¹D) produced reacts with H₂O to generate OH [Seinfeld and Pandis, 1997].

The presence of ozone in the troposphere is due to several different processes. Ozone certainly is diffusing to the troposphere from the stratosphere across the tropopause. Another important source of ozone is linked to the hydrocarbon oxidation in the presence of NO_x that may be summarized by the following chemical scheme [Finlayson-Pitts and Pitts, 1986]:



NMHC refers to non-methane hydrocarbons.

The OH-radical is very reactive towards most hydrocarbons (RH) and undergoes hydrogen abstraction reactions which initiate hydrocarbon oxidation:



Reaction (R 2.2.4) is followed by additional reactions leading to the oxidation of the hydrocarbon. Figure 2.2.1 gives a summary of the oxidation mechanism for a typical hydrocarbon (RH) in the atmosphere. In this scheme the hydrocarbon serves as the fuel that is controlling and driving the production/consumption cycles of O₃, OH and NO. The energy that is required to initiate this complex and interlocked cycle is delivered by sunlight which forms the free radicals O(¹D) and NO by photodissociation.

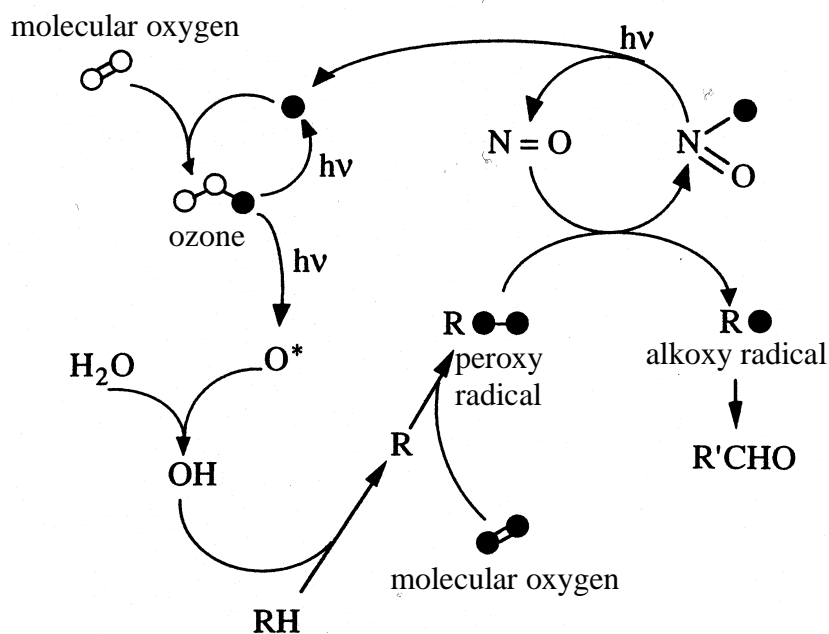


Figure 2.2.1: Scheme of hydrocarbon (RH) oxidation in the atmosphere. Initiation of the hydrocarbon oxidation is afforded by the abstraction mechanism (R. 2.2.4).

Figure 2.2.1 illustrates furthermore that an additional source of OH-radicals will accelerate the rate of formation of O₃ if a sufficient amount of hydrocarbons is present. Such sources for OH-radicals, are formaldehyde and nitrous acid (HONO). Formaldehyde may photolyze to hydrogen atoms and produce OH-radicals according to the following reaction scheme:



The reaction mechanism that is forming OH-radicals from HONO is much simpler. The strength of the N-O bond (as marked in Figure 2.2.2) is only 206.3 kJ/mol [McMillan and Golden, 1982]. Therefore, the energy of the sunlight is high enough to dissociate the molecule and to directly produce OH-radicals:



Thus, any reaction leading to the formation of HONO will immediately influence the oxidizing capacity of the atmosphere which governs the residence time and distribution of organic pollutants.

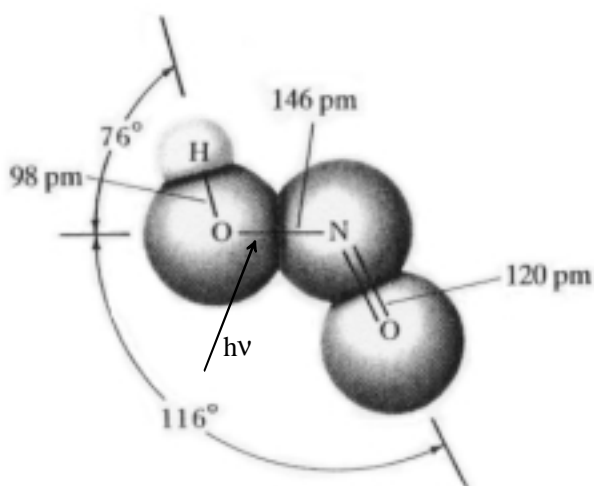


Figure 2.2.2: The structure of the HONO molecule. The arrow is marking the N-O bond that is dissociated by sunlight.

2.2.2 HONO: Techniques of detection and results of field measurements.

HONO was observed for the first time in tropospheric field measurements by Nash [1974] and Perner and Platt [1979]. Most of the data of field measurements that have been performed during the last years have been obtained using either differential optical absorption spectroscopy (DOAS) or denuder tube techniques.

Spectroscopy as an *in situ* method is clearly advantageous when dealing with molecules which are reactive on surfaces. The sensitivity of the method increases with the path length, which can be up to approximately 10 km. On the other hand, this gain in sensitivity must be paid for by a loss of spatial resolution of the data.

In a denuder tube, trace gases are separated from the aerosols in sampled air by diffusion. Gases diffuse from a laminar flow through the denuder to the walls, where they are absorbed by an appropriate coating, while aerosols, having much smaller diffusion rates, pass through the denuder without being trapped. A denuder system that is often used for HONO measurements consists of a first tube coated with NaCl followed by two additional tubes with Na₂CO₃ coatings. The weakly alkaline NaCl tube is meant for removing nitric acid from the sampled air flow which otherwise would interfere with the detection of HONO in a first step. HONO itself is only trapped by the more alkaline Na₂CO₃ coating of the second tube. From this tube it can be washed-off and analyzed as nitrite by ion chromatography. The third tube serves to correct the nitrite contribution of NO₂ which in part is also absorbed by Na₂CO₃. However, as the collection efficiency for NO₂ is relatively low, the amounts of NO₂ absorbed are approximately the same for tubes 2 and 3. HONO on the other hand, is almost quantitatively absorbed by tube 2. Thus, the amount of HONO can easily be calculated by subtracting the amount of nitrite of tube 3 from that of tube 2. Although various artifacts can be identified and avoided, undetected reactions of the nitrogen oxides on the denuder surfaces cannot be completely excluded. For instance, it has been found that at elevated levels of SO₂, an interference of NO₂ may cause significant positive artifacts in HONO detection when Na₂CO₃ coatings are used [Febo and Perrino, 1991].

In field experiments, HONO was measured at various sites such as in polluted atmospheres [Platt et al., 1980; Febo et al.1996], rural areas [Harrison and Kitto, 1994; Neftel et al., 1996; Staffelbach et al., 1997b] or remote regions [Li, 1996]. The results of these measurements show, as reviewed by Lammel and Cape [1996], that the HONO concentrations in urban sites are generally ranging between 0.1 and 15 ppb. The values for rural and remote sites are lower and attain maximum values of 10 and 1 ppb, respectively.

During the night, HONO is accumulating to reach concentrations of up to 14 ppb [Appel et al., 1990; Febo et al., 1996]. HONO absorbs light in the near UV with maxima at 354 and 368 nm and an absorption cross section at these wavelengths of 5.0×10^{-19} cm² and 4.5×10^{-19} cm² per molecule, respectively [Bongartz et al., 1994, and references therein]. HONO lifetimes from approximately 1 hour (early morning) to 10 minutes (midday) are calculated as a function of the temporal variation of the actinic flow on a sunny day [Bongartz et al., 1991]. As a consequence, the high nighttime concentrations of HONO decay by photolysis according to (R. 2.2.8) on the time scale of hours and a concomitant peak of NO and OH-radicals is observed at sunrise early in the morning. This OH pulse in the early morning is of great importance because OH production rates from other sources such as

photolysis of O₃ (R. 2.2.1-2) or formaldehyde (R. 2.2.5-7) are slow at this time. As a consequence of the increasing efficiency of (R. 2.2.8) daytime concentrations of HONO are strongly reduced, however values of up to 200 ppt have nevertheless been observed [Staffelbach et al., 1997b]. Figure 2.2.3 shows an example for the described diurnal variation of the HONO concentration. Jenkin et al. [1988] calculated the contribution of HONO to the photochemical reaction cycle as shown in Figure 2.2.1 in a model study. The main results were a five-fold increase in OH density at 0600h, a 14% increase in OH present at the daily maximum (1200h) and a 16% increase in net photochemical ozone production.

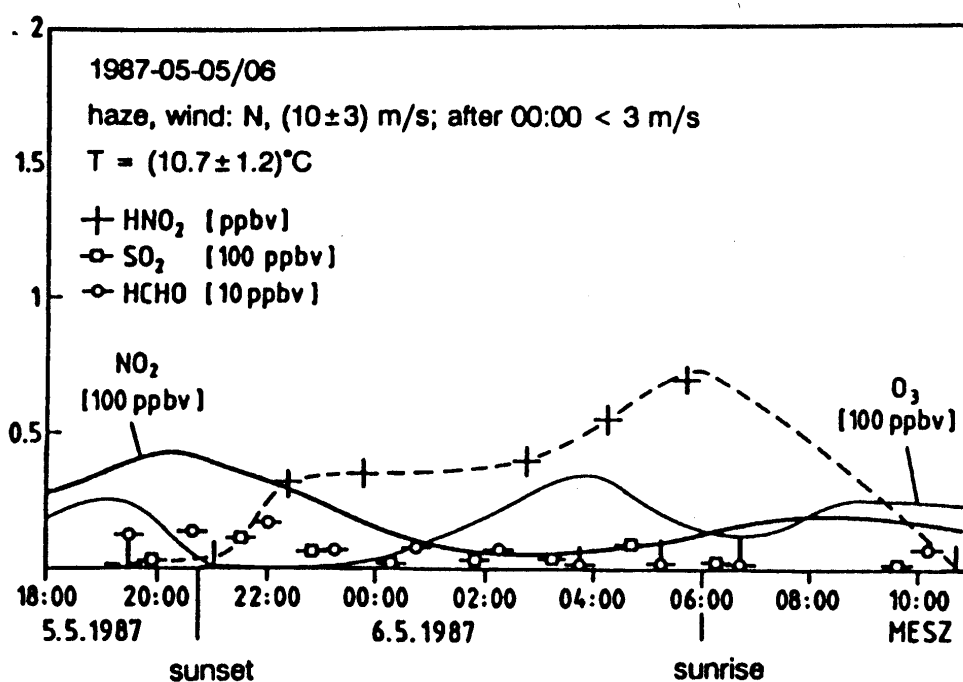
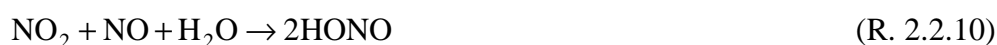


Figure 2.2.3: Measured HONO concentrations at Mainz, in a heavily industrialized area (Graph from Lammel and Cape, 1996).

2.2.3 Sources of HONO.

A) Gas phase reactions

Several well known gas phase reactions have been suggested in order to explain the formation of HONO in the atmosphere (R. 2.2.9-11):



However, reactions (R. 2.2.9-10) are much too slow to explain the observed night-time HONO production rates and reaction (R. 2.2.11) can only be significant during daytime as OH levels are very low during the night [Junkermann and Ibusuki, 1992]. Calculations demonstrate that reactions (R. 2.2.9-11) could account for at most 0.5% HONO relative to NO_x whereas field measurements show that the HONO/NO₂ ratio typically reaches a few percent [Lammel and Cape, 1996, and references therein].

B) Direct emission of HONO.

Another possible source of HONO is its emission as a primary pollutant from combustion engines or biomass burning. Exhaust gases from different vehicles have been examined and the results revealed that the mole ratio HONO/NO_x is approximately 0.15% and may increase only to 0.5% by rapid reactions subsequent to emission [Perner, 1987]. Measurements during the burning season in the tropical savanna suggested that HONO is only a minor by-product [Rondón and Sanhueza, 1989]. Thus, direct emission of HONO by combustion processes cannot explain the high levels that have been measured neither in urban nor in rural areas.

C) Heterogeneous reactions of HONO.

Neither gas phase reactions nor direct emissions are able to explain the observed HONO levels so far. Therefore, more and more interest is directed to heterogeneous reactions. Studies that have been performed in smog chambers often reported the formation of HONO. This process could finally be identified as a heterogeneous hydrolysis of NO₂ on the reactor walls [Finlayson-Pitts and Pitts, 1986]:



Species in curved brackets refer to adsorbed molecules. This reaction has been examined for many different surfaces such as glass, quartz, metal oxides, fluorinated polymers etc. but significant rates of HONO formation have never been observed [Lammel and Cape, 1996, and references therein]. Only recently, Kleffmann et al. [1998] have suggested that this reaction may be faster under certain conditions on Pyrex glass.

A similar process that has been observed in laboratory studies consists of the hydrolysis of N₂O₃ [Calvert et al., 1994]:



In the environment there are two types of surfaces: ground surfaces such as soil, biological surfaces, buildings, paved roads etc. and the surface of airborne particles. Over grassland in SE England an upward flux of 5-25 ng HONO m⁻² s⁻¹ (which would correspond to tenths of a ppbV HONO h⁻¹ under the influence of a low night-time boundary layer) was observed when NO₂ concentrations exceed 10 ppbV, while at lower concentrations a net downward flux occurred [Harrison and Kitto, 1994]. A strong coincidence of HONO and Radon concentrations (which has sources exclusively on the ground) suggested a ground-based source of HONO [Allegrini et al., 1994]. The surfaces of buildings and streets are substrate candidates as NO₂ is known to be efficiently absorbed by cement and building stone [Baumgärtner et al., 1992].

The importance of aerosol surfaces was suggested by the observation that the production of HONO was particularly effective under hazy conditions [Lammel et al., 1990]. A correlation between HONO mixing ratios and particulate matter surface area was observed at Jülich, Germany [Kessler and Platt, 1984]. A clear correlation has also been observed in rural air in northern Italy, where co-variation with the boundary layer depth was minimized [Andrés-Hernández et al., 1996]. Furthermore, whenever aerosol has been analyzed for nitrite, it has appeared that atmospheric aerosol was a source of gaseous HONO [Li, 1994; Lammel and Perner, 1988]. It is unclear, however, whether the aerosol surface was the only or the dominant source.

2.2.4 Soot aerosols as a potential HONO source.

Although a lot of different surfaces have been examined in relation to their potential to form HONO, a conclusive heterogeneous reaction mechanism with which the observed HONO levels could be explained is still missing.

The variety of airborne particulate matter is quite high. There are on the one hand inorganic aerosols like sea salts or mineral dust and on the other hand organic materials such as for instance soil particles or aerosols that are formed by the photooxidation of hydrocarbons according to the reactions described in Figure 2.2.1. The situation can be even more complex as a lot of aerosols are in fact external mixtures of several phases.

A particularly interesting group of aerosols is represented by soot. The fact that it is emitted by combustion processes is logically leading to the result that it is always accompanied by increased concentrations of other pollutants such as NO_x or SO₂. Therefore, it is not surprising that an increasing number of research groups started to explore their role in atmospheric chemistry. The present study is thought to make a contribution to the question how nitrogen oxides such as NO, NO₂ or HONO interact with soot. Although numerous studies have already been performed a lot of open questions still exist in this field. One reason

for this lack of knowledge is certainly due to the enormous complexity that the soot substrate represents. The next Section will therefore give a short survey of the manner how soot is formed, of its distribution in the atmosphere is and how it may be characterized from a chemical point of view.

2.3 Soot particles in the atmosphere.

2.3.1 Atmospheric burden and impact of soot particles.

Atmospheric soot particles, also called black carbon, are produced by the incomplete combustion of fuel with the main sources being fossil fuel and biomass burning. Global emissions of soot were estimated to be between 12.6 and 24 Tg C per year [Penner, 1993] leading to loadings of elemental carbon in the boundary layer ranging from 1.5-20 $\mu\text{g}/\text{m}^3$ (urban areas) to 0.2-2 $\mu\text{g}/\text{m}^3$ (rural areas) [Seinfeld, 1998, and references therein]. Soot particles in the concentration range of 0.05-4.2 ng/m^3 have been detected also along aircraft flight corridors in the higher troposphere and the lower stratosphere [Pueschel, 1992 and 1997; Blake, 1995; Chuan, 1984]. Black carbon particles can be transported on the global scale and so are able to reach remote regions. Trace element and meteorological analysis suggest that even long-range transport from mid-latitudes takes place to the extent between 5'000 and 10'000 km [Rahn, 1980; Barrie, 1981].

The presence of these aerosols in the atmosphere is problematic for several reasons. Soot aerosols strongly absorb the incoming solar radiation, and, thereby, may contribute directly to climate forcing [ICCP,1996]. The opposite effect is produced if they act as cloud condensation nuclei. Their role in the formation of contrails, which may develop into large scale cirrus has been discussed in several studies [Kärcher, 1996; Minnis, 1998; Strom, 1998]. A further area of interest is their potential to interact with gaseous pollutants. An increasing number of laboratories are examining the heterogeneous reactions of trace gases such as NO₂, NH₃, HONO, O₃ or SO₂ with the surface of soot particles [Kleffmann, 1999; Koehler, 1999; Longfellow, 1999]. The special feature of freshly emitted soot is that its surface presents reductive sites in an environment that otherwise is oxidative. Such heterogeneous reactions have been proposed in order to explain discrepancies between field measurements and model calculations [Hauglustaine, 1996; Bekki, 1997; Aumont, 1999]. Finally, soot aerosols also represent a direct risk for human health. Its fine fraction ($\varnothing \leq 1 \mu\text{m}$) can enter the human respiratory system and advance even into the alveoli where carcinogenic polycyclic aromatic compounds such as benzo(a)pyrene that are adsorbed on the surface of soot particles may develop their fatal activity [Schlesinger, 1995].

2.3.2 Chemical characterization of soot particles.

Soot is not only an undesired pollutant but also a commercial product that is manufactured on an industrial scale for more than 50 years. It is basically used as a pigment for printing inks and coatings or as an additive in order to improve the mechanical properties and UV resistance of polymers such as automobile tires. Within the scope of product development industrial research made big efforts to characterize the chemical groups that are present on soot particles. An often used method consists of the titration of aqueous suspensions of soot particles. Acidic surface groups such as –COOH, lactones or C₆H₅-OH have been detected with traditional titration agents such as NaHCO₃, Na₂CO₃ and NaOH [Hofmann, 1950; Boehm, 1966]. However, many types of industrial soot undergo an oxidative after-treatment and may therefore not be representative of environmental soot samples.

The industrial research on soot cited above has been continued in more recent years but now from an environmental point of view. A better understanding of the composition of soot should lead to more precise predictions concerning its role as a cloud condensation nucleus, its participation in climate forcing or its importance as a reactive surface in heterogeneous atmospheric chemistry. Many studies have been performed in order to identify the chemical functionalities and compounds that are present in soot both for environmental samples as well as for laboratory-generated soot. Akhter et al. [1985] showed using FTIR and mass spectroscopy that on laboratory-generated n-hexane soot a multitude of different PAH's are condensed on the non-extractable elemental carbon backbone structure of soot. In addition, they have shown that both the elemental carbon backbone as well as the PAH's present all kinds of functionalities such as –aryl-C=O, aryl-OH, aryl-COOH, anhydride etc. It is very important to know whether these findings are transferable to environmental soot samples or not. Larichev et al. [2000] performed a comparative study between laboratory-generated soot and aircraft soot using different techniques such as PTD, BET, elemental analysis etc. They found that laboratory-generated soot has different properties compared to aircraft soot in many respects. These results show that one has to be very careful when results based on laboratory-generated soot are to be transferred into the environment. One of the main problems in the analysis of environmental aerosols is that most analytical methods require substantial quantities of substrate material which has the consequence that long sampling times are necessary. This not only decreases the temporal resolution of the monitoring but also favors desorption/adsorption artifacts [Bidleman, 1987; König, 1980]. Therefore, many efforts have been expended in order to develop analytical methods that allow the examination of small quantities of aerosol samples. Haefliger et al. [1999] used a laser desorption/laser photoionization mass spectrometry system to analyze urban aerosol samples on the scale of several micrograms. They found that single compounds of the adsorbed PAH

fraction show a strong variation during the course of a day which may lead to conclusions concerning the source of the particles.

2.3.3 The diffusion flame.

The physico-chemical characteristics of a diffusion flame will be presented below because it is the type of combustion that has been used in the present work in order to produce the soot samples (see Sections 4.1 and 4.2).

A) General properties of a diffusion flame.

Combustion is a phenomenon caused by a self-supported, exothermic reaction. The physical processes involved are principally those which pertain to transport of material and energy. The conduction of heat, the diffusion of chemical species and the bulk flow of gas may all develop from the release of chemical energy in an exothermic reaction as a consequence of the thermal and concentration gradients that are set up in the vicinity of the reaction zone. It is the interaction of these various processes that leads to the phenomenon that is observed.

The chemical reaction usually involves two components, one of which is termed fuel and the other the oxidant. In the case of a diffusion flame combustion occurs at the interface of the fuel and the oxidant gas. A classic fuel/oxidant interface is for instance the wick of a petroleum lamp where the liquid fuel is transported by capillary forces to the top where it is instantaneously evaporated by the heat that is emitted by the diffusion flame. The oxidant is in this case oxygen that is delivered from the ambient air. A turbulent flame is resulting if the oxygen/fuel mixing occurs by eddy diffusion. Such a mixing is reflected by a flickering flame whose thermal and chemical properties are strongly varying, both temporally as well as spatially. In slow-burning diffusion flames on the other hand where the fuel and the oxygen are moving upwards in laminar flows at the same speed mixing process occurs solely by molecular diffusion. The result is a temporally stable 'laminar' diffusion flame that is much easier to characterize than a turbulent one.

It is a characteristic of the diffusion flame that the burning process depends more on the rate of mixing than on the rates of chemical processes involved. This can be seen in Figure 2.3.1 where the spatial concentration profiles for fuel, oxygen and reaction products through a cross-section of a laminar diffusion flame are presented. It is found that the fuel concentration has a maximum on the axis and falls rapidly at the boundary. The oxygen concentration also decreases close to the flame and falls approximately to zero at the boundary. By contrast, the concentrations of products is at a maximum at the boundary, where the major extent of reaction occurs, and falls away both towards the axis and into the surrounding atmosphere. It

is evident that due to this inhomogeneous distribution of fuel and oxygen zones of quite different reactivities can be distinguished within a diffusion flame.

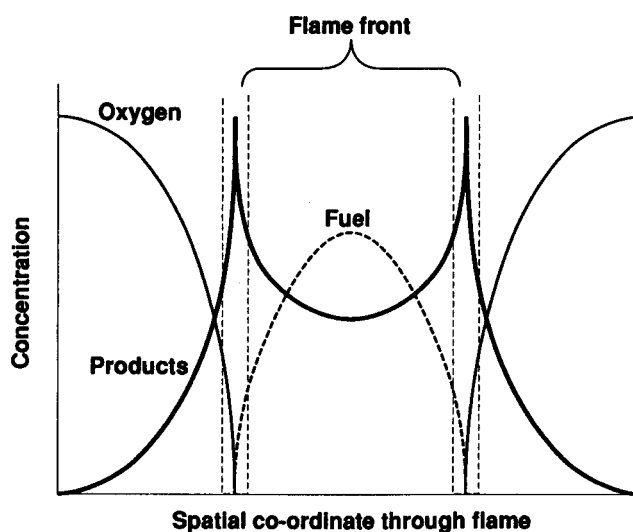


Figure 2.3.1: Spatial concentration profiles for fuel, oxygen and reaction products through a cross-section of a laminar diffusion flame (picture from Griffith and Barnard, 1995)

Samples taken of the inner zone showed that primary chemical processes involve pyrolysis. In the absence of oxygen alkanes are cracked in order to form lower molecular alkenes and molecular hydrogen but also radicals that can undergo polymerization and cyclization which results in the formation of large and highly unsaturated compounds [Medalia and Rivin, 1976]. These products are subsequently transported to the oxygen rich boundary zone where they are oxidized [Barnard, 1962]. Figure 2.3.2 shows the possible mechanisms for methane oxidation according to Warnatz [1984]. The combustion of higher alkanes is closely connected to this scheme, insofar as these processes are the final stages of the reaction chains involved, regardless of the molecular mass of the primary fuel. Degradation of the molecular structure of the fuel by pyrolysis is favored at high temperatures, yielding a predominance of free radicals and molecular intermediates which contain only a small number of carbon atoms. In particular the formation of alkyl radicals in any free radical abstraction process, for example ($X = O, OH, \text{etc.}$):



is followed by



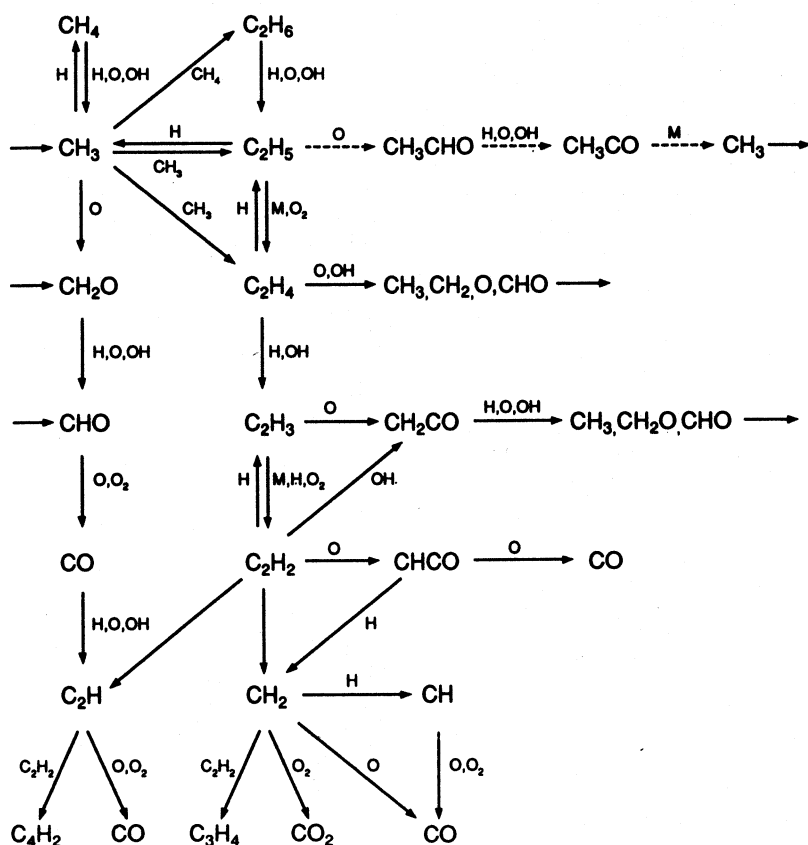


Figure 2.3.2: Schematic representation of a mechanism for methane oxidation at high temperature (after Warnatz, 1984).

Figure 2.3.2 shows that the formyl radical (CHO) is a major product of the oxidation of C₁ and C₂ hydrocarbon fragments. This fragment may be a source of hydrogen atoms, via



or it may be oxidized and give rise to HO₂ formation, via



Hydrogen that is formed in this way may further interact with molecular oxygen in two different ways:



These reactions are crucial because they describe the formation of the radicals H, O, OH and HO₂ that are the most important oxidant in a flame. In addition, (R. 2.3.7) is very important because it is a radical chain branching reaction mode. That means that two highly reactive radicals are formed from one. This particular reaction, coupled to



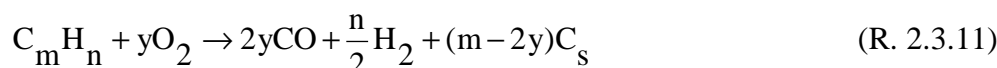
and the principal propagation reaction, which is highly exothermic:



are crucial to the branching chain thermal interaction that gives rise to the self-sustaining properties of hydrocarbon flames.

B) Soot formation in a diffusion flame

From a thermodynamic point of view, the formation of soot should start when in reaction (R. 2.3.11)



$2y$ becomes equal to or smaller than m [Homann, 1967] which means when the O/C ratio remains below one or when there is not enough oxygen available in order to enable a complete oxidation of the present carbon to CO₂. Experimentally however, limits of soot formation that have been determined in premixed flames do not occur at O/C = 1 but usually close to O/C ≈ 2.0 [Wagner, 1978, and references therein]. In the inner zone of a diffusion flame the O/C ratio is generally far below this critical limit. That means that almost every diffusion flame is producing soot which is also testified by the yellow/orange luminosity of this flame zone. In fact, the soot particles approach black body properties and are emitting radiation of a bright yellow to orange color according to their temperature [Kunugi, 1967]. The general sooting tendency of different fuels in a laminar diffusion flame is [Herbst, 1968] given by the series

aromatics > alkynes > alkenes > alkanes.

The detailed mechanism of formation of soot particles has not been completely established. However, a scheme for which considerable evidence exists is shown in Figure 2.3.3 [Homann, 1968]. It has been mentioned above that in the inner, oxygen poor zone of a diffusion flame cracking, polymerization and cyclization processes occur. These reactions may convert the hydrocarbon fuel into polycyclic aromatic molecules and radicals, which owe their stability to a high resonance energy. The stable, planar polycyclics condense into very

small droplets, which collide and coalesce to form larger droplets or semi-liquid “particles”. The polycyclic species tend to orient themselves predominantly concentrically parallel to the surface. Progressive dehydrogenation and linking together of the polycyclics leads to an increase in viscosity so that on further collision the droplets stick together in the form of aggregates, but do not coalesce into spherical form. Further dehydrogenation converts the polycyclic species to carbon.

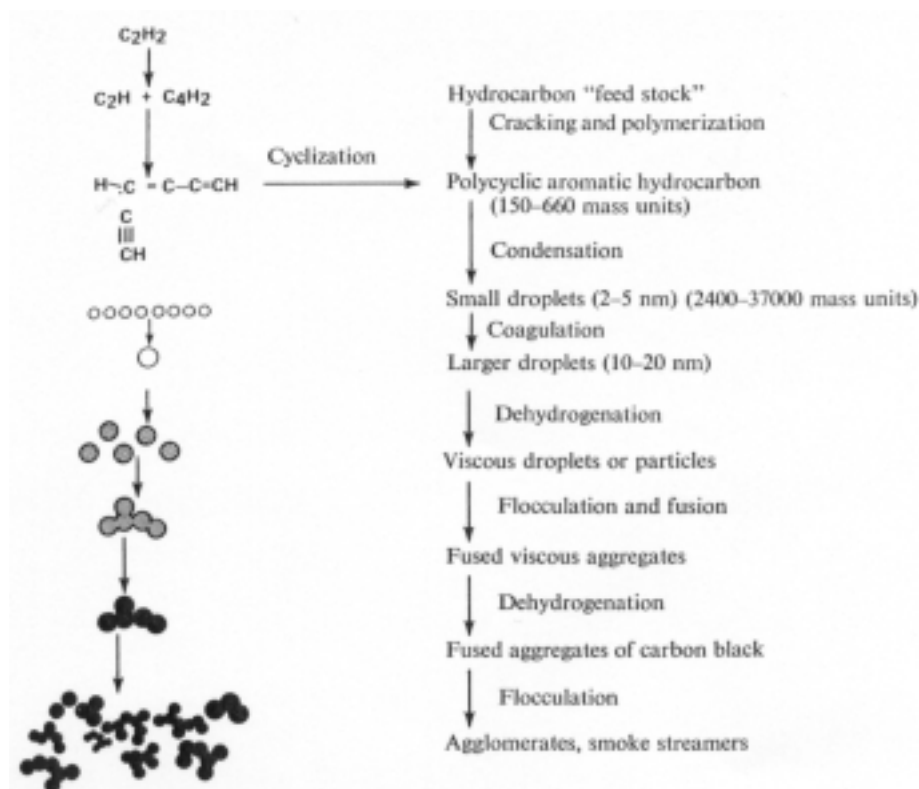


Figure 2.3.3: Schematic mechanism of carbon black formation (based on Homann, 1968, and Medalia and Rivin, 1976).

The tendency of polycyclic aromatic hydrocarbons to orient themselves concentrically parallel to the surface leads to a microstructure that reminds one of an equatorial slice of an onion. Figure 2.3.4 shows a simplified scheme of the currently accepted concentric layer model of the carbon black microstructure [Harling, 1969]. It can be seen that the concentric layers are less ordered in the inner region of the spheroid leading to the false impression that the particle is hollow. The small packets correspond to microcrystalline regions of 3 to 4 graphitic layers containing each 20-35 six-membered carbon rings [Ullmann, 1977]. However, even in these microcrystalline regions the degree of perfection and ordering can be highly decreased compared to pure graphite. This is reflected by the distance between the

adjacent layers which can vary between 3.5 and 3.7 Å [Heidenreich, 1968] which is higher than the distance of 3.35 Å that is measured for pure graphite.

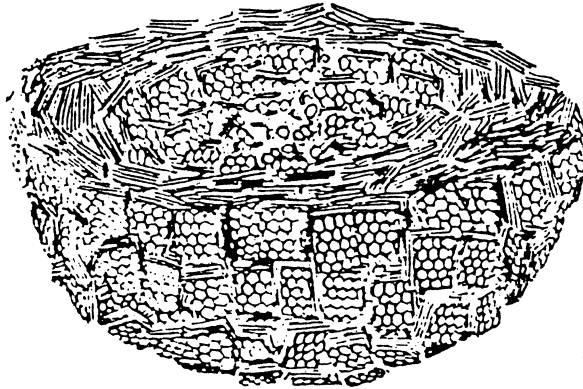


Figure 2.3.4: Schematic structure of a soot particle (picture from Heddrich, 1986)

Pyrolytic soot formation is competing with oxidative soot consumption. The latter is predominating in the outer oxygen rich zone of a diffusion flame. If the residence time of the particles in the outer, oxidative zone is sufficiently long all the soot will be consumed and transformed into CO₂ and H₂O. If on the other hand soot formation processes prevail the soot particle will leave the combustion zone in form of a plume.

3 Experimental set-up.

3.1 The Knudsen flow reactor.

The technique applied to the kinetic measurements in this work is based on a Knudsen cell, a low pressure flow reactor that operates under molecular flow conditions [Golden et al., 1973]. In practice, one may proceed on the assumption that molecular flow conditions are attained if the dimensionless ratio between the mean free path and the diameter of the escape orifice is at least 3:

$$\frac{\lambda}{\varnothing_{\text{escape orifice}}} > 3 \quad \Rightarrow \quad \text{molecular flow regime} \quad (\text{E. 3.1})$$

Where λ is the mean free path of the molecules and $\varnothing_{\text{escape orifice}}$ the diameter of the escape orifice. Maximum pressures of about 6×10^{-3} mbar in the 1mm escape orifice reactor lead to λ 's of at least 10 mm for NO_2 , NO and HONO in the present study. The division of this number by the diameter of the escape orifice gives 10. Consequently, all the experiments of the present study were definitely performed under molecular flow conditions. This low pressure regime ($P_{\text{tot}} < 10$ mbar) represents two major advantages: First it ensures that the dominant collision mode inside the reactor is of the type gas-wall, which is quite appropriate when studying heterogeneous processes, since gas phase reactive perturbations are thus minimized. Second, essential parameters like the residence time and the collision frequency of the gas molecules with the substrate can be accurately determined using gas kinetics theory because of the absence of any gas phase diffusion limitations. The gas-wall collision frequency ω per molecule per cm^2 per second is defined by equation (E. 3.2):

$$\omega = \frac{\langle c \rangle}{4V} = \frac{1}{4V} \sqrt{\frac{8RT}{\pi M}} \quad (\text{E. 3.2})$$

where $\langle c \rangle$ is the mean molecular speed of the gas species, M the molar mass for this species, R the ideal gas constant, T the gas temperature and V the volume of the reactor. The fact that there are no gas phase diffusion limitations leads to very short mixing times within the reactor which is enabling the observation of processes with very fast kinetics.

The reactor developed in our laboratory (see Figure 3.1) consists of two compartments: one used for reference experiments and the second containing the substrate of

interest and which can be isolated from the reference part through an O-ring sealed movable plunger. The internal surfaces of the reactor (made of Pyrex glass and stainless steel) are entirely coated with fluorinated ethylene-propylene (Teflon® FEP 100, Dupont) to limit potential interactions between gas phase species and the walls. The versatility of this reactor in the context of heterogeneous studies has been discussed by [Caloz et al., 1997].

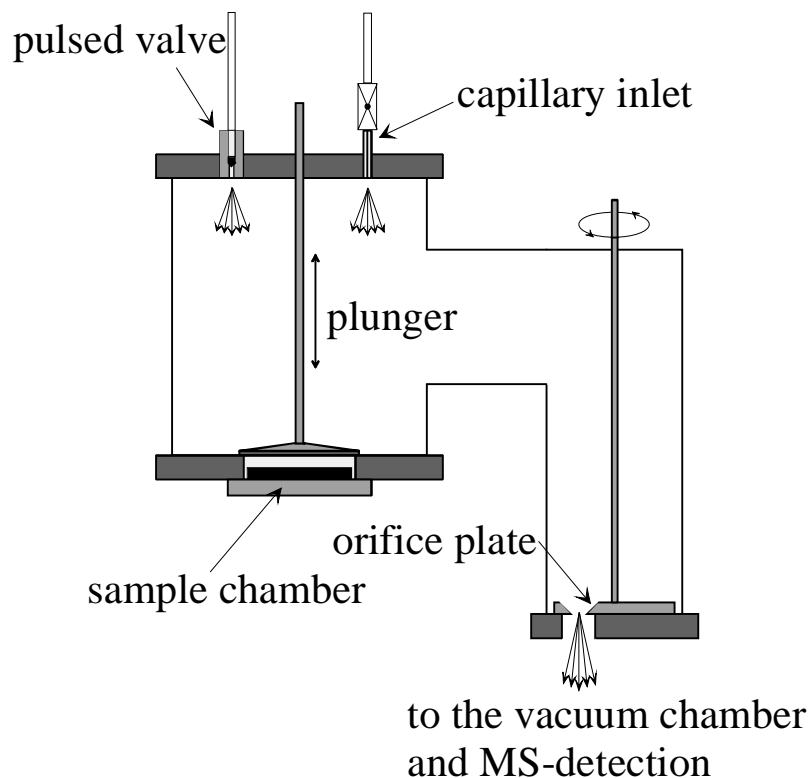


Figure 3.1: The Knudsen cell reactor.

3.2 General description of the experiment.

The apparatus is equipped with a standard vacuum line from which the gas species of interest can be admitted into the reactor. There are two types of injectors: glass capillary inlets (diameter of 0.1mm) and a pulsed solenoid valve.

The residence time of the gas in the reactor is controlled by means of a variable size orifice through which molecules escape into the vacuum chamber. By changing the orifice cross section one affects the molecules' rate of effusion out of the reactor and can thus vary their residence time (τ) by up to two orders of magnitude. This effusion rate constant referred to as k_{ESC} solely depends on the gas-wall collision frequency ω (E. 3.2) and the orifice surface A_h .

$$k_{esc} = \omega A_h \quad (\text{E. 3.3})$$

The instantaneous pressure or gas phase concentration in the reactor also depends on the selected orifice size according to the formula:

$$[\text{gas}] = \frac{N}{V} = \frac{F}{k_{esc} V} \quad (\text{E. 3.4})$$

where N is the total number of molecules in the reactor and F the flow of molecules into the reactor.

This means that the concentration may be chosen either by adjusting the inlet flow F or at a given flow by changing the orifice size. Thus we can vary the density within a range of three orders of magnitude and gain access to mechanistic information on the heterogeneous process taking place. The general parameters of our Knudsen reactor are listed in Table 3.1a. whereas the specific conditions for the study of the soot/ NO_2 interaction may be found in table 3.1b.

Volume ^A = 2000 cm ³ Surface area ^B = 1300 cm ² $\omega^C = 35.6 \times (T/M)^{0.5} \text{ s}^{-1}$		
Orifice diameter [mm]	$k_{esc} [\text{s}^{-1}]$	Residence time [s]
Ø 1.0	$0.013 \times (T/M)^{0.5}$	$76.5 \times (M/T)^{0.5}$
Ø 4.0	$0.245 \times (T/M)^{0.5}$	$4.04 \times (M/T)^{0.5}$
Ø 8.0	$0.796 \times (T/M)^{0.5}$	$1.23 \times (M/T)^{0.5}$
Ø 14.0	$1.880 \times (T/M)^{0.5}$	$0.528 \times (M/T)^{0.5}$

Table 3.1a: General parameters of the Knudsen cell used in this work. k_{esc} , ω and the gas phase residence time were experimentally determined using NO_2 .

A) The total volume is increased only by 1% upon opening the sample chamber. Therefore no distinction concerning the volume is made between a reference and an uptake experiment.

B) Estimated total surface area of the Knudsen cell.

C) This formula applies to the maximum reactive area of 19.6 cm² and the molar mass M expressed in g/mole.

3 Experimental set-up

Volume $V = 2000 \text{ cm}^3$		Reactive area $A_S^A = 19.6 \text{ cm}^2$		$\omega(\text{NO}_2)^B = 90.6 \text{ s}^{-1}$	
escape orifice	$k_{\text{ESC}}(\text{NO}_2)$	typical collision rates of NO_2		typical concentrations of NO_2	
\varnothing [mm]	$[\text{s}^{-1}]$	lower limit $[\text{molec cm}^{-2} \text{ s}^{-1}]$	upper limit $[\text{molec cm}^{-2} \text{ s}^{-1}]$	lower limit $[\text{molec cm}^{-3}]$	upper limit $[\text{molec cm}^{-3}]$
14	4.4	6.0E+14	1.0E+16	6.5E+10	1.1E+12
4	0.56	4.2E+15	8.0E+16	4.5E+11	8.6E+12
1	0.034	8.4E+16	1.4E+18	9.1E+12	1.5E+14

Table 3.1b: Specific parameters for the study of the NO_2 /soot interaction.

- A) Reactive surface area refers to the geometric surface area of the sample chamber. The reactive surface area of the 1,2,10-trihydroxyanthracene samples discussed in Section 10 was only 10.5 cm^2 .
- B) Calculated according to formula C) of Table 3.1a for a temperature of 298K and a reactive surface area of 19.6 cm^2 .

Molecules escape from the reactor forming an effusive (thermal) molecular beam collected by an electron impact quadrupole mass spectrometer QMS (Balzers QMA 421) lodged in the lower part of a differentially pumped vacuum chamber. The ion source of the mass spectrometer is located inside an annular concentric trap that can be filled with liquid nitrogen. This cold trap significantly lowers the background pressure around the ion source and thus improves the signal-to-noise ratio. The choice of Phase Sensitive Detection (PSD) was made to discriminate the signal of the molecular beam from the background signal which originates from interactions of the reactants with the walls of the detection chamber. To this end the beam effusing from the cell is modulated by a tunable chopping wheel (20 - 350Hz) prior to ionization and detection. The PSD is then processed by a lock-in amplifier (Stanford Research System SR 830). All this is schematically summarized by Figure 3.2.

3 Experimental set-up

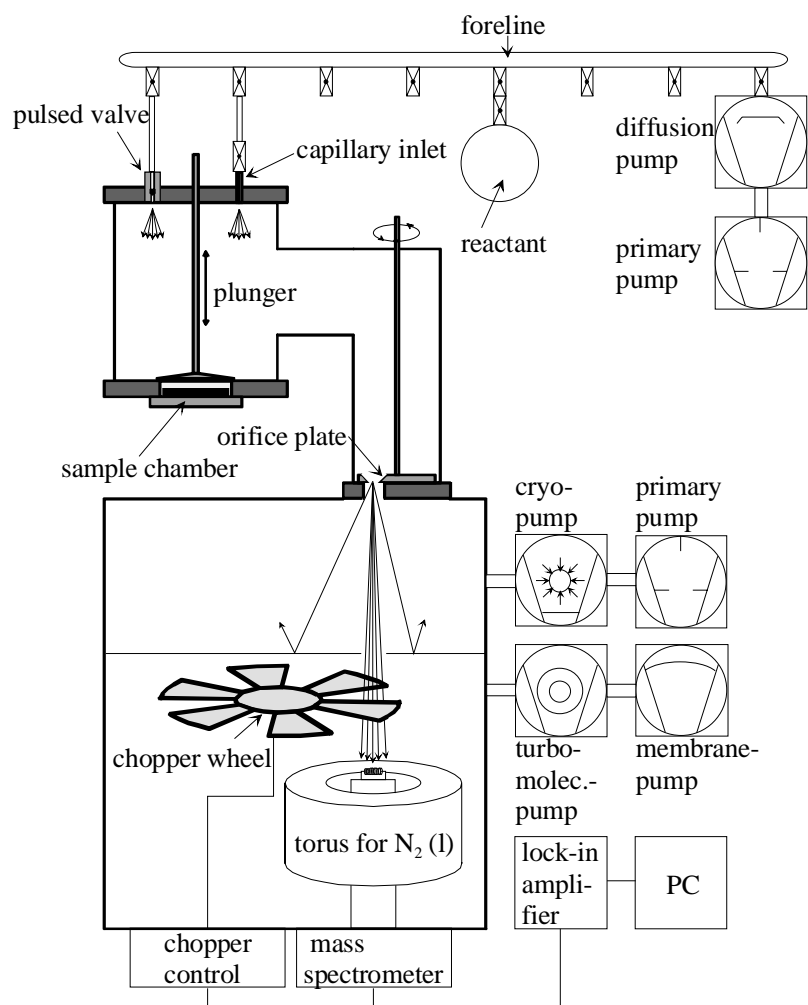


Figure 3.2: Schematic description of the experimental system.

Two types of experiments are routinely performed using this design which hence will be referred to as continuous-flow and pulsed-valve experiments.

In a **continuous-flow experiment** (Figure 3.3) a constant flow F_{in} of molecules is admitted into the cell. Once the equilibrium established in the reactor and in the absence of reaction, the steady state equation $F_{\text{in}} = F_{\text{out}}$ results in the following relation:

$$\begin{aligned} \frac{dN}{dt} &= F_{\text{in}} - F_{\text{out}} = F_{\text{in}} - k_{\text{esc}} N_0 \\ \Rightarrow N_0 &= \frac{F_{\text{in}}}{k_{\text{esc}}} \end{aligned} \quad (\text{E. 3.5})$$

When a reactive surface is exposed the new steady state at molecular flow conditions may be expressed as

$$\begin{aligned} \frac{dN}{dt} &= F_{\text{in}} - k_{\text{esc}} N_{\text{r}} - k_{\text{uni}} N_{\text{r}} \\ \Rightarrow N_{\text{r}} &= \frac{F_{\text{in}}}{k_{\text{esc}} + k_{\text{uni}}} \end{aligned} \quad (\text{E. 3.6})$$

where N_{r} is the number of surviving molecules leaving the reactor and k_{uni} is the first order rate constant of the uptake of the gas on the reactive surface. The mass spectrometric signal, directly proportional to the flow of molecules leaving the reactor, drops from S_0 to S_{R} (see Figure 3.3). One may then determine k_{uni} by measuring both signals S_0 and S_{R} , that is non-reactive and reactive signals, respectively, and calculate k_{uni} using equation (E. 3.7):

$$k_{\text{uni}} = \left(\frac{S_0}{S_{\text{R}}} - 1 \right) k_{\text{esc}} \quad (\text{E. 3.7})$$

To make this value independent of the geometrical characteristics which are specific to our reactor it is convenient to express the kinetic result in the form of a dimensionless uptake coefficient γ defined as:

$$\gamma = k_{\text{uni}} / \omega_{\text{S}} \quad (\text{E. 3.8})$$

where ω_{S} ist the collision frequency of the molecule on the surface area of the sample ($\omega_{\text{S}} = \omega A_{\text{S}}$). This uptake coefficient represents the fraction of all collisions leading to the net removal of the reactant molecule from the gas phase.

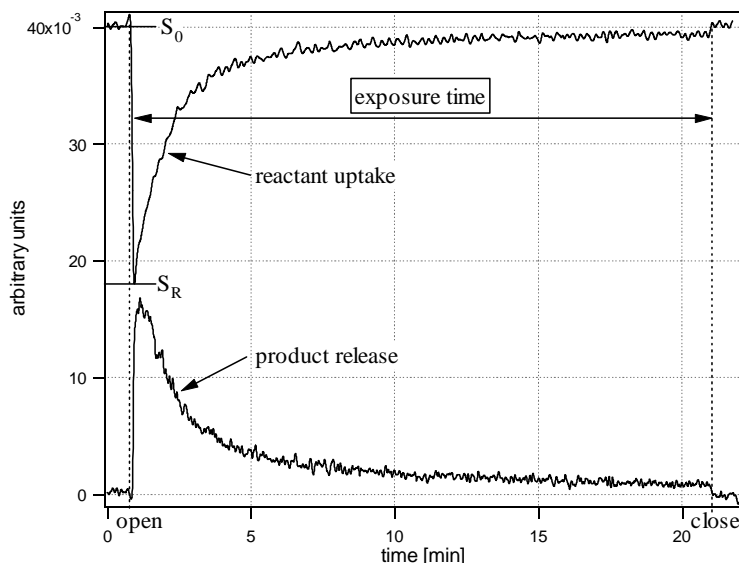


Figure 3.3: Typical continuous-flow experiment profile performed on decane soot at ambient temperature in a 4 mm aperture reactor with a NO_2 flow of $4.5 \times 10^{15} \text{ molecule s}^{-1}$. The upper trace monitors the fate of the reactant, namely NO_2 at m/e 46, while the lower indicates the release of nitrous acid (HONO) in the gas phase monitored at m/e 47.

In the case of **pulsed-valve experiments** (Figure 3.4), pulses of reactive gas are admitted into the cell by briefly opening the solenoid valve on the millisecond time scale. Having isolated the reactive substrate from the admitted gas, we inject a first pulse which is referred to as the reference pulse. The corresponding mass spectrometric (MS) signal decays following a single exponential and gives us a measured value of k_{esc} for the reactant monitored according to the equation :

$$\frac{dN}{dt} = k_{\text{esc}} N \quad (\text{E. 3.9})$$

A "reactive pulse" of equal dose follows for which the reactive surface is exposed. The resulting MS signal, assuming the process is first order, is again of single exponential type with a decay rate k_{dec} which amounts to the sum of k_{esc} and k_{uni} . Thus by comparing the two pulses we obtain $k_{\text{uni}} = k_{\text{dec}} - k_{\text{esc}}$. By applying the same procedure outlined in (E. 3.8) we obtain $\gamma = k_{\text{uni}} / \omega_s$

This type of kinetic measurement not only allows us to validate the kinetics obtained in a continuous-flow experiment, but provides us with more specific information as follows:

- The injected dose of reactant may be minimised, typically down to 5×10^{13} molecules per pulse. This represents only a fraction of a formal monolayer which is equivalent to approximately 1×10^{16} molecule for our samples of approximately 19.6 cm^2 surface area. In many cases we may ignore any desorption on the time scale of the pulse [Chaix et al, 1998] and what we observe is therefore a real-time kinetic process. Our measured γ corresponds therefore to a mass accommodation coefficient. However, we will see that in the case of the interaction of NO_2 on soot even that small a dose will lead to saturation effects and the calculated value of k_{uni} therefore does not correspond to an unimolecular uptake process.
- Not only the reactant but the expected products may be monitored. Kinetic information such as the shape of the "product pulse" and the delay with which it appears can eventually lead to insights in terms of potential interaction of the product with the surface and the associated mechanism.
- The integral of the MS trace resulting from a pulse may be set equal to an absolute dose once the calibration procedure described in the next Section will have been performed (3.3). By comparing the respective integrals of non- reactive and reactive pulses we are able to establish a mass balance for the reaction of interest.

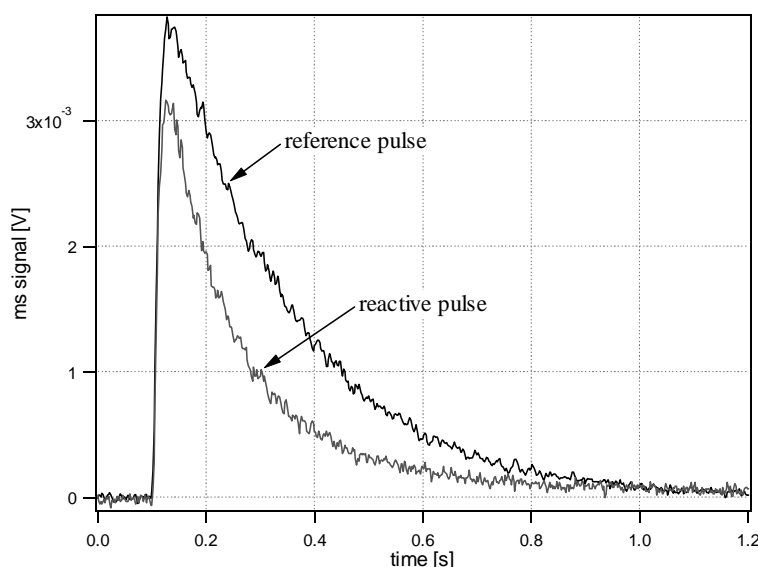


Figure 3.4: Typical pulsed-valve experiment of NO_2 on decane soot at ambient temperature monitored at m/e 46. The reference pulse is monitored in the absence of any substrate, while the reactive pulse corresponds to the same injected dose in the presence of the substrate.

3.3 Gas flow calibration technique.

The mass-spectrometric signal measured at any time S_t is directly proportional to the flow of the monitored species F_{out} effusing out of the reactor. Under continuous-flow conditions and no reaction the following equation applies:

$$F_{\text{in}} = F_{\text{out}} = \frac{dN}{dt} = K_{\text{cal}} S_t \quad (\text{E. 3.10})$$

where K_{cal} is a calibration constant for the species of interest depending on the QMS set-up parameters such as ionization efficiency or SEM voltage.

To determine this calibration constant, we measure the instant flow of a pure gas sample out of a calibrated storage volume V_{cal} into the reactor by monitoring the progressive pressure drop. Initial pressures are ranging from 1 to 4 Torr. If we assume ideal gas behaviour we obtain:

$$\frac{dN}{dt} = \frac{V_{\text{cal}} N_A}{RT} \frac{dP}{dt} \quad (\text{E. 3.11})$$

where P is the pressure and N_A Avogadro's constant.

This technique can be applied providing the species is stable enough to be stored in a closed volume for some time without suffering decomposition. This was not the case for HONO which is quite a reactive molecule and decomposes easily at higher pressures. The calibration method that was used for HONO is described in Section 4.3.3.

3.4 Errors and uncertainties.

In continuous-flow experiments, the use of equation (E. 3.8) to determine the uptake coefficient γ involves an uncertainty proportional to the error in estimating the ratio S_0/S_R and k_{esc} [Caloz et al., 1997]. The former essentially depends on the signal-to-noise characteristics of the detection and varies as a function of flow, amplification and QMS settings. Other sources of error are the zero drift and non-linear response in the detection as well as the accurate knowledge of the reactor volume. In addition, some sticky reactants as for example HONO are adsorbed to some extent on the walls of the reactor. This reservoir represents an additional source whenever a sudden concentration drop of the corresponding molecule occurs. S_0/S_R is therefore slightly underestimated.

The escape rate constant k_{esc} is measured directly, by either (1) stopping abruptly the continuous flow of gas into the cell and following the first order disappearance of that species, or (2) admitting a short pulse of gas into the cell using the pulsed valve inlet and monitoring the first-order decay. Sticky molecules are posing some problems for the determination of k_{esc} : In the case of method (1) the surface of the reactor represents an additional source of molecules for the measurement of γ_0 as it has been mentioned. k_{esc} determined in this way will therefore be underestimated. In the case of method (2) the surface of the reactor represents an additional sink which has previously not been saturated by a continuous flow of the molecule of interest. k_{esc} determined in this way will therefore be overestimated.

Thus the total error in the determination of the uptake coefficient must be evaluated on a case-by-case basis, but usually does not exceed 30% [Caloz et al., 1997].

4 Reactant preparation.

4.1 Preparation of soot samples from hexane and decane.

A simple co-flow system has been developed in order to produce fresh soot samples from liquid fuels in a reproducible way. As shown in Figure 4.1.1 it basically consists of a diffusion flame that is maintained in a controlled stream of air (5% rh). The glass cover is double-walled in order to enable air-cooling of the lamp. First tests without the cooling facility revealed that the flame gets unstable without sufficient removal of the heat. Fuel transport is afforded by the capillarity of a small cylinder of sintered ceramics which replaces the wick of a traditional petroleum lamp. The use of ceramic cylinders of different porosity allowed us to regulate the fuel flow that is feeding the flame in a coarse manner. An additional advantage of the ceramics is that it is not consumed and the geometry therefore not changed during the collection time of a soot sample. The stream of air which is feeding the flame with oxygen has been controlled by mass flow meters. Soot samples between 1 and 20 mg have been collected approximately 1 cm above the flame on glass plates of 19.6 cm² surface area. For decane and hexane fuel (both reagent grade, Fluka) two different types of soot have been produced: one type generated in a lean flame (low fuel/air ratio) and the other in a rich flame (high fuel/air ratio). The lean flame is characterized by a rather low rate of soot production compared to the rich flame. In addition, the flame temperatures in the lean flame are considerably higher which is reflected by a yellow/white emission as opposed to the orange/red emission of the rich flame. In order to obtain the lean flame ceramic cylinders with small pores (\varnothing 4-10 μm) and flow rates of air between 1.3 – 1.5 l/min have been used whereas the rich flame is obtained using ceramic cylinders with large pores (\varnothing 17-40 μm) and air flows between 1.2 – 1.4 l/min. Table 4.1 summarizes the characteristic parameters of the two types of flames. Soot from the rich flame has a greyish color, whereas soot produced in the lean flame is pitch 'black' when observed with the naked eye. The soot samples of the two types will therefore also be referred to as 'grey' decane soot and 'black' decane soot. It is noteworthy that there is no significant difference of the NO_x production between the rich and the lean flame whereas the soot formation rate is almost three times higher in the case of the rich flame.

The fuel/air ratio is a key parameter in combustion technology. In the present study, however, its value can only be roughly estimated because it has not been measured. Therefore the fuel/air ratio will from now on only be qualified as 'high' or 'low' respectively 'rich' or 'lean'. In addition, it must be stressed that a good reproducibility concerning the observed soot properties has only been achieved when the air flow has been continuously adjusted

during sample collection in order to maintain a flame of constant appearance (emission and dimension of the flame and the soot plume).

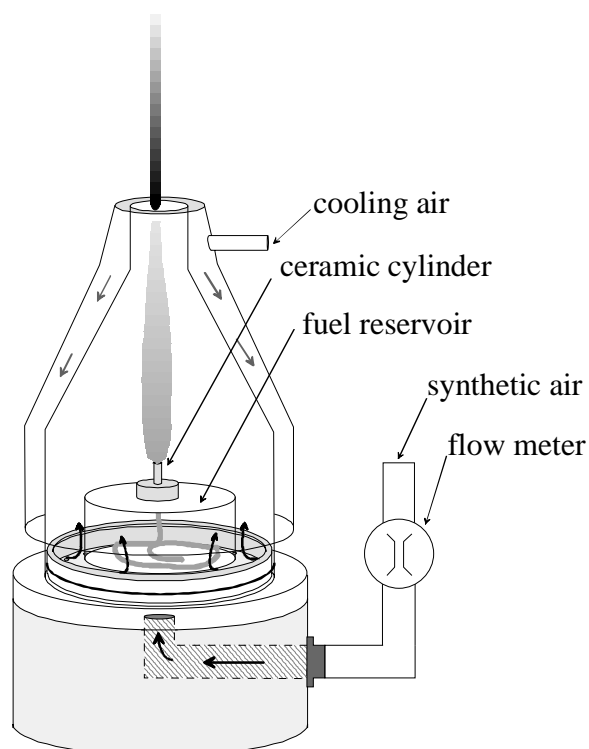


Figure 4.1.1: Co-flow system for a laminar diffusion flame based on liquid fuels.

flame type	height [mm]	emission	[NO _x] in the plume (NO ₂ / NO) [ppm]	soot formation [mg min ⁻¹]	air flow [l min ⁻¹]	fuel duct (pore Ø) [µm]	soot type
rich ^A	~60	orange/red	5.0 ± 0.3 / 18.9 ± 0.5	2.8 ± 0.7	1.3-1.5	17-40	"grey"
lean ^B	~55	white/yellow	5.2 ± 0.5 / 19.4 ± 0.4	1.0 ± 0.3	1.2-1.4	4-10	"black"
acetylene ^C	~50	orange/red	not measured	0.7 ± 0.2 ^D	- ^E	-	acetyl.

Table 4.1: Characteristic parameters of flames that have been used to produce decane, hexane and acetylene soot.

- A) The parameters of the rich flame are the same for 'grey' decane and 'grey' hexane soot.
 B) The parameters of the lean flame are the same for 'black' decane and 'black' hexane soot.
 C) For acetylene gas only one type of flame has been used to produce soot (see Section 4.2).
 D) The effective rate of soot formation was higher but acetylene had the particularity to produce large smoke streamers which detached from the sample support.
 E) The flame was maintained in the free laboratory air and thus was not fed with a controlled flow.

4.2 Preparation of soot samples from acetylene gas.

Soot samples of acetylene gas (Carbagas) have been produced using a commercial gas burner. The standard flame was fed with 135 ml/min of acetylene gas and maintained in the free laboratory air. As in this system the fuel arrives already in the gas phase there were much less problems of flame stability compared to the system for liquid fuels described above.

4.3 Production/purification of gas phase reactants.

4.3.1 NO₂.

NO₂ (Carbagas) is diluted in oxygen (1:10) and stocked in darkness during approximately 14 hours in order to convert traces of NO into NO₂ that are always present as a contaminant. Subsequently, NO₂ is frozen out at approximately –80°C in darkened vessel and O₂ pumped off.

4.3.2 NO.

The NO (Matheson) is purified by condensing the NO₂ contamination in a cold trap at – 100°C. Whereas the NO₂ impurity is frozen out the remaining NO can be pumped into a second vessel.

4.3.3 HONO.

HONO has been generated *in situ* in the low pressure reactor by flowing gaseous HCl through a vessel coated with solid KNO₂ (puriss. p.a. ≥98.8%; Fluka) as shown on Figure 4.3.1. The coating was obtained by spraying a saturated ethanol solution of KNO₂ on the walls of the vessel. The solvent was removed by heating and pumping. The monitoring of mass 36 confirmed that HCl was entirely absorbed by the KNO₂ coating and therefore could not enter into the sample compartment and thus interact with the soot sample. For the HONO calibration the assumption has been made that for every molecule of HCl lost a molecule of HONO is generated. Pure gaseous HCl has been produced by dripping concentrated sulphuric acid (puriss. p.a. 98%; Fluka,) onto solid NaCl grains (puriss. p. a. ≥99.5%, Fluka). The emerging gaseous HCl has been frozen out at – 200 °C in a system which previously had been evacuated.

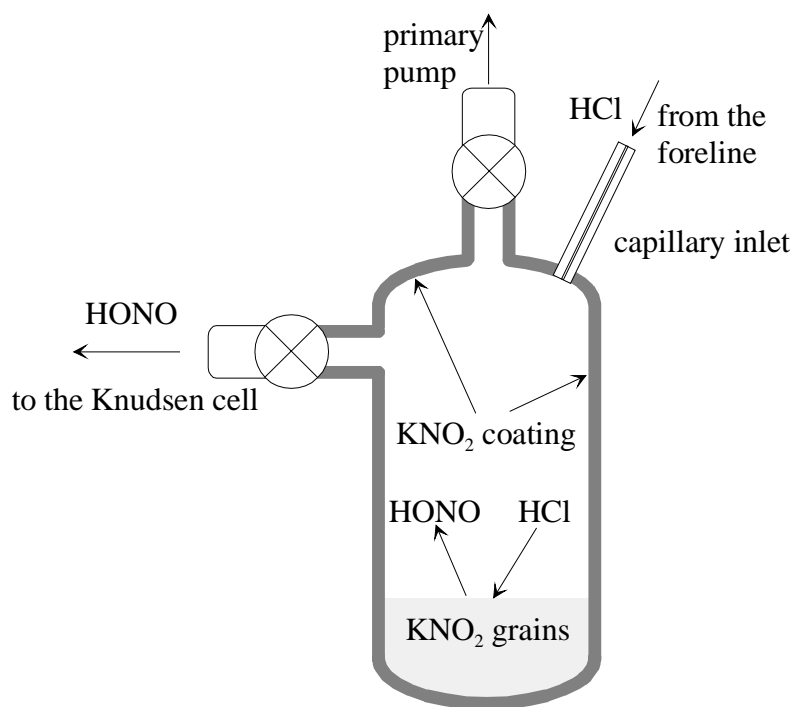


Figure 4.3.1: Supplementary vessel that is connected to the Knudsen cell in order to produce HONO.

The purity of all the gaseous reactants mentioned above has regularly been checked using mass spectrometry.

4.4 Soxhlet extraction of ‘grey’ decane soot.

In order to examine the reactivity of the organic fraction of soot two extractions of each 500 mg of freshly prepared decane soot generated in a rich flame (“grey” decane soot) have been performed in a Soxhlet apparatus in 200 ml benzene and tetrahydrofuran, respectively. The extractions have been performed for 24 hours under nitrogen in order to avoid oxidation of the organic components. Subsequently, the extractions have been sprayed onto thin layer chromatographic plates with polar (silica gel 60; Merck) and non polar surface groups (RP-C18; Merck), respectively, and examined in the Knudsen-cell after evaporation of the solvent. The RP-C18 surface consists of octadecylsilane groups which are chemically bond to the siloxane surface groups of the silica gel. The residual soot has been dried, spread out on a metal plate and also tested in the Knudsen flow reactor. The metal plate had previously been coated with halocarbon wax (series 1500; Halocarbon Products Corp.) in order to improve the adhesion of the loose powder onto the sample support.

4.5 Deposition of 1,2,10-trihydroxyanthracene films.

Thin films of 1,2,10-trihydroxyanthracene (“anthrarobin”, techn. 85%, Aldrich) have been deposited from the vapor phase onto the thinlayer chromatography plates cited above. The technique consisted in heating some milligrams of anthrarobin-powder in a stainless steel cell up to 250°C. The vapors were then condensed on the water-cooled TLC plates. The cell has previously been evacuated to pressures below 1×10^{-3} mbar in order to avoid oxidation of the reactant and accelerate its diffusion to the TLC plate. The whole process has been performed during 12-14 hours.

5 Characterization of the soot samples.

5.1 BET surface areas.

In each system where a gas phase species enters into contact with the surface of a solid sample, an equilibrium will be formed between the portion of gas phase molecules which remains in the gas phase and a portion adsorbed on the surface of the solid sample. The equilibrium for a given temperature may be expressed in the form of the adsorption isotherm. It describes how much of the species is adsorbed as a function of its partial pressure in the gas phase.

Adsorption isotherms have been measured for acetylene soot and for both types of decane soot. Each sample consisted of approximately 400 mg of soot that had been recycled from uptake experiments in the Knudsen cell. The measurements have been performed using a Sorptomatic 1990 (Fisons Instruments) at 77 K with nitrogen as adsorbate. The samples have been pumped at ambient temperature during 2 hours prior to the start of nitrogen adsorption.

The adsorption isotherms show the same characteristics for all three types of soot. Figure 5.1.1 shows as an example the adsorption/desorption isotherms of 'black' decane soot.

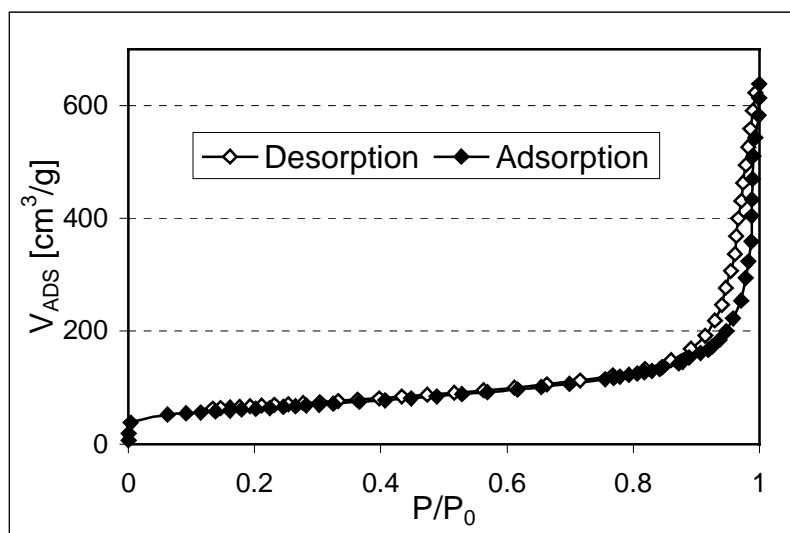


Figure 5.1.1: Adsorption/desorption isotherm of N_2 on 'black' decane soot at 77K.

According to the BDDT classification (Brunauer, Deming, Deming and Teller) [Brunauer, 1944] the isotherms which were obtained for the three different types of soot may be related to group IV. The surface area of this type of adsorbents can be obtained by plotting the

volume of adsorbed N_2 (V_{ADS}) versus P/P_0 according to (E. 5.1). The resulting curve, also called BET plot, should yield a straight line whose slope and intercept serve to calculate the volume of one monolayer of adsorbed N_2 (V_{MONO}):

$$\frac{P}{(P_0 - P)V_{ADS}} = \frac{1}{cV_{MONO}} + \frac{c-1}{cV_{MONO}} \frac{P}{P_0} \quad (\text{E. 5.1})$$

P is the vapor pressure of N_2 in the system, P_0 its saturation vapor pressure, V_{ADS} the volume of N_2 adsorbed at STP and c a constant that is related exponentially to the heat of adsorption of N_2 on the adsorbent:

$$c \approx \exp\left(\frac{\Delta H_{ADS} - \Delta H_V}{RT}\right) \quad (\text{E. 5.2})$$

where ΔH_{ADS} is the adsorption enthalpy of N_2 on the soot surface and ΔH_V the condensation enthalpy of N_2 at 77 K.

The BET plot obtained for ‘black’ decane soot is displayed in Figure 5.1.2.

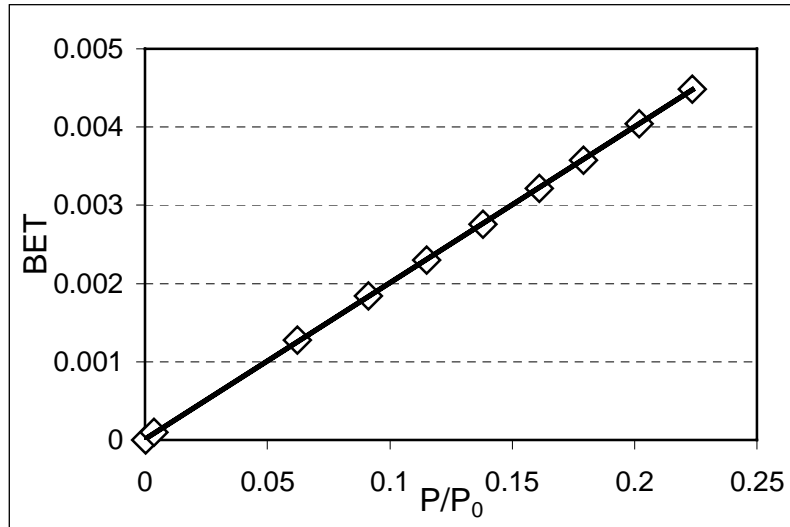


Figure 5.1.2: BET-plot of the adsorption isotherm displayed in Figure 5.1.

Figure 5.1.1 reveals that the adsorption and the desorption isotherm are not identical at higher pressures of N_2 . This adsorption/desorption hysteresis is generally associated with capillary condensation of the adsorbate in mesopores (\varnothing 2-50 nm). Dollimore and Heal [1973] described this phenomenon based on the Kelvin effect and developed a method in order to calculate the size distribution and the related surface of the mesopores. The results of

the BET plots and of the Dollimore-Heal calculations are summarized in **Table 5.1.1** for all three types of soot.

type of soot	surf. area [m ² g ⁻¹]	surf. area m. p. ^A [m ² g ⁻¹]	pressure range ^B (P/P ₀)	Δ _{ADS} H ^C [kJ/mole]
"grey" decane	69	69	0.0284-0.300	8.3
"black" decane	218	174	0.0001-0.22	10.1
acetylene	72	67	0.0258-0.297	8.9
n-hexane ^D	46	-	-	-
kerosene ^D	91	-	-	-
n-hexane ^E	89	-	-	-
carb. black ^F	-	-	-	11.3-11.7
graph. carb. black ^F	-	-	-	12.7

Table 5.1.1: Results of the interpretation of the adsorption/desorption isotherms according to Brunauer, Emmet and Teller (BET) and Dollimore & Heal.

A) Values in this column represent the surface areas of the mesopores calculated according to Dollimore&Heal.

B) This column contains the pressure range over which the BET-plot has been performed.

C) Δ_{ADS}H was calculated according to (E. 5.2) with a heat of condensation for N₂ (Δ_vH) of 5.577 kJ/mole.

D) Choi and Leu [1998].

E) Akhter et al. [1985].

F) Reference data from Parfitt and Sing [1976] for 'carbon black' and 'graphitized carbon black'.

A comparison of 'grey' decane with acetylene soot shows that both types of soot have a BET surface area of roughly 70 m²/g. In addition, in both cases the total BET surface area can be attributed almost entirely to the presence of mesopores. Finally, a comparison with soot generated in other studies shows that the BET surface areas of 'grey' decane and acetylene soot are in the same range.

'Black' decane soot on the other hand is different with respect to several parameters. First, the BET surface area is higher by a factor of about 3 compared to 'grey' decane and acetylene soot. Second, only about 80% of the total BET surface can be attributed to the presence of mesopores. This indicates a significant contribution of micropores (Ø < 2 nm) to the total surface area. The presence of micropores is also indicated by a weak concave curvature of the BET plot at higher pressures. This is the reason why the upper limit of P has been chosen lower for 'black' decane soot in order to draw the BET plot.

The heats of adsorption (ΔH_{ADS}) of all three types of soot are quite similar and slightly lower than the values indicated by Sing and Parfitt [1976]. However, it must be mentioned

that this parameter is – above all for ‘black’ decane soot - very sensitive to the fitting range that has been used in order to obtain the BET plot. The values may therefore only serve as a rough estimation of a mean heat of adsorption for N₂.

As a final remark we want to remind of the fact that BET surface area measurements are based on a theoretical concept containing many assumptions and approximations. A huge number of publications is available explaining difficulties and proposing different interpretations of surface area measurements. Therefore, the results presented in this Section must not be taken as an absolute number of high accuracy but rather as a value of relative nature indicating trends and differences between the different types of soot.

5.2 Elemental analysis.

The principle of the elemental analysis consists of the transformation of an unknown sample into products of a known composition. These products are then quantitatively measured which allows the calculation of the composition of the original sample. The process that is used to form products of a known composition is the complete oxidation (combustion) of the sample in a pure oxygen atmosphere at 925°C. The elements C, H, N and O are transformed under appropriate conditions quantitatively into CO₂, H₂O and NO_x. These products are subsequently separated in a chromatography column and quantitatively measured by a thermal conductivity detector (TCD). The NO_x is quantitatively reduced to N₂ in a copper column prior to detection by the TCD. In this way it is possible to directly determine the mole or weight fractions of the elements C, H and N. Oxygen on the other hand can only be quantified indirectly as the combustion takes place in an environment containing an excess of oxygen. Therefore that mole or weight fraction is attributed to oxygen that is needed to complete the mass balance. This is only valid if other elements such as S or P are present in negligible amounts.

In the present work a PE 2400 CHN Analyser (Perkin-Elmer) has been used for elemental analysis. Each sample of approximately 2 mg has been freshly prepared immediately before the analysis. As the examined samples were produced using decane and acetylene of reagent grade quality we assumed that elements other than C, H, N and O were only present in traces. The content of oxygen can therefore be calculated using the method cited above.

Table 5.2.1 gives a survey of the results of the elemental analysis. The mean values of each type of soot are based at least on three different soot samples. In addition to the standard types of ‘grey’ and ‘black’ decane and acetylene soot another type denominated acetylene_{LEAN}

has been examined. Whereas the standard acetylene flame was fed with a gas flow of 135 ml/min, the one leading to acetylene_{LEAN} soot was fed with only half the fuel flow, i.e. 67.5 ml/min.

type of soot	C [%weight]		H [%weight]		N [%weight]		O [%weight]	
	mean	σ	mean	σ	mean	σ	mean	σ
acetylene _{LEAN}	98.26	0.08	0.15	0.02	0.16	0.08	1.41	0.02
acetylene	98.57	0.27	0.20	0.01	0.33	0.11	0.90	0.26
"black" decane	96.39	0.22	0.19	0.01	0.27	0.09	3.22	0.25
"grey" decane	97.27	0.05	0.83	0.04	0.20	0.18	1.65	0.19
n-hexane ^A	85.1-90.5		0.10-0.13		-		7.8-14.3	

Table 5.2.1: Results of the elemental analysis. Uncertainties correspond to one standard deviation.

A) Akhter et al. [1985]. The values correspond to the lower and upper limits.

The table clearly reveals that the composition of the soot for a given fuel depends on the combustion conditions i.e. the fuel/air ratio. As explained in Section 4.1 the fuel/air ratio is lower for 'black' decane compared to 'grey' decane soot. The oxidative conditions in the lean flame of 'black' decane soot are reflected by a higher oxygen content compared to 'grey' decane soot. The same trend may be stated if the oxygen content of 'acetylene_{LEAN}' is compared to that of standard acetylene soot which was generated in a rather rich flame.

The opposite trend is visible if the hydrogen contents are examined. In this case the soot samples from the leaner flames ('black' decane and acetylene_{LEAN}) show lower values in comparison with those from rich flames ('grey' decane' and acetylene). This result is noteworthy because one would assume that the amount of adsorbed water should be higher in the case of the samples generated in a lean flame because its surface should be more polar owing to a higher oxygen content. The fact that 'grey' decane and acetylene soot nevertheless contain more hydrogen than the corresponding samples from a lean flame means therefore that it refers primarily to hydrogen that is contained in organic compounds as opposed to adsorbed H₂O.

Akhter et al. [1985] produced soot from n-hexane by igniting the vapors of some milliliters of fuel that have been poured into a beaker. A comparison of their results with those from the present work reveals two facts: First) the oxygen content of the soot samples produced by Akhter et al. have much higher oxygen contents than those found in the present work, and Second) the method of soot production used in the present work seems to be much more reproducible than that by Akhter et al.

Figure 5.2.1 shows that the results of the presented elemental analysis are not only precise but also accurate. Control measurements of acetanilide have regularly been performed in between the analysis of the soot samples. It may be seen that the measured elemental composition corresponds to the real values.

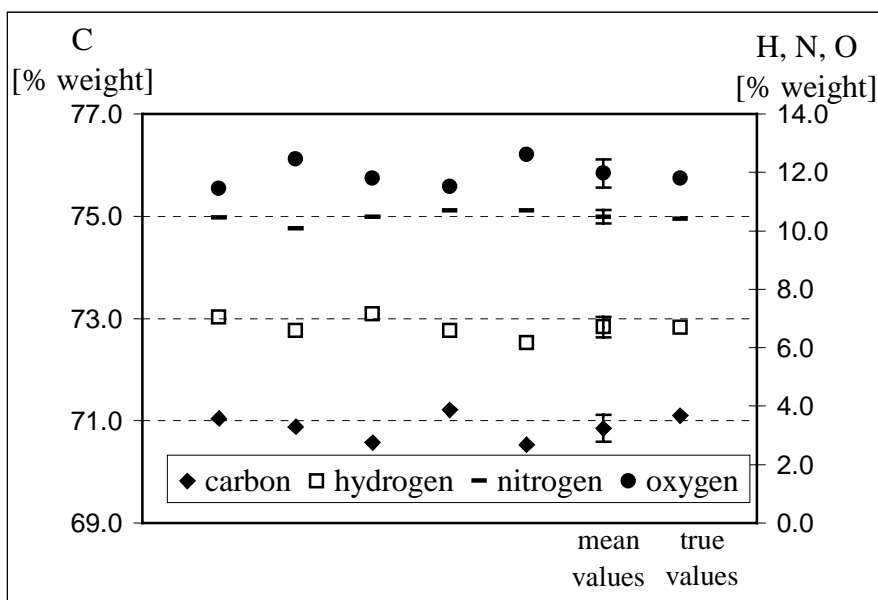


Figure 5.2.1: Control measurements of acetanilide samples performed between the measurements of the soot samples. The second last column contains the mean values with error bars corresponding to two standard deviations. The last column contains the true values.

6 Interaction of NO₂, NO and HONO with soot particles generated in the laboratory.

6.1 The reproducibility of the generation of soot samples.

The device used in the first instance to produce soot samples from liquid fuels consisted of a simple oil lamp equipped with a cotton wick for fuel transport. The flame was located within a glass tube which in turn was held by a metal rim on top of the fuel reservoir. The exothermicity of the flame created an up-draft which sucked air through slits cut into the metal rim. Soot production was enabled by blocking some of the air slits in order to obtain a fuel/oxygen ratio which prevented complete combustion of the fuel carbon. However, the air flow could not be controlled in a reproducible manner which resulted in a highly unstable flame. Turbulent conditions in the flame zone resulted in a flickering flame whose height, emission and rate of soot production changed permanently. Figure 6.1.1 reveals that these unstable conditions affected the reproducibility of the soot samples as studied by the kinetics of NO₂ uptake.

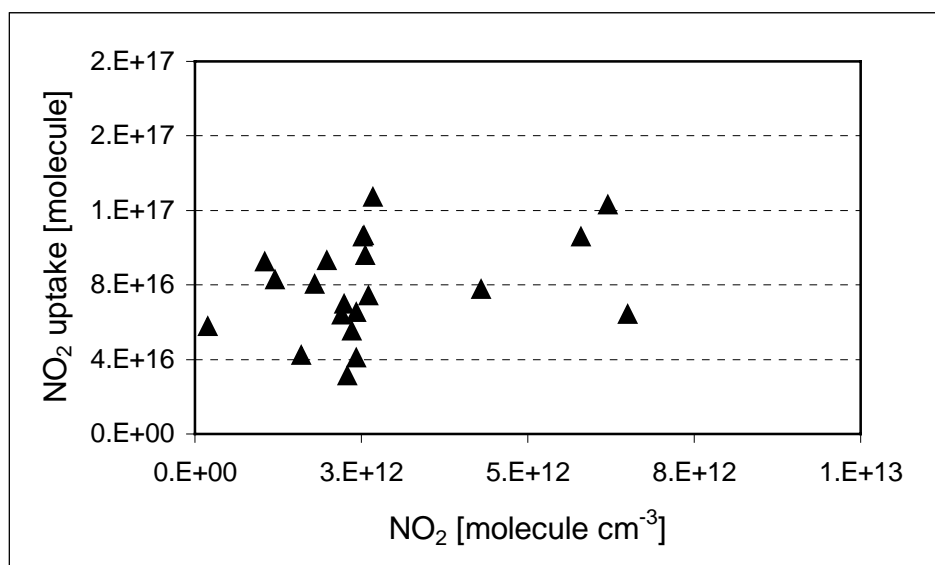


Figure 6.1.1: Uptake of NO₂ on decane soot as a function of the NO₂ concentration. Soot samples were produced using a simple oil lamp; 4 mm diameter escape orifice, integrated over 100 seconds, mean sample weight was 17.3 mg.

The NO₂ uptake clearly varied by more than a factor of three for steady state concentrations that were almost identical. A concentration dependence of the NO₂ rate of uptake could not be stated under those conditions. These results were of course highly

disappointing but at the same time they conveyed the message that the reactivity of flame soot depends very much on the conditions of its production.

As a consequence we devoted some effort into the development of a device which allows the production of flame soot under more controlled conditions. The design has been presented in Section 4.1. The main advantage of the new device is that the air flow which feeds the flame can be controlled. Figure 6.1.2 shows results that correspond to those displayed in Figure 6.1.1 with the only difference being that the soot samples were produced using the new co-flow device.

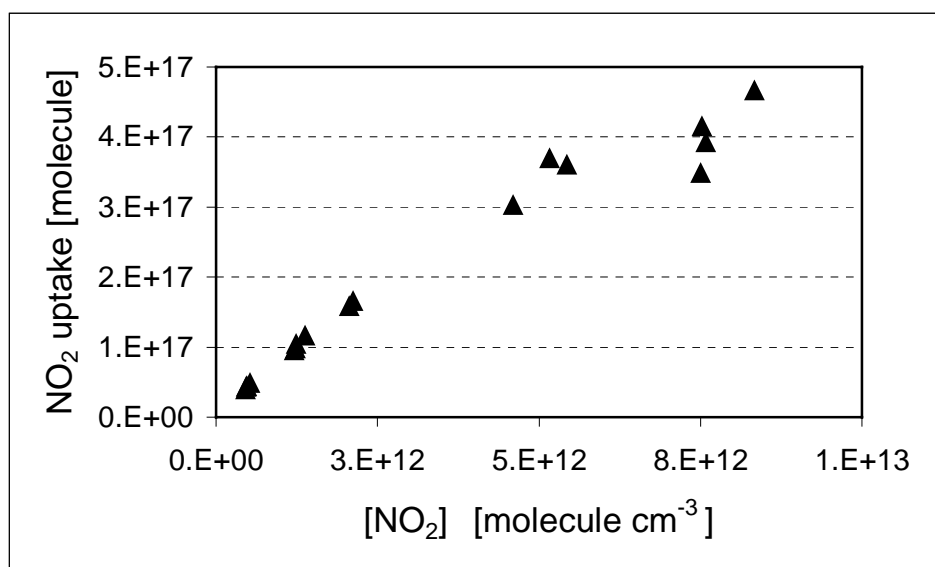


Figure 6.1.2: Uptake of NO₂ on decane soot as a function of the NO₂ steady state concentration. Soot samples were produced using the new co-flow device; 4 mm diameter escape orifice, integrated over 100 seconds, mean sample weight was 16.4 mg.

A comparison of Figures 6.1.1 and 6.1.2 demonstrates the improved reproducibility of the soot samples as far as the rate of NO₂ uptake is concerned. In contrast to the results of Figure 6.1.1 a distinct concentration dependence may now be recognized in Figure 6.1.2.

Thus, the co-flow system allowed us to produce soot samples in a reproducible manner at different fuel/air ratios and to examine the influence of the combustion conditions on its reactivity towards gas phase molecules such as NO₂, HONO and NO.

6.2 Interaction of NO₂ and HONO with decane soot from a rich flame ('grey' decane soot).

6.2.1 Products and mechanism of NO₂ interacting with decane soot from a rich flame.

The interaction of NO₂ and decane soot originating from a rich flame has been examined in a series of steady-state experiments by exposing each time approximately 16.4 ± 1.5 mg of freshly prepared soot to a continuous flow of NO₂. A detailed description of the production of 'grey' decane soot can be found in Section 4.1. By performing measurements using two different escape orifices (14 and 4 mm) a concentration range of more than a factor of 100 has been covered. Figure 6.2.1 shows the results of a typical uptake experiment.

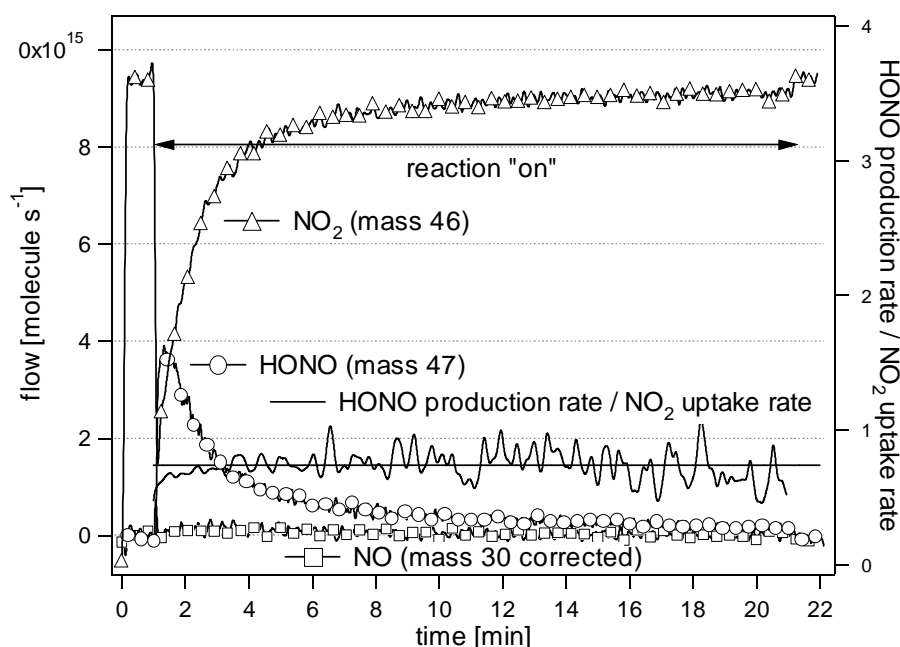


Figure 6.2.1: Uptake experiment of NO₂ on 'grey' decane soot; sample mass = 16.3 mg, 4 mm diameter escape orifice, NO₂ concentration = 8.3×10^{12} molecule cm⁻³.

The soot sample is exposed to the NO₂ flow at $t = 1$ min: A large and instantaneous rate of uptake is observed. However, saturation of the soot sample is occurring quickly so that after 3 minutes of interaction the effusing NO₂ flow attains already 85% of the initial value. At the same time it must be stressed that even after 20 minutes of exposure corresponding to an integrated flux to the geometric sample surface of 5.6×10^{17} molecule cm⁻² of NO₂ complete saturation of the sample does not occur. This may be seen from the fact that the NO₂ signal increases again after the closing of the sample chamber at $t = 21$ min. Simultaneously to the uptake of NO₂ a large product peak of HONO is appearing which shows that the conversion of NO₂ into HONO is a fast process. The fast decrease of the NO₂ uptake correlates with the

rate of HONO formation which is still observable even after 20 minutes of exposure. A look at the signal of NO at m/e 30 after correction reveals that no measurable amounts of NO are produced.

Figure 6.2.2 summarizes the observed HONO yields defined as the ratio of the amount of HONO released to the amount of NO₂ taken up during the same time span as a function of the concentration of NO₂.

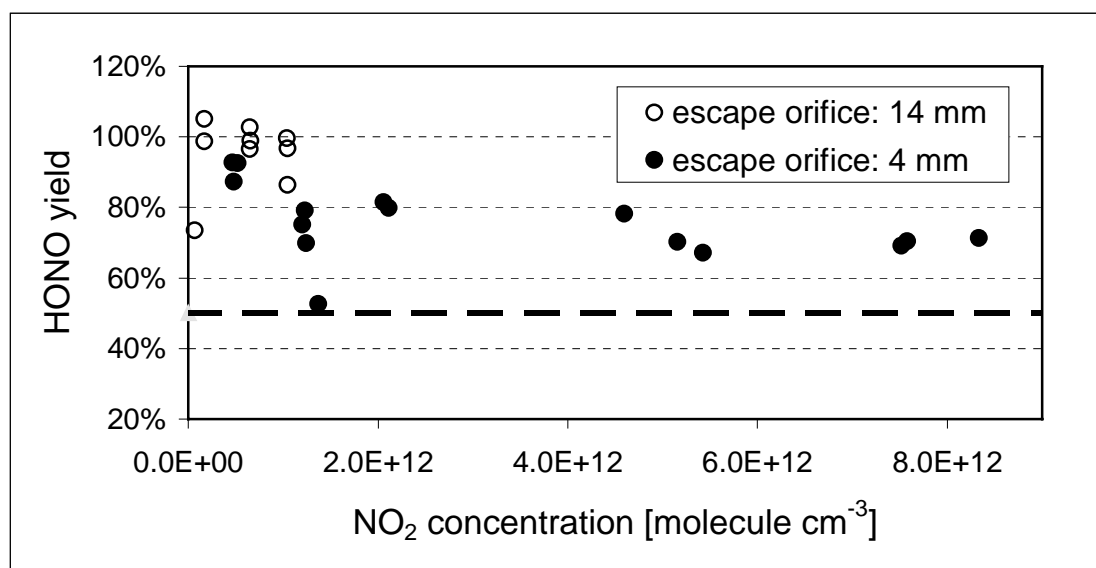
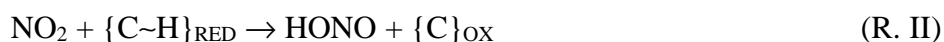


Figure 6.2.2: HONO yield relative to NO₂ taken up on ‘grey’ decane soot as a function of the NO₂ concentration; yields are calculated for the first 20 minutes of interaction, mean sample mass = 16.4 ± 1.5 mg. The dashed line indicates the maximum HONO yield for the disproportionation process, reaction (R. I).

A HONO yield of up to 100% is attained at low concentrations of NO₂ and decreases to approximately 60% at high concentrations. However, HONO yields in excess of 50% unambiguously exclude the classical surface catalyzed disproportionation as the dominating process for HONO generation according to reaction (R. I).



Instead, we propose a redox-mechanism where reducing surface sites of soot convert NO₂ into HONO:



{C~H}_{RED} represents a surface site that is reducing NO₂ to HONO, and which shall remain unspecified as to the nature of the hydrogen for the time being. The species listed in curved brackets refer to surface adsorbates.

HONO could also be observed in other studies where freshly prepared soot was exposed to NO₂. Gerecke et al. [1998] and Kleffmann et al. [1999] always observed both products that is HONO as well as NO. Ammann et al. [1998], Kalberer et al. [1999] and Longfellow et al. [1999] on the other hand only observed HONO as a product in significant amounts, however the HONO yields relative to NO₂ taken up were all clearly below 100%. ‘Grey’ decane soot generated in the present work has the property that it is able to quantitatively convert NO₂ into HONO. The relative HONO yields are 100% for NO₂ concentrations up to 6.5×10^{11} molecule cm⁻³ corresponding to a partial pressure of 26 ppb. The relative yields start to decrease at concentrations in excess of 6.5×10^{11} molecule cm⁻³ but still amount to approximately 60% at a concentration of 8.3×10^{12} molecule cm⁻³ which corresponds to a partial pressure of 338 ppb. This latter value corresponds to the upper limit of the concentration range of NO₂ covered by the experiments.

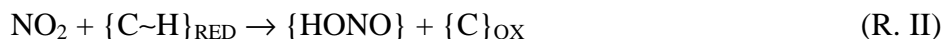
Chughtai et al. [1994] also examined laboratory-generated soot but contrary to the studies cited above they dried their n-hexane soot samples over night at 120 °C before exposing them to NO₂ concentrations of 9-35 ppm. As a consequence they did not observe HONO but products such as CO₂, CO, N₂O and NO when this soot interacted with NO₂ at ambient temperature. The heat treatment may have led to desorption losses of volatile organic compounds and/or H₂O. Even an oxidation of reactive surface sites at higher temperatures cannot be excluded in order to explain the missing HONO formation.

Results of studies with commercial soot are inconclusive. NO as the only gas phase product upon interaction with NO₂ has been observed for soot types such as Printex 60 or Flame Soot 101 in Knudsen cell studies [Tabor et al., 1994; Rogaski et al, 1997] whereas Kleffmann et al. [1999] also insisted on the formation of HONO. It seems that both the total as well as the partial pressure of water will have an influence on the rate of product formation. Unanimity reigns on the other hand in the case of FW2 (Degussa). For this type of soot which undergoes an oxidative after-treatment by the manufacturer NO was the only product observed in every study. The fact that NO which represents a more reduced species than HONO is formed incidentally on FW2 whose surface is oxidized is quite surprising.

6.2.2 Interaction of HONO with decane soot from a rich flame (‘grey’ decane soot).

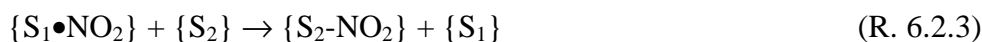
As mentioned above HONO yields are significantly below 100% at high concentrations of NO₂ as may be seen in Figure 6.2.2. This may be due to the fact that NO₂ is either going to be adsorbed in a second pathway not leading to HONO formation or to

increasing adsorption and/or decomposition of HONO at higher concentrations of NO₂. In order to distinguish between these two possibilities a series of uptake experiments of pure HONO on soot has been performed with HONO concentrations ranging from 1.4×10^{11} up to 4.3×10^{13} molecule cm⁻³. No significant uptake has ever been observed. Therefore, a non-reactive adsorption pathway for NO₂ must be responsible for the decrease of the HONO yields at higher NO₂ fluxes. Thus, reaction (R. II) must be in competition with a reaction describing the irreversible uptake of NO₂, reaction (R. III):



At high concentrations of NO₂ the uptake rate of reaction (R. II) is saturating so that reaction pathway (R. III) becomes significant. In the present study we did not have the technical means to measure NO₂ remaining on the soot surface. However, such experiments have been performed by Chughtai et al. [1994] using FTIR who detected the appearance of surface functionalities such as -NO₂, -ONO and -N-NO₂ upon interaction with NO₂. Kleffmann et al. [1999] detected nitrogen-containing surface anions such as NO₂⁻ and NO₃⁻ by ion chromatography after extraction. They observed that the yield of NO₃⁻ significantly increased with increasing NO₂ consumption.

A closer analysis of the experimental traces in Figure 6.2.1 allows an even more detailed description of the uptake mechanism: the solid line represents the ratio of the rates of HONO release to NO₂ uptake during the experiment. As can be clearly seen this ratio has a constant value of 0.74 over the whole time scale except for the very first few seconds. This initial delay of the HONO flow was much smaller in experiments that were performed in a freshly cleaned reactor. We therefore regard it as an artifact caused by interaction of HONO with the walls of the reactor and not as a characteristic property of the NO₂/soot interaction. The missing fraction of 26% corresponds to NO₂ that is irreversibly adsorbed according to reaction (R. III). This leads us to conclude that the branching ratio (R. II)/(R. III) is independent of time although both rates are varying by a factor of 25 during the uptake experiment. This statement is valid for all the measurements represented in Figure 6.2.2 which means that the values indicated represent not only mean ratios of the relative yields but values that are valid at every instant during the course of a standard uptake experiment. The conclusion is that both processes (R. II and R. III) must have a common rate limiting step involving a common adsorption site. After passing through this gateway NO₂ has a choice of either forming HONO or adsorbing irreversibly. Thus reactions (R. II) and (R. III) may be further specified in equations (R. 6.2.1) to (R. 6.2.3):



The interaction of NO₂ with the adsorption site {S₁} leading to {S₁•NO₂} is probably weak which means more probably owing to physisorption than to chemisorption, otherwise NO₂ would not be sufficiently mobile to subsequently encounter other surface sites such as {C~H}_{RED} and {S₂}. An initial physisorption or ‘reversible adsorption’ of NO₂ has also been postulated by other groups such as Tabor et al. [1994], Kalberer et al. [1999] or Kleffmann et al. [1999] in order to explain the kinetics of the NO₂/soot interaction.

According to reactions (R. 6.2.2) and (R. 6.2.3) the surface sites {C~H}_{RED} and {S₂} are consumed and soot therefore does not act as a catalyst as proposed by Longfellow et al. [1999]. However, the fast decrease of the HONO formation rate during our experiments as displayed in Figure 6.2.1 must be primarily due to a temporary depletion of the surface adsorption site {S₁} and not of the reducing site {C~H}_{RED} otherwise the branching ratio (R. 6.2.2)/(R. 6.2.3) would most probably change during the course of an experiment.

6.2.3 Quantitative aspects of the NO₂ uptake and product formation on ‘grey’ decane soot.

The mean sample weight of soot in the standard uptake experiments of NO₂ described in Section 6.2.1. was 16.4 ± 1.5 mg. The interaction of bulk soot samples with NO₂ is limited to the upper layers at the beginning of the uptake experiment. In order to estimate the depth of the interaction as a function of time, a series of experiments as a function of the mass of soot has been performed. Figure 6.2.3 shows that for sample masses of approximately up to 17 mg both the amount of NO₂ taken up as well as the amount of HONO produced are linearly increasing over the time scale of 20 minutes. As we routinely use soot masses lower than 17 mg we may assume that NO₂ has probed the whole soot sample at the end of standard experiments. If, on the other hand, only the first 100 seconds of interaction are considered the HONO yield becomes independent of mass at approximately 10-12 mg indicating that deeper soot layers have not yet been probed in this time period.

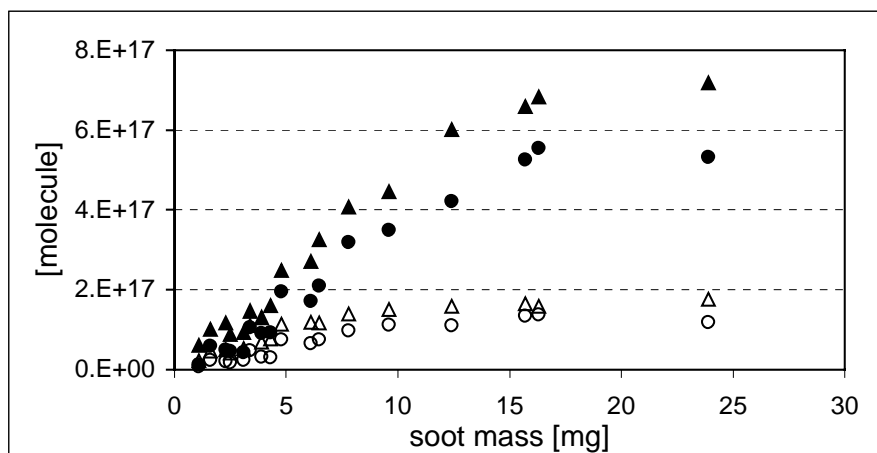


Figure 6.2.3: Mass dependence of NO₂ uptake (triangles) and formation of HONO (circles) on 'grey' decane soot; yields are integrated over 100 seconds (open symbols) and 20 minutes (filled symbols), respectively at 4 mm diameter escape orifice and at a mean concentration of 2.2×10^{12} molecule cm⁻³ corresponding to a partial pressure of 90 ppb.

This result allows us to express the NO₂ uptake and the HONO formation on a per mass basis as displayed in Figure 6.2.4. Both the amount of NO₂ taken up as well as the HONO yield are progressively saturating with increasing concentration of NO₂. We attribute this to the limiting uptake rate of the initial adsorption step, reaction (R. 6.2.1). The maximum amount of released HONO of approximately 4×10^{16} molecule mg⁻¹ is of the same order as in other studies where the samples have been presented in bulk form [Gerecke et al., 1998, Kleffmann, 1999] but approximately 25 times lower than the value given by Kalberer et al. [1999] who presented the soot as an aerosol. Kalberer et al. speculated whether the limitation in water vapor is reducing the rate of HONO formation in experiments that are performed in low-pressure reactors. However, this reasoning is defeated by the fact that Kleffmann et al. observed quantities of HONO that are similar to those in the present work at relative humidities of up to 80%. In addition, it must be mentioned that Kalberer et al. did not directly measure the mass of soot they introduced into the flow reactor. They used a differential mobility analyzer and a condensation nuclei counter in order to determine the total surface and volume of the soot aerosols. These results were then transformed into a total mass by assuming a mean density of soot of 0.5 g cm^{-3} . This indirect determination of the soot mass may in fact lead to an underestimation of the soot mass and thus to an overestimation of the mass specific reactivity concerning HONO formation. If such an overestimation can be excluded on experimental grounds one may ask whether or not the sample presentation such as suspended aerosols vs. bulk phase may be responsible for the observed differences or whether the soot that has been produced by Kalberer et al. may have been unusually reactive.

Finally, it must be stated that the HONO production potential of 'grey' decane soot is rather underestimated by the values given in Figure 6.2.4 because it has been shown in **Figure**

6.2.1 that the samples are generally not completely exhausted after 20 minutes. The long term behavior of soot samples concerning saturation will be discussed in Section 6.5.

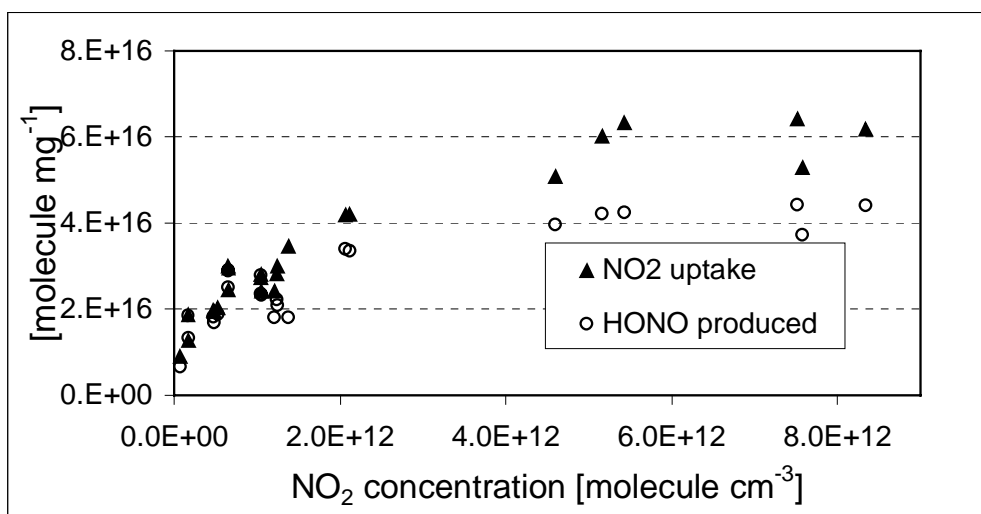


Figure 6.2.4: Mass specific NO₂ uptake and HONO formation on 'grey' decane soot as a function of the NO₂ concentration; 14 and 4 mm diameter escape orifice, integrated over 20 minutes.

6.3 Interaction of NO₂ and HONO with decane soot from a lean flame ('black' decane soot')

6.3.1 Products of NO₂ interaction with decane soot from a lean flame ('black' decane soot).

A series of experiments with 'black' decane soot has been performed akin to the measurements with 'grey' decane soot discussed in Section 6.2.1. Figure 6.3.1 shows raw data of an uptake experiment of NO₂.

Again, an instantaneous large uptake of NO₂ with a fast consecutive saturation of the soot sample may be observed. HONO formation is observable only during the initial 4 minutes of the uptake and consists of a very small MS signal. On the other hand, the NO signal is observed to rise slowly at the beginning to reach a constant value.

Figure 6.3.2 shows the yields of NO formation relative to the NO₂ uptake as a function of the NO₂ concentration with the sample surface. It clearly is approaching 50 % at high NO₂ concentrations and suggests a disproportionation process somewhere in the mechanism. We assume that for each molecule NO formed a corresponding fragment of higher oxidation state remains on the soot surface. It may clearly be seen that, especially at low NO₂ concentrations, the mass balance is not closed. Based on the NO yields presented in Figure 6.3.2 we postulate another reaction pathway for irreversible adsorption of NO₂ which corresponds to reaction (R. 6.2.3) observed for the interaction of NO₂ on 'grey' decane soot. Contrary to 'grey' decane

soot the importance of reaction (R. 6.2.3) is decreasing with increasing NO₂ concentration as indicated by the dashed line in Figure 6.3.2.

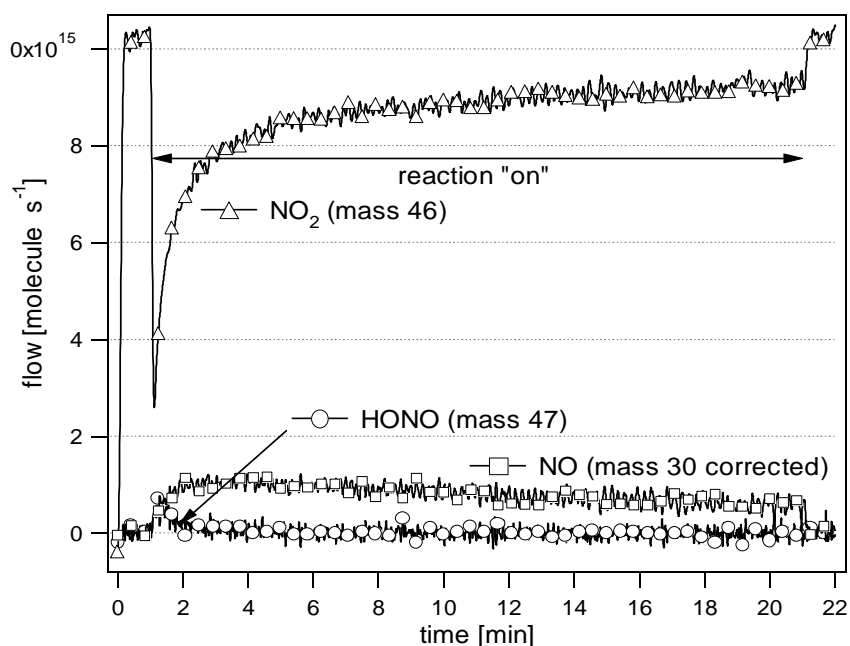


Figure 6.3.1: Uptake experiment of NO₂ on 'black' decane soot; sample mass = 15.8 mg, 4 mm diameter escape orifice, NO₂ concentration = 9.1×10^{12} molecule cm⁻³.

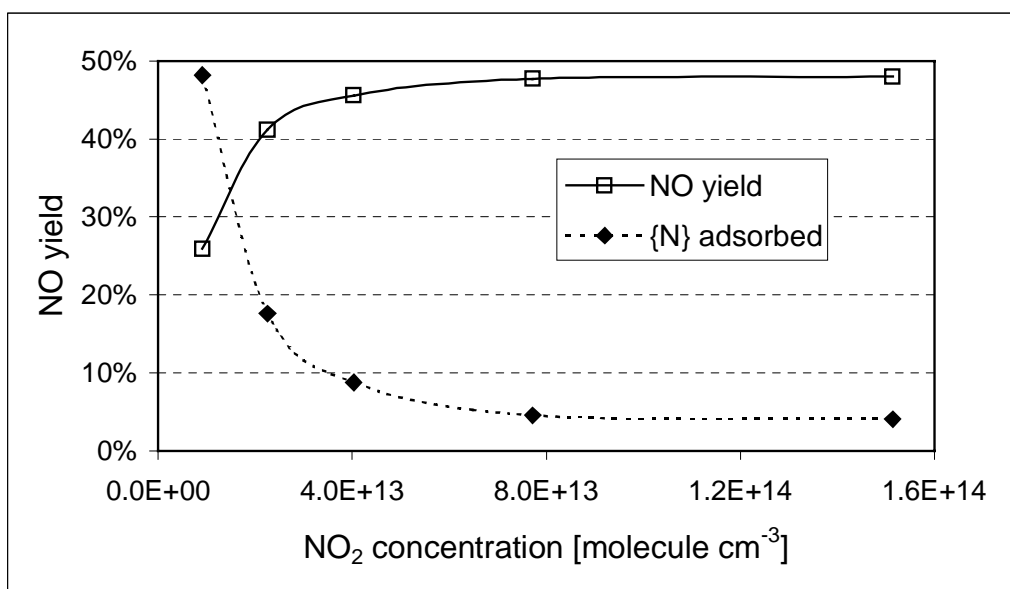


Figure 6.3.2: Relative yields of NO (open squares) and {N} that is adsorbed on 'black' decane soot either as NO₂ or HONO (filled diamonds) as a function of the NO₂ concentration; 1mm diameter escape orifice, integrated over 20 minutes, mean sample weight = 18.0 ± 1.0 mg.

Data in Figure 6.3.3 yield further insight into the interaction of NO₂ with 'black' decane soot: NO₂ uptake and production of NO are continuously increasing up to a mass of 12 mg, whereas HONO formation is low and varying randomly. Apparently only HONO formed in the uppermost soot layers is observed whereas HONO formed in deeper layers is either adsorbed or decomposes to NO.

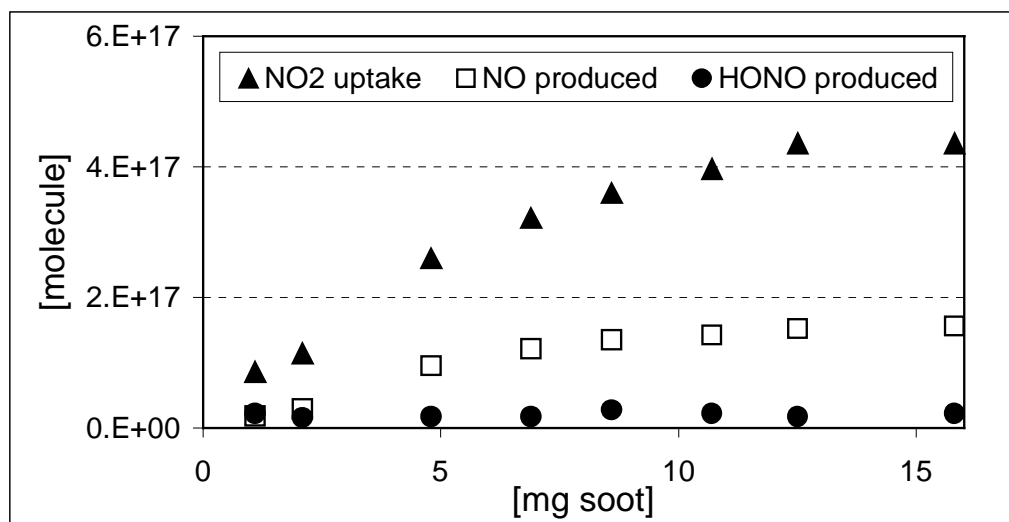


Figure 6.3.3: Mass dependence of NO₂ uptake, formation of NO and HONO on 'black' decane soot: 4 mm diameter escape orifice, mean NO₂ concentration = 2.2×10^{12} molecule cm⁻³, integrated over 20 minutes.

6.3.2 Interaction of HONO with decane soot from a lean flame ('black' decane soot).

We speculated in Section 6.3.1 that HONO produced on 'black' decane soot may irreversibly adsorb on its surface or decompose to NO. In order to decide which of these two processes takes place, 'black' decane soot has been exposed to a flow of pure HONO in a series of experiments using reactors with 14, 4 and 1 mm escape orifice. Figure 6.3.4 shows raw data of a typical uptake experiment performed at a high concentration of HONO in the 1 mm escape orifice reactor. The uptake of HONO is instantaneous and, in contrast to the interaction of NO₂ on 'black' decane soot, no saturation of the uptake is occurring over the time scale observed. The NO flow slowly rises on the time scale of 2 min. and reaches a steady-state that is stable during the whole uptake experiment. Thus, the NO formation shows the same kinetic characteristics as for the interaction of NO₂ on 'black' decane soot displayed in Figure 6.3.1. Moreover, a small but steadily increasing signal of NO₂ is observed starting at $t \approx 1.5$ min. The fact that the NO₂ signal is disappearing after the closure of the sample chamber at $t = 5.5$ min clearly shows that it is formed on the soot and not by secondary reactions of HONO on the KNO₂ surface.

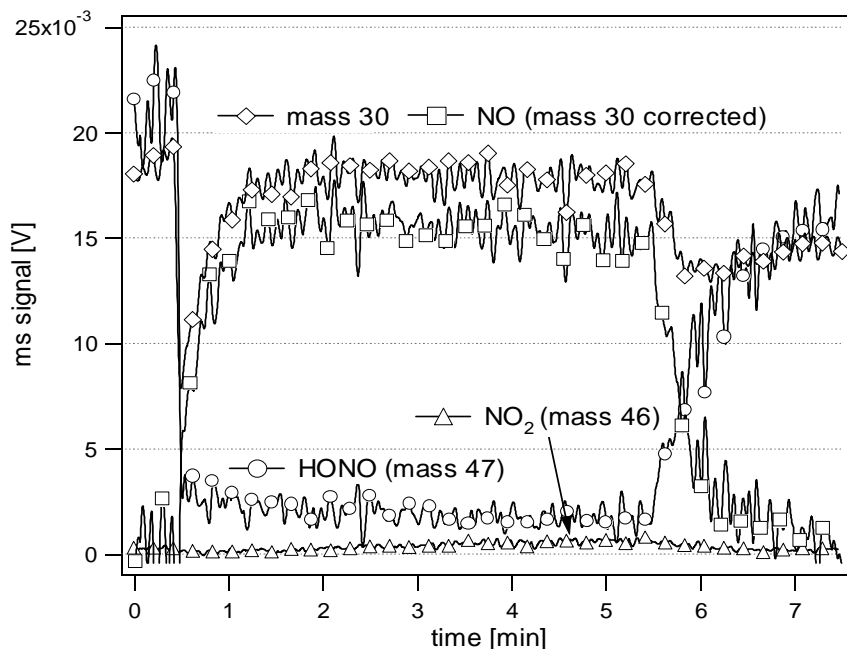
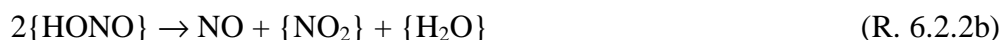


Figure 6.3.4: Raw data of an uptake experiment of HONO on 'black' decane soot; sample mass 10.9 mg, 1 mm diameter escape orifice, initial HONO concentration = 3.7×10^{13} molecule cm^{-3} .

The series of experiments revealed a total product yield of 50% whereof 40% NO and 10% NO₂ for a HONO concentration of approximately 3.3×10^{11} up to the maximum concentration of 3.7×10^{13} molecule cm^{-3} . Total product yields below 50% have only been observed at concentrations below 3.3×10^{11} molecule cm^{-3} . The missing balance of nitrogen probably represents a reservoir of HONO which is temporarily adsorbed on the soot surface.

The results of the HONO/soot experiments suggest, together with the conclusions from Section 6.3.1, that NO₂ interacts with 'black' decane soot resulting in the formation of HONO, which to a large extent is decomposed by disproportionation into NO and a fragment that is remaining on the soot surface.

It has been confirmed by ancillary experiments that NO does not interact with soot, neither with a fresh sample nor with a sample that previously has been exposed to NO₂. Thus, NO is desorbing instantaneously and represents a tracer for the disproportionation process and the reservoir of {HONO} that is temporarily adsorbed on the soot surface. We assume that HONO is produced in a first step by the same process as resulting from the interaction of NO₂ with 'grey' decane soot so that we may add reaction (R. 6.2.2b) in order to define the reaction mechanism describing the interaction of NO₂ with 'black' decane soot.



'Black' decane soot may therefore be regarded as a variant of 'grey' decane soot on which HONO undergoes fast decomposition to NO and a N(IV) species that may either

remain on the soot surface or undergo an additional reaction according to reaction (R. 6.2.1). As we may see in Figure 6.3.4, part of this N(IV) species is observable as NO₂ only at longer times of exposure to HONO.

6.3.3 Quantitative aspects of the NO₂ uptake and product formation on ‘black’ decane soot.

The mean sample weight of soot in the standard experiments was 18.0 ± 1.0 mg, but its exposure to NO₂ is limited to the upper layers of the bulk sample at the beginning, as discussed above. In order to estimate the probe depth as function of time another look at Figure 6.3.3 reveals that the rate of NO₂ uptake and NO formation are not increasing for masses exceeding 12 mg. We conclude that only the upper 12 mg of the soot sample are probed by NO₂ during the first 20 minutes of interaction. Thus, we divide by 12 the amount of NO₂ taken up and the product formed, in order to present the results on a per mg basis shown in Figure 6.3.5. Within the experimental uncertainty both the NO₂ uptake and NO formation are linearly increasing over the whole concentration range examined: even at high concentrations NO₂ is converted into NO without apparent saturation of the reaction rate as displayed in Figure 6.3.5. (as opposed to ‘grey’ decane soot whose results are displayed in Figure 6.2.4). As mentioned above (Section 6.3.2) this is probably due to the fact that at high concentrations the NO₂ flux is directed almost exclusively into the disproportionation branch (R. 6.2.2.b) for which we did not observe saturation of its rate (see Figure 6.3.4).

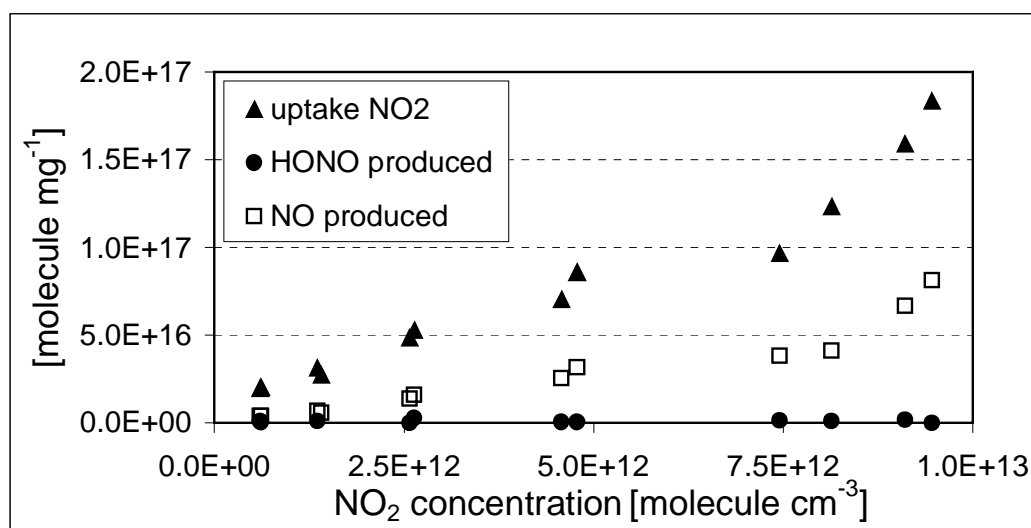


Figure 6.3.5: Mass specific NO₂ uptake, formation of NO and HONO on ‘black’ decane soot as a function of the NO₂ concentration at 4 mm diameter escape orifice integrated over 20 minutes.

6.4 ‘Grey’ vs. ‘black’ decane soot. – What are the differences?

It has clearly been demonstrated in Sections 6.2 and 6.3 that the different combustion conditions during the production of ‘grey’ and ‘black’ decane soot strongly influence their reactivity towards NO₂. We therefore want to summarize the observed differences and try to explain them with our knowledge on the properties of the two types of soot.

HONO is produced by both types of soot according to our reaction scheme. Whereas HONO is quantitatively released according to (R. 6.2.2a) by ‘grey’ decane soot, it is to a large extent decomposed according to (R. 6.2.2b) on ‘black’ decane soot. (R. 6.2.2a) and (R. 6.2.2b) are in competition on both ‘black’ as well as ‘grey’ decane soot. The principal difference between the two types is that for ‘black’ decane soot $k_{6.2.2b}\{\text{HONO}\} \gg k_{6.2.2a}$ whereas the opposite is true for ‘grey’ decane soot.

One reason for the different ratios $k_{6.2.2b}\{\text{HONO}\}/k_{6.2.2a}$ of ‘grey’ and ‘black’ decane soot may be due to the fact that the surface of ‘black’ decane soot is more polar. The results of the elemental analysis showed that the mass fraction of oxygen is approximately two times higher for ‘black’ decane soot compared to ‘grey’ decane soot (see Table 5.2.1). The real difference of the surface polarity is most probably even higher because the results of the elemental analysis represent mean values of the bulk samples whereas oxidation of the soot particles in the diffusion flame predominantly takes places on the surface of the particles.

Another aspect is the fact that the two types of soot encounter different amounts of NO₂ during sample collection. One can infer from Table 4.1 that the sampling time for a mean soot mass of 15 mg roughly amounts to 5 minutes for ‘grey’ and 15 minutes for ‘black’ decane soot. During this time the sample is exposed to an air flow containing approximately 5 ppm of NO₂ for both ‘grey’ as well as ‘black’ decane soot. By multiplication of the used air flow (1.3 l/min for ‘grey’ decane soot and 1.4 l/min for ‘black’ decane soot) with the sampling time and the NO₂ concentration one can estimate the maximum amount of NO₂ which has collided with the soot during the sample preparation. This calculation indicates only an upper limit as the flux of NO₂ to the sample surface is limited by diffusion. The results are approximately 8×10^{17} and 2.6×10^{18} NO₂ molecules for ‘grey’ and ‘black’ decane soot, respectively. However, the fact that ‘black’ decane soot encounters approximately three times more NO₂ than ‘grey’ decane soot during the time of sample preparation can hardly explain the dramatic differences in reactivity that are observed in the uptake experiments.

On the other hand, these amounts of NO₂ can be compared to those that a sample encounters in an uptake experiment in the Knudsen cell. Based on Table 3.1b amounts ranging from 1.4×10^{19} (14 mm diameter escape orifice at minimum collision rate) to 1.9×10^{21} molecules (4 mm diameter escape orifice at maximum collision rate) are calculated for the

standard interaction time of 20 minutes. The ‘worst case scenario’ occurs for a ‘black’ decane sample which undergoes uptake in the 14 mm diameter reactor at low collision rate. In this case the maximum NO₂ dose to which the sample is exposed during the time of collection amounts to almost 20% of the amount to which the sample is subsequently exposed in the Knudsen cell. The corresponding ratio for a sample of ‘grey’ decane soot is approximately 6%. One could therefore argue that both samples, that is ‘black’ as well as ‘grey’ decane soot, are to a large extent saturated prior to the actual uptake experiment whereas the same effect would not be observed for soot particles that are emitted by the exhaust pipe of a car because in this case the gas plume undergoes fast dilution.

Even if we cannot completely exclude partial saturation of the soot particles during sample preparation we estimate its extent as rather small. The temperatures 1 cm above the flame tip where the samples are collected are several hundred degrees °C. At these temperatures the NO₂/soot interaction seems to be strongly reduced. This is suggested by measurements where the exhaust gases of different vehicles have been analyzed directly at the outlet of the exhaust pipe [Perner,1987]. HONO could only be detected in minor concentrations although both NO₂ as well as soot particles were present in high concentrations. A possible explanation is that the surface residence time of NO₂ on the soot surface is drastically reduced at higher temperatures.

A further difference between ‘grey’ and ‘black’ decane soot is the dependence of the branching ratio (R. 6.2.2)/(R. 6.2.3) on the concentration of NO₂. As shown in Figure 6.3.2 the higher the NO₂ concentration in uptake experiments on “black” decane soot the more the branching ratio between reaction (R. 6.2.2) and (R. 6.2.3) is shifted towards reaction (R. 6.2.2). This may be explained by secondary reactions in which a product of the HONO formation/disproportionation branch, reaction (R. 6.2.2) followed by (R. 6.2.2b), is either masking {S₂} which would lead to a decrease of the rate of reaction (R. 6.2.3) or is interacting with {C-H}_{RED} in order to catalyze reaction (R. 6.2.2). Possible candidates for this interaction are either {HONO} or the products of the disproportionation reaction (R. 6.2.2b) such as {NO₂} and {H₂O}. A comparison with the corresponding branching ratio found on ‘grey’ decane soot reveals that the situation is exactly opposite there: The branching ratio (R. 6.2.2)/(R. 6.2.3) is high at low NO₂ concentration and decreases with increasing concentration, as shown in Figure 6.2.2. The most probable explanation therefore is that the ratio of sites {C-H}_{RED}/{S₂} is much higher in the case of ‘grey’ decane soot compared to ‘black’ decane soot. In addition, there are no products such as {NO₂} or {H₂O} which could interact with the surface sites on ‘grey’ decane soot and which would change the branching ratio as there is no disproportionation (R. 6.2.2b) taking place on ‘grey’ decane soot. Finally, {HONO} cannot build up to a significant reservoir on the surface because it does not adsorb on ‘grey’ decane soot as mentioned in Section 6.2.2.

The different behavior of the branching ratio (R. 6.2.2)/(R. 6.2.3) may also be responsible for the higher turnover rate of ‘black’ decane soot at high NO₂ concentrations. It can be seen in Figure 6.3.5 that on ‘black’ decane soot NO₂ is converted into NO without apparent saturation of the reaction rate even at high concentrations. This is probably due to the fact that at high concentrations the NO₂ flux is directed almost exclusively into the disproportionation branch (R. 6.2.2.b) for which we did not observe saturation effects (see Figure 6.3.4). For ‘grey’ decane soot on the other hand, a clear saturation of the NO₂ uptake rate is discernible (see Figure 6.2.4). The fact that ‘black’ decane soot has a BET surface that is three times higher than that of ‘grey’ decane soot (see Table 5.1.1) may also contribute to the different turn-over rates at high NO₂ concentrations.

A comparison of our reaction mechanism with the one recently proposed by Kleffmann et al. [1999] shows that they are essentially identical. This makes us quite confident in our data, all the more so as the studies have been performed using different techniques. Nevertheless, some minor differences exist: Kleffmann et al. postulate that a reducing agent on the soot surface (‘red. soot’) is converting NO₂ into HONO after which this site is oxidized (‘red. soot’ → ‘ox. soot’). This oxidized site in turn would have the capability to irreversibly adsorb NO₂. If this were true we would expect that the branching ratio between HONO formation and irreversible adsorption of NO₂ would shift with increasing sample exposure towards irreversible adsorption as ‘ox. soot’ is increasing to the same extent as ‘red. soot’ is decreasing. In our case, such a behavior has not been observed in the course of the standard experiments (see Figures 6.2.1). As the next Section will show, the same also is true for soot samples that have been exposed to NO₂ 5 times in succession each time for 20 minutes (see Figures 6.5.3 and 6.5.5). We therefore postulate that irreversible adsorption of NO₂ is taking place on an adsorption site that is independent of the HONO formation (see reaction (R. 6.2.3)).

Kleffmann et al. [1999] observe that HONO yields are increasing with a decrease of the total pressure in the flow reactor. Based on this observation they propose that disproportionation is taking place according to a Langmuir-Rideal mechanism. However, from our point of view a distinction between a Langmuir-Hinshelwood or a Langmuir-Rideal mechanism is – in any reactor – very difficult based on total pressure variation. In our case, HONO would have to survive a large number of collisions within the bulk phase of the sample before it desorbes in order to be detected. This is not probable in view of the strong reactivity of HONO on ‘black’ decane soot. Therefore, the absence of HONO in the gas phase is in our case no evidence for a Langmuir-Hinshelwood process.

The soot samples used in the study of Kleffmann et al. produced always both NO as well as HONO at low pressures whereas in our study ‘grey’ decane soot only produced HONO and ‘black’ decane soot only significant amounts of NO. We therefore assume that the

characteristics of the soot samples used by Kleffmann et al. can be placed somewhere between 'black' and 'grey' decane soot.

That the reactivity of soot particles concerning HONO formation depends on the combustion conditions has also been shown by a study of Arens et al. [1999]. They produced soot aerosols with a diesel engine by operating it under full load and idling conditions. The result was that the HONO formation rate under full load conditions was two times higher than under idling conditions. However, the differences observed in this study were rather small and limited to the kinetics. Conclusions concerning the mechanism or differences in the total HONO yields could not be deduced.

6.5 Multiple exposure experiments.

6.5.1 Multiple exposure of 'grey' decane soot.

We have seen in Figures 6.2.1 and 6.3.1 that the reactivity of both types of decane soot is never completely saturated during a standard experiment which lasts for 20 minutes. Therefore, a series of standard experiments has been performed where the same sample has been consecutively exposed 5 times to a mean NO₂ concentration of 2.5×10^{12} molecule cm⁻³. The samples have been stored in a dark container filled with dry synthetic air for 24 hours both before the first experiment as well as between subsequent uptake experiments. The identical procedure has been adopted for a reference sample, the only difference being that the container was filled with synthetic air at a relative humidity of 100%. After a total interaction time of 100 minutes we obtain yields of NO₂ uptake and HONO production which still correspond to 40 and 50% of the initial values as shown in Figure 6.5.1 'dry' and 'humid', respectively. Such uptake yields could never be observed if the samples were not partially regenerated. As a matter of fact, Figure 6.5.2 shows that the NO₂ uptake rate at the beginning of exposure n° 5 is much higher than that at the end of exposure n° 4. Therefore, it is obvious that some of the elementary steps in the reaction mechanism must be reversible on the time scale of the experiments discussed in this Section.

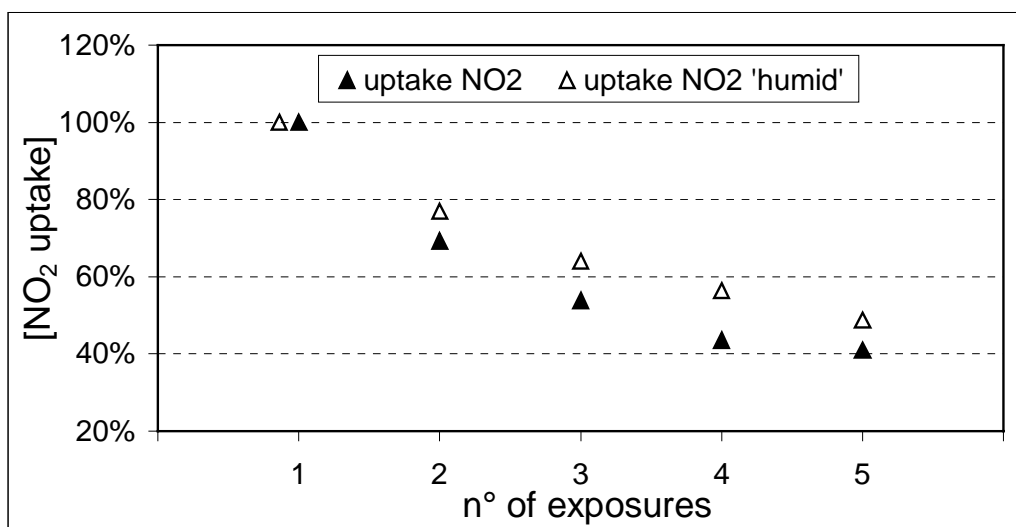


Figure 6.5.1: NO₂ uptake upon multiple exposure of a 'dry' and a 'humid' 'grey' decane soot sample integrated over 20 minutes; 4 mm diameter escape orifice, mean NO₂ concentration = 2.52×10^{12} molecule cm⁻³, sample weight 16.6 ('dry') and 15.8 mg ('humid'), respectively.

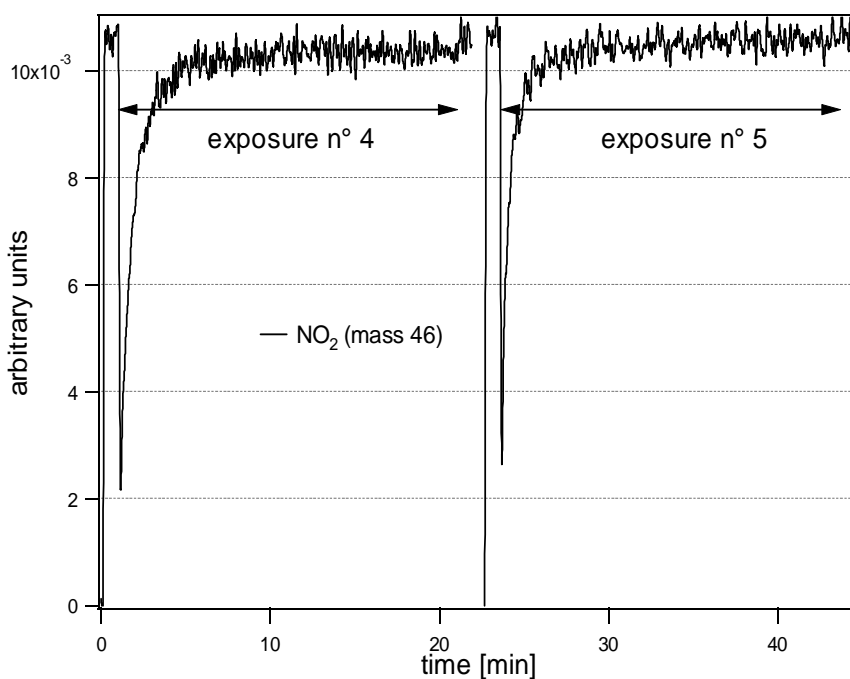


Figure 6.5.2: NO₂ uptake on 'grey' decane soot ('dry') at exposures n° 4 and 5; 4 mm diameter escape orifice, NO₂ concentration = 2.49×10^{12} and 2.53×10^{12} molecule cm⁻³, respectively, sample weight 16.6 mg, time between the two exposures = 24 hours

In Figure 6.2.1 we have seen that the branching ratio between reactions (R. 6.2.2) and (R. 6.2.3) is constant for the duration of a standard experiment. Data of Figure 6.5.3 show that this observation is still valid for samples for which the absolute yields are reduced by at least a factor of 2. It may be concluded that the saturation of the sample is not caused by the depletion of the surface sites $\{C-H\}_{RED}$ or $\{S_2\}$ because this would most probably also change the branching ratio (R. 6.2.2)/(R. 6.2.3). We therefore surmise that the reduced reactivity of the soot is caused by saturation of the adsorption sites $\{S_1\}$. A possible interpretation of this observation is that products such as $\{C\}_{OX}$ or $\{S-NO_2\}$ may interact with $\{S_1\}$ thereby deactivating the primary adsorption sites. Furthermore, it may be seen in Figure 6.5.3 that relative HONO yields are higher for the ‘humid’ sample compared to the ‘dry’ sample, that is 48.0% vs. 38.6% on average. According to our reaction scheme this would indicate that the presence of humidity slows down the saturation of $\{S_1\}$ adsorption sites. In addition, the humidity is shifting the branching ratio between reactions (R. 6.2.2) and (R. 6.2.3) towards reaction (R. 6.2.2). However, this interpretation may be highly speculative as the observed differences between ‘dry’ and ‘humid’ samples are rather small and based on only one sample of each type. The effects of H₂O in the present study are relatively weak and we therefore forego to include it explicitly in the mechanism. It must be kept in mind that the soot samples were pumped down in the low-pressure reactor for five minutes before each experiment. Therefore a large amount of H₂O may desorb from the soot prior to the actual uptake experiment. On the other hand, a strong influence of H₂O has been unambiguously observed in studies performed at higher total pressures [Kalberer et al., 1999, Kleffmann et al., 1999]. A comparison of the results observed in this Section with those from experiments performed several weeks before as displayed in Figure 6.2.2 shows that the relative HONO yields are significantly lower in the case of the multiple exposure experiments. For this observation we do not have conclusive explanation except that the response factor of the mass spectrometer may have changed in the meantime.

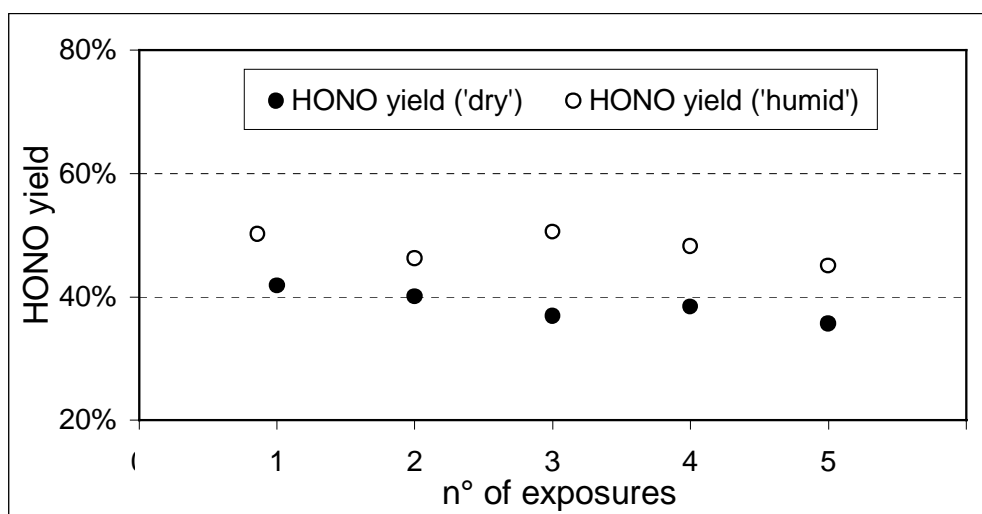


Figure 6.5.3: HONO yields relative to NO₂ taken up for the multiple exposure of a ‘dry’ and a ‘humid’ ‘grey’ decane sample as shown in Figure 6.5.1.

6.5.2 Multiple exposure of 'black' decane soot.

An identical series of repeated exposure experiments to NO₂ has been performed for 'black' decane soot. It has been observed that the uptake of NO₂ is decreasing continuously with repeated exposure just as in the case for 'grey' decane soot. The corresponding rate of NO production decreases to the same extent so that relative NO yields are constant between 19-23%. Even after the fifth exposure amounts of NO₂ taken up and NO released attain approximately 50% of the initial values displayed in Figure 6.5.4. In contrast to 'grey' decane soot there is no observable difference between dry and humid samples. This is somewhat surprising because soot samples stored in humidified air have changed their macroscopic aspect. The longer the sample was stored in humidified air the more its surface has been furrowed by cracks. This may be due to capillary pore filling with water resulting in an increase of the internal stress within the soot sample. In Section 6.4 we postulated that a product of the HONO-formation/disproportionation branch shifted the branching ratio between reaction (R. 6.2.2) and (R. 6.2.3) towards reaction (R. 6.2.2). Based on the results of multiple exposure we may exclude H₂O and favor {HONO} or {NO₂} as the species responsible for this shift. Another important observation is that relative yields of NO are constant from the start to the end of the multiple exposure series leading to the conclusion that in this case as well the decrease in reactivity may primarily be due to the depletion of adsorption sites {S₁}. The same conclusion has been reached for the NO₂/'grey' decane soot interaction based on results displayed in Figures 6.5.1 and 6.5.3.

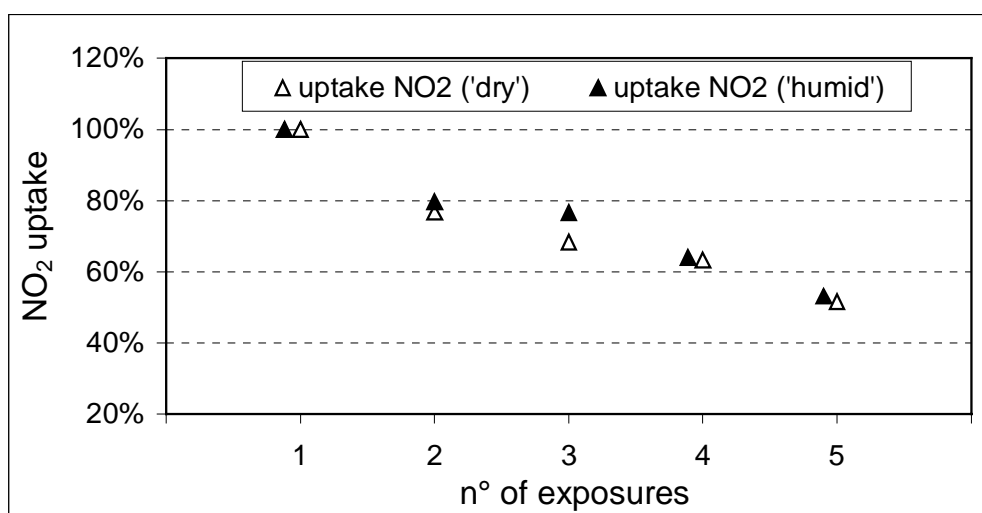


Figure 6.5.4: NO₂ uptake upon multiple exposure of a 'dry' and a 'humid' 'black' decane sample integrated over 20 minutes; 4 mm diameter escape orifice, mean NO₂ concentration = 2.5×10^{12} molecule cm⁻³, sample weight 17.2 ('dry') and 15.2 mg ('humid'), respectively.

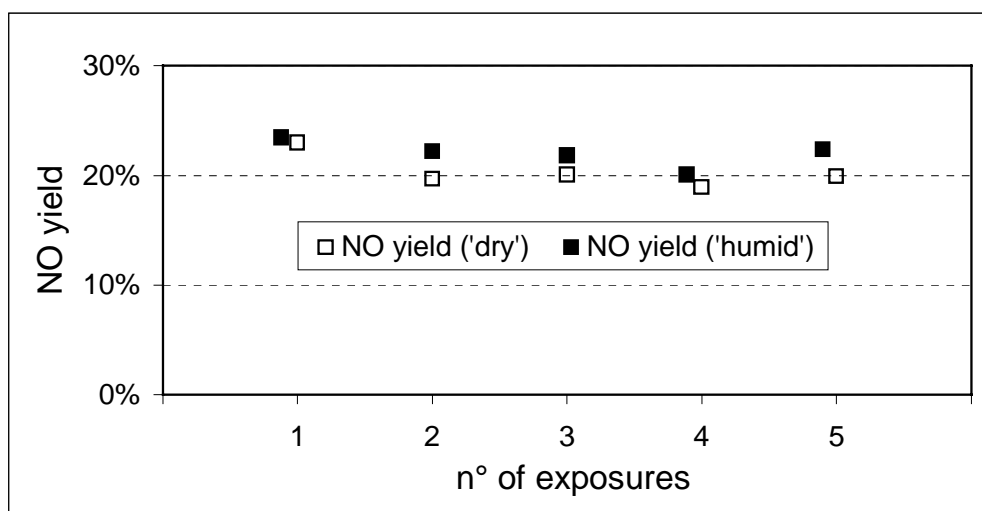


Figure 6.5.5: HONO yields relative to NO₂ taken up for the multiple exposure of a 'dry' and a 'humid' 'black' decane sample as shown in Figure 6.5.4.

6.6 NO₂/decane soot interaction with a concomitant flow of H₂O.

We have seen in Section 6.5.2 that the reactivity of 'black' decane soot towards NO₂ did not change when the soot samples had been exposed to water vapor prior to the uptake experiment. For 'grey' decane soot a very weak influence could be noted at best. In order to explain the missing water effect we speculated whether any adsorbed H₂O molecules would just be pumped off prior to the uptake experiment. This was the reason why we performed a few experiments in which the soot samples were simultaneously exposed to a concentration of NO₂ of 2.5×10^{12} molecule cm⁻³ and varying concentrations of H₂O. It is quite easy to summarize the observed results. Even H₂O concentrations of up to 2×10^{14} molecule cm⁻³ had absolutely no influence on the NO₂ rate of uptake on 'grey' or on 'black' decane soot. This is not surprising as a measurable uptake of H₂O could not be observed neither on 'grey' nor on 'black' decane soot. The partial pressures that may be obtained in the Knudsen flow reactor are obviously not high enough in order to adsorb significant amounts of H₂O. This speculation is supported by the fact that for the interaction of H₂O on graphitized carbon adsorption isotherms have been observed which correspond to type III of the BDDT classification [Parfitt and Sing, 1976]. This type is convex to the pressure axis over its entire range which means that significant amounts of H₂O are only adsorbed at high partial pressures. We therefore have to conclude that a low pressure reactor is not an appropriate experimental device with which to examine the influence of water towards the soot/NO₂ interaction.

6.7 Uptake kinetics of NO₂ on ‘grey’ and ‘black’ decane soot.

6.7.1 Continuous-flow experiments.

Raw data on the NO₂ interaction with decane soot clearly show that the uptake rate of NO₂ is strongly decreasing during the course of an experiment such as displayed in Figures 6.2.1 and 6.3.1. After an initial fast uptake of NO₂ saturation is approaching fast. Thus, it is obvious that the uptake probability γ strongly depends on the number of collisions the sample has experienced. This fact may also be found in the literature where γ values varying by several orders of magnitude have been published depending on the time resolution of the experiment [Tabor et al., 1994, Rogaski et al., 1997, Gerecke et al., 1998, Ammann et al., 1998, Kalberer et al., 1999, Kleffmann et al., 1999, Longfellow et al., 1999]. Therefore, we have calculated both initial uptake probabilities (γ_0) as well as uptake probabilities for exposure times of 10 and 20 minutes, respectively (γ). Figure 6.7.1 displays γ_0 of ‘black’ and ‘grey’ decane soot as a function of the NO₂ concentration. γ_0 has been calculated in relation to the geometric surface area of the samples (19.6 cm²). This is a reasonable approximation as only data from the first second or so of sample exposure are considered when only the upper soot layers are probed. It may be seen that γ_0 is continuously decreasing with increasing concentration of NO₂. The γ_0 value of NO₂ on soot cannot be described by a pseudo first order rate law even at the lowest concentrations of NO₂ used. Figure 6.7.1 shows that γ_0 for ‘black’ and ‘grey’ decane soot are almost identical. At higher concentrations of NO₂ γ_0 seems to be a bit larger for ‘grey’ compared to ‘black’ decane soot, although its BET surface is smaller by a factor of three compared to ‘black’ decane soot (see Table 5.1.1). The measured values of γ_0 from this work are approximately the same as γ_0 of NO₂ uptake on commercial soot samples [Tabor et al., 1994, Rogaski et al., 1997] or on laboratory-generated ethylene soot [Gerecke et al., 1998].

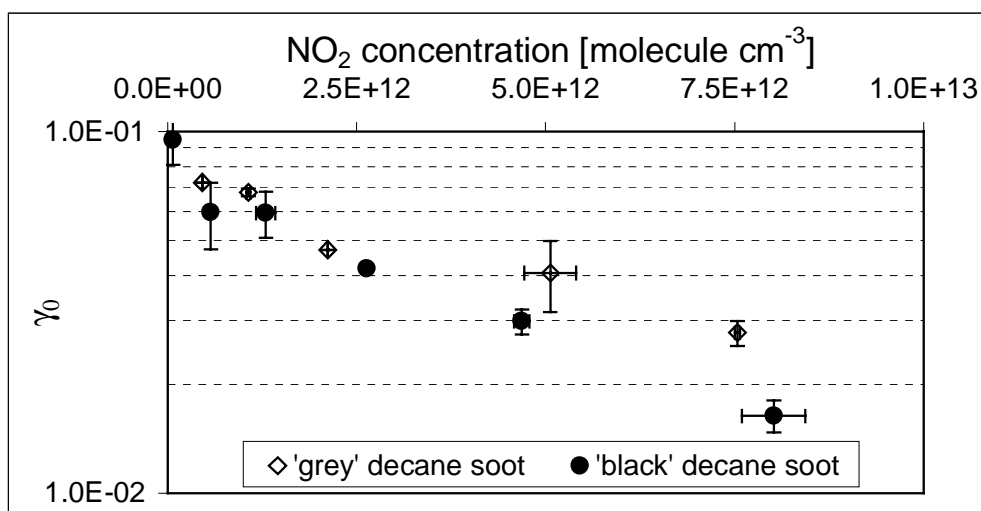


Figure 6.7.1: Initial uptake coefficient (γ_0) of NO₂ on 'grey' and 'black' decane soot as a function of the NO₂ concentration; 14 mm diameter escape orifice, mean sample weight 16.2 mg. γ_0 has been calculated using the geometric surface area of the samples (19.6 cm²).

Uptake probabilities after longer interaction times are calculated using BET surface areas of the soot sample because deeper layers are probed as shown in Figures 6.2.3 and 6.3.3. This leads to small γ values based on surface areas larger by a factor of 560 for 'grey' decane soot and by 1290 for 'black' decane soot, respectively. Figure 6.7.2 displays the resulting γ values as a function of NO₂ taken up which are lower by several orders of magnitude compared to γ_0 reflecting both the progressing saturation of the samples as well as the large surface areas. In contrast to γ_0 , distinct differences between 'black' and 'grey' decane soot may be noted. In the case of 'grey' decane soot, γ is continuously decreasing from 1.4×10^{-5} down to 3×10^{-7} with increasing quantities of NO₂ taken up. γ values for 'black' decane soot, on the other hand, are quickly decreasing at the beginning but then remain almost constant for amounts of NO₂ taken up above 2×10^{13} molecule cm⁻². This behavior is surprising on first view, but is understandable if one takes into account that the data points at low NO₂ uptake were obtained in experiments in which the samples have been exposed to low NO₂ concentrations whereas the opposite is true for data points at high NO₂ uptake. We have seen in Section 6.3.1 that at low concentrations almost all NO₂ is taken up on 'black' soot in reaction (R. 6.2.3) whereas at high concentrations reaction (R. 6.2.2) is predominant, as displayed in Figure 6.3.2. We thus conclude that saturation is mainly due to reaction (R. 6.2.3) and should appear for low concentrations of NO₂ in Figure 6.7.2. This hypothesis is also confirmed by the observation that no saturation has been observed during the experiments where samples of 'black' decane soot were exposed to a flow of HONO (see Figure 6.3.4). The conclusion following our reaction scheme is that the complex {S₂-NO₂} that is formed by reaction (R. 6.2.3) interferes on longer time scales with the adsorption site {S₁} in order to reduce its adsorption capacity. In the case of 'grey' decane soot the situation is simpler

because the more NO₂ is taken up the more reaction (R. 6.2.3) is becoming important as shown in Figure 6.2.2. This leads to γ values that are continuously decreasing, as shown in Figure 6.7.2.

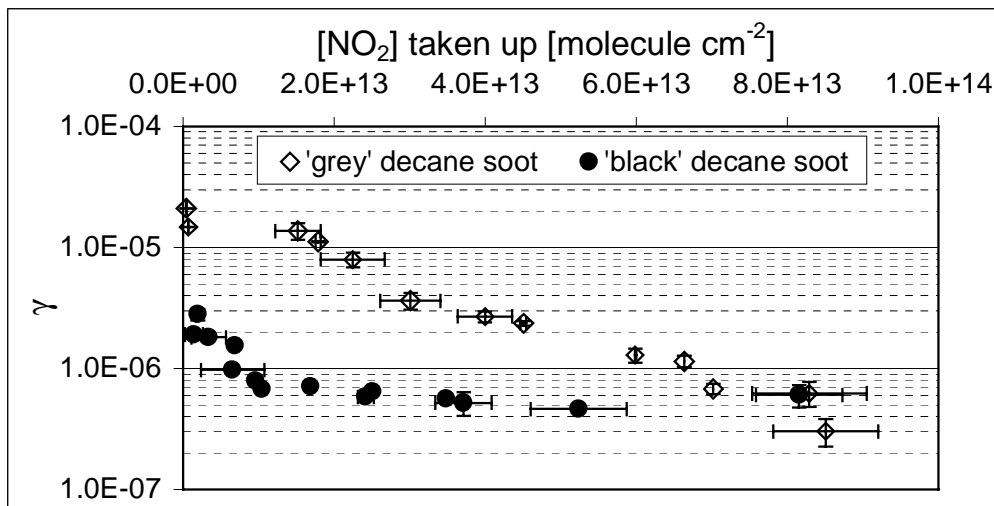


Figure 6.7.2: Uptake coefficient (γ) of NO₂ on 'grey' and 'black' decane soot depending on the amount of NO₂ taken up; 14 and 4 mm diameter escape orifices, mean sample weight 16.6 mg, duration of exposure = 10 or 20 min., amount of NO₂ taken up is expressed relative to the BET surface area of the samples.

6.7.2 Pulsed valve experiments.

In Section 6.7.1 we have seen that the initial uptake coefficients (γ_0) of NO₂ on 'grey' and 'black' decane soot do not pertain to a pseudo first order reaction even at the lowest concentration of NO₂ used. In order to verify this observation we performed some uptake experiments using the pulsed-valve technique. Figure 6.7.3 shows the measured uptake coefficients (γ_0) as a function of the dose of the NO₂ pulses.

A linear dependence of γ_0 on the dose may be noted for both 'grey' as well as 'black' decane soot. At a dose of 5×10^{13} molecules which corresponds to the detection limit of the mass spectrometer γ_0 amounts to 0.12 and 0.15 for 'grey' and 'black' decane soot, respectively. This value is slightly higher than the maximum values observed in the continuous-flow experiments.

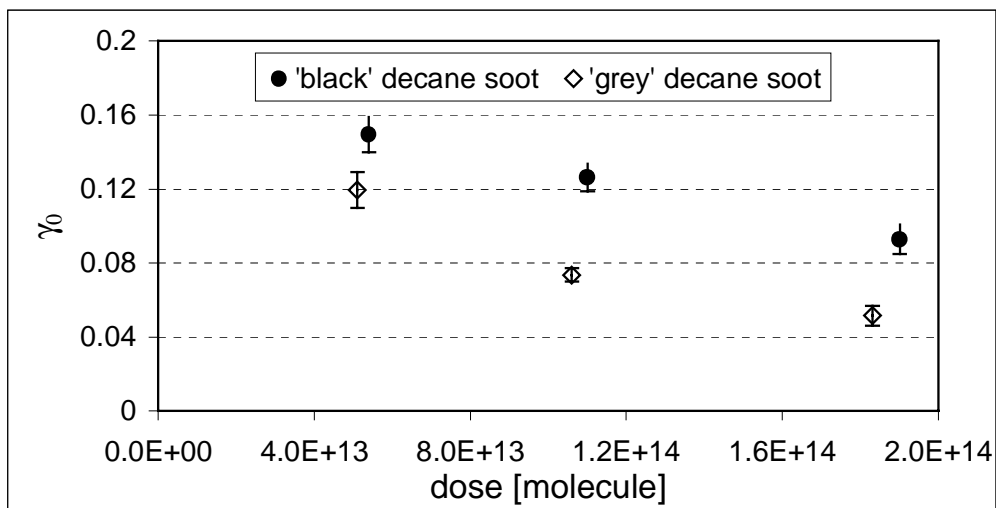


Figure 6.7.3: Initial uptake coefficients γ_0 of NO₂ on 'grey' and 'black' decane soot as a function of the pulse dose; 14 mm diameter escape orifice, sample weight 6.1 mg for 'grey' and 5.0 mg for 'black' decane soot, respectively.

If we assume that NO₂ has a surface area of 16.2 Å² it would take 1.2×10^{16} molecules to cover the 19.6 cm² of the sample surface in a formal monolayer. If we relate this number to the minimum detectable dose of 5×10^{13} molecules it is clear that the soot surface has been probed with a number of NO₂ molecules which corresponds only to 4×10^{-3} of a monolayer. However, even the uptake of such small doses of NO₂ cannot be described by a pseudo first order rate process. This may be seen from the fact that γ_0 is decreasing with increasing dose and from the decay curve of the reactive pulse which was not single-exponential.

Another way to evaluate the pulsed-valve experiments is to compare the integrals of the reactive with those of the reference pulses. The difference of a reference and a reactive pulse indicates how many molecules have been taken up by the soot. The relative yield of uptake is shown in Figure 6.7.4 as a function of the dose. All the data points were obtained on the same soot sample by introducing a pulse approximately every two minutes. It may be seen that the sample is progressively saturating with each additional pulse. The relative yield of uptake diminished by 10% between the first and the tenth pulse. However, it has been shown in Figure 6.5.2 that some of the saturation effects are reversible on a longer time scale.

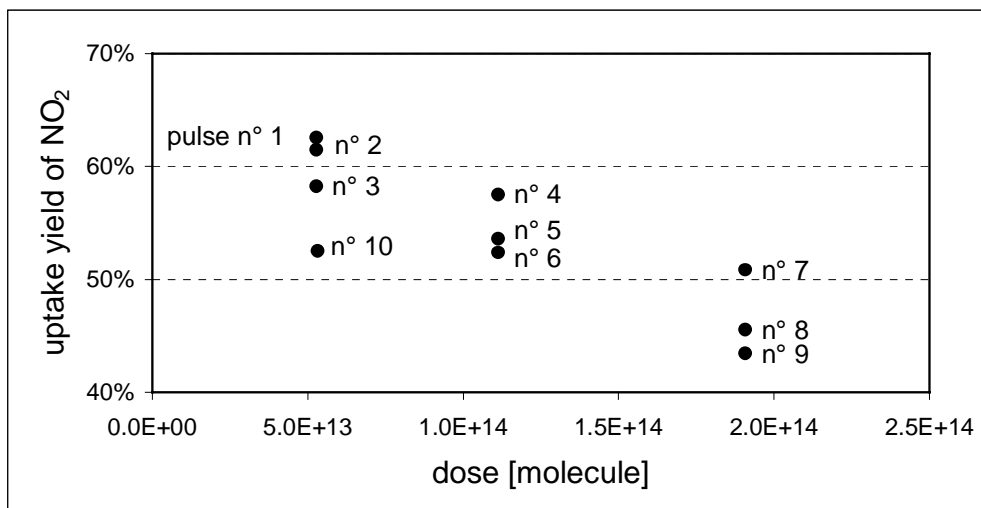


Figure 6.7.4: Relative yields of NO₂ uptake on a 'black' decane soot sample as a function of the dose; 14 mm diameter escape orifice, sample weight 5.0 mg.

The pulsed-valve technique has not been performed using phase sensitive detection. This means that fast secondary reactions on the walls of the detection chamber will interfere with the molecular beam effusing from the Knudsen reactor. As a consequence we were not able to detect the HONO product pulse because the difference of the HONO signal between the reference and the reactive pulse was too small. We assume that the HONO signal of the reference pulses originated from the interaction of NO₂ with soot that was deposited on the walls of the detection chamber. In fact, it was unavoidable that small quantities of soot were sucked into the detection chamber upon the lifting of the plunger sealing of the sample chamber.

6.8 Uptake kinetics of HONO on 'black' decane soot.

Results in Section 6.3.2 showed that HONO undergoes a fast uptake on 'black' decane soot. In addition, saturation of the samples have never been observed during the 5 minutes that it took to perform the standard exposure experiment. An additional feature may be seen in Figure 6.8.1. where the initial uptake coefficients (γ_0) are shown as a function of the HONO concentration. The values have been calculated using the geometric surface area of the samples (19.6 cm²). Uptake coefficients obtained in the 14 mm reactor are varying randomly and do not show a clear saturation with increasing HONO concentration as it is the case for the corresponding data of NO₂ uptake on 'black' decane soot (see Figure 6.7.1). The mean value amounts to 0.027. A decrease of γ_0 with increasing HONO concentration is observed only at higher concentrations in the 4 mm reactor: In this case γ_0 slowly decreases from a value of 0.022 at a concentration of 9.1×10^{11} molecule cm⁻³ to a value of 0.01 at a

concentration of 3.3×10^{12} molecule cm^{-3} . Uptake coefficients that were obtained in the 1 mm escape orifice reactor at concentrations between 1.6×10^{13} and 3.8×10^{13} molecule cm^{-3} varied only slightly and had a mean value of approximately 1.8×10^{-3} .

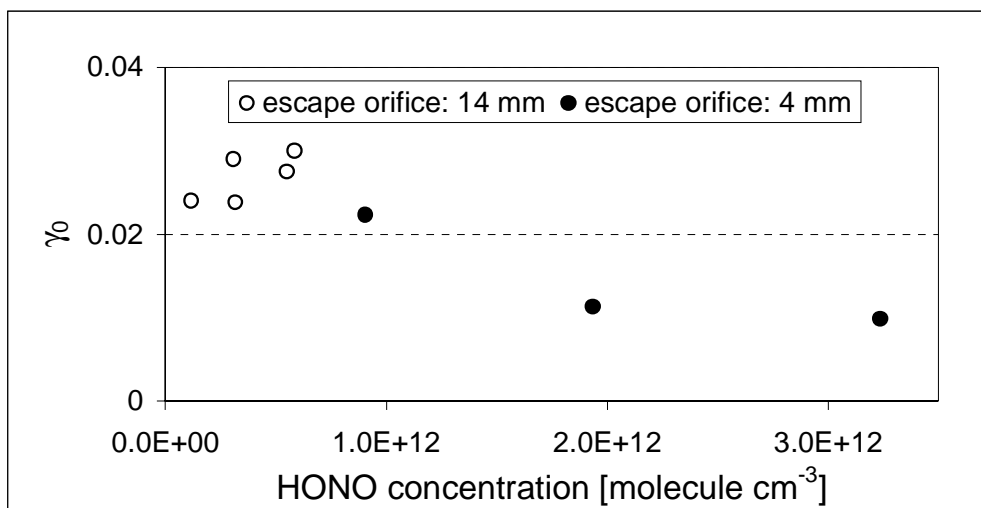


Figure 6.8.1: Initial uptake coefficient (γ_0) of HONO on ‘black’ decane soot as a function of the NO₂ concentration; mean sample weight 11.9 ± 1.8 mg. γ_0 has been calculated in relation to the geometric surface area of the samples (19.6 cm^2).

As already mentioned above we were unable to observe saturation of the samples during the 5 minutes of HONO exposure. Nevertheless, it may not be concluded that the uptake coefficient will stay constant because it is not known how the probing depth is evolving with time. A conservative estimate would be that HONO has probed not only the geometrical but the total internal BET surface area after 5 minutes. According to this assumption one obtains values for $\gamma_{5\text{min}}$ that are roughly 1000 times lower than those shown in Figure 6.8.1 ($1000 \approx \{11.9 \text{ mg} \times 2180 \text{ cm}^2 \text{ mg}^{-1}\} / 19.6 \text{ cm}^2$). This means that $\gamma_{5\text{min}}$ for 14 and 4 mm diameter escape orifices ranges from 2.7×10^{-5} to 1.0×10^{-5} . The corresponding correction for data obtained in the 1 mm diameter escape orifice reactor gives a mean value of 1.8×10^{-6} .

The only uptake coefficients for HONO that have been published so far as we know are those of Kleffmann et al. [1999] measured on commercial ‘lamp black 101’. They reported an uptake coefficient of approximately 2.0×10^{-8} for an interaction time of 5 minutes. This value continuously decreased during the first 30 minutes of interaction and then stabilized at $\gamma < 10^{-8}$ for several hours. Unfortunately, we were not able to produce a constant flow of HONO for longer time spans. However, the lowest limit of $\gamma_{5\text{min}}$ measured in the present study amounts to 1.8×10^{-6} which is about 100 times higher as the value reported by Kleffmann et al. This difference is not surprising as we have already postulated in Section 6.4

that 'black' decane soot produces high amounts of HONO upon interaction with NO₂ but converts it in a second step almost quantitatively into NO and {NO₂}. Thus, there must be strong interactions between HONO and 'black' decane soot also leading to high uptake coefficients. 'Lamp black 101' on the other hand releases significant amounts of HONO. This observation alone indicates that the interaction of HONO with 'lamp black 101' must be weaker and the uptake coefficients therefore lower than in the case of 'black' decane soot.

6.9 Heating of soot samples.

The most important limitation of the experimental set-up used in this work is that only gas phase species can be detected. On the other hand it has been shown in Sections 6.2.1 and 6.3.1 that depending on the flux significant amounts of NO₂ may stay adsorbed on the surface of both 'grey' as well as 'black' decane soot. The only way to make these reservoirs accessible to detection by mass spectrometry is to transfer the molecules into the gas phase. We have done this by heating the soot samples in the Knudsen cell across Pyrex walls using a heating lamp (Philips, IR, 375 W) for four minutes. Compared to programmable temperature desorption (PTD) our procedure was quite crude because we did not have appropriate means to measure the temperature nor to control the heating rate. Nevertheless, by heating every sample for the same time from an identical distance we measured desorption rates with good reproducibility. The products we were looking for were CO and CO₂ at m/e 28 and 44. They represent tracers for the oxidation of the soot surface. Furthermore, we were screening m/e 30, 46 and 47 in order to control whether nitrogen species such as NO, NO₂ or HONO may desorb upon heating. Finally, signals at m/e 62 and 63 have been recorded in order to examine whether species such as NO₃ or HNO₃ had been formed on the soot surface. For 'grey' as well as 'black' decane soot three different types of samples have been examined: One that previously had been exposed to NO₂ during twenty minutes and one that had been exposed to HONO during 5 minutes. The third sample was untreated soot which served as a reference.

Only a few experiments have been performed for each type of treated soot. In addition, the mass spectrometer signals often cannot be unambiguously attributed to a well defined product. We therefore will content ourselves with a qualitative discussion. The intensity of all observed signals strongly depended on the pumping time prior to heating of the sample. Therefore, each sample was pumped exactly 45 minutes prior to the start of the heating in order to enable a comparison of the different experiments. We forego to show MS signals at m/e 62 and 63 as they never significantly increased upon heating. However, the signals of the molecular ions of NO₃ (m/e 62) and HNO₃ (m/e 63) only amount to 15% and 1% of the corresponding signals at m/e 46 [Caloz, 1997]. Therefore, only high amounts of these two products could have been detected.

Figure 6.9.1 shows experiments performed on 'grey' decane soot. Graph A) presents the results on the heating of an untreated reference sample. It may be seen that the signals at m/e 28, 30 and 44 are clearly increasing after the start of the heating cycle at $t = 2.5$ min. Signals at m/e 46 and 47, on the other hand, only show a weak increase. It is obvious that products such as CO (m/e 28) and CO₂ (m/e 44) are always present in the soot matrix because they are major products of the combustion process in the diffusion flame. Signals at m/e 30, 46 and 47, on the other hand, may be caused by fragments of organic compounds or by nitrogen species that have been generated during the combustion of decane fuel. NO_x are present in the gas plume of both the rich as well the lean flame as we have seen in Section 4.1. A general feature of all the samples is that the increase of the MS signal m/e 28 is much faster than the one at m/e 44. The reference sample (A) and the sample that had been exposed to HONO (C) do not show significant differences. This was expected as we have seen in Section 6.2.2 that HONO does not interact with 'grey' decane soot. On the other hand, it can be seen that several traces of graph B) show different characteristics when compared to the reference sample A). The desorption flows at m/e 28 and 44 clearly increase. Assuming that these signals represent CO and CO₂ this would mean that the observed signals correspond to reaction sites that have been oxidized either by (R. 6.2.2) or by reactions involving NO₂ that has been irreversibly adsorbed by (R. 6.2.3). A distinct increase can also be observed for MS signals at m/e 30 and 46. An additional flow monitored by these signals can be observed above all at the beginning of the heating. This suggests that these signals refer to weakly bound compounds. The initial ratio of 30/46 is approximately two which corresponds to the fragmentation pattern of NO₂. However, this ratio increases to 4.4 for the signals which are integrated over the whole heating period. As a consequence, NO₂ cannot be responsible for the total signal observed at m/e 30. If the difference of the m/e 46 MS signal between sample B) and A) is integrated and completely attributed to NO₂ one calculates an amount of 8.6×10^{15} molecules which have been released upon heating. This number would approximately correspond to the amount of NO₂ that is expected to have irreversibly adsorbed according to (R. 6.2.3) in the uptake experiment prior to the heating.

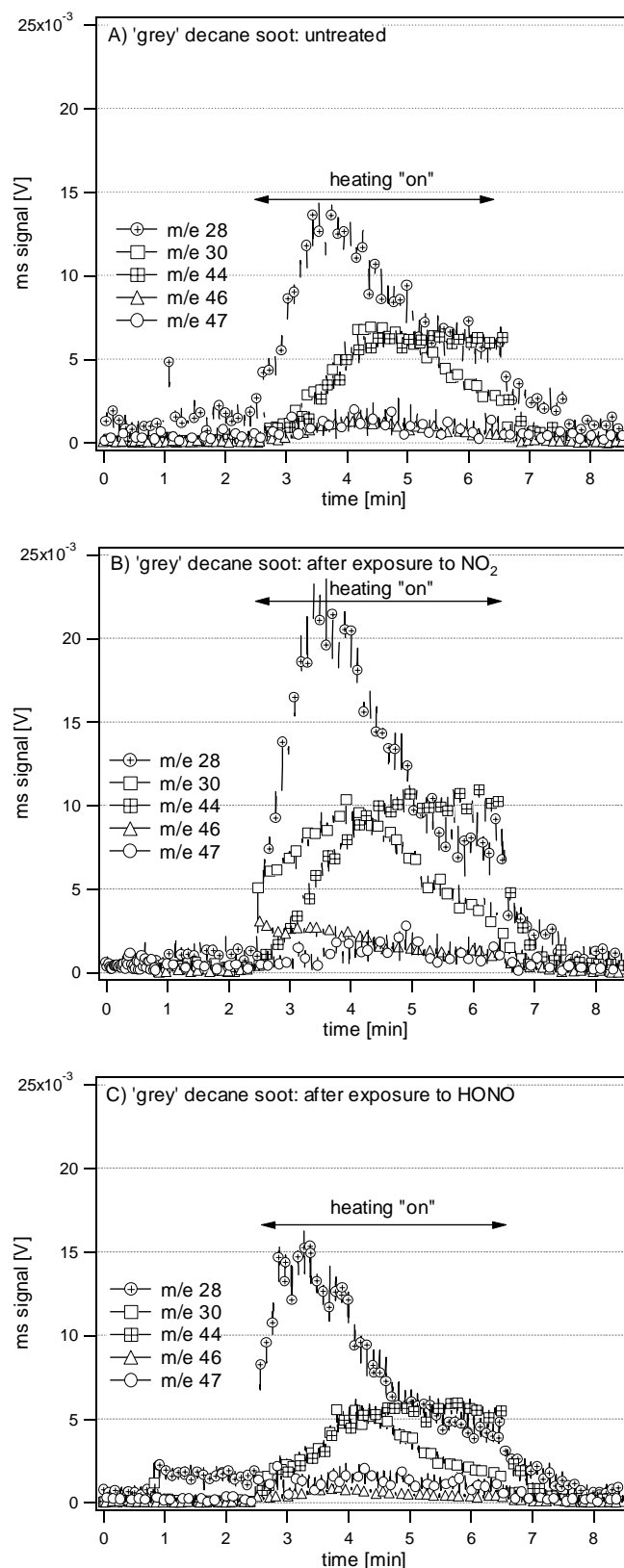


Figure 6.9.1: Heating of 'grey' decane soot: A) untreated sample, mass = 10.5 mg; B) sample exposed to a NO₂ concentration of 2.19×10^{12} molecule cm⁻³ during 20 min. prior to heating, mass 10.2 mg; C) sample exposed to a HONO concentration of 1.93×10^{12} molecule cm⁻³ during 20 min. prior to heating, mass = 11.1 mg. All the heating experiments were performed using the 4 mm diameter escape orifice.

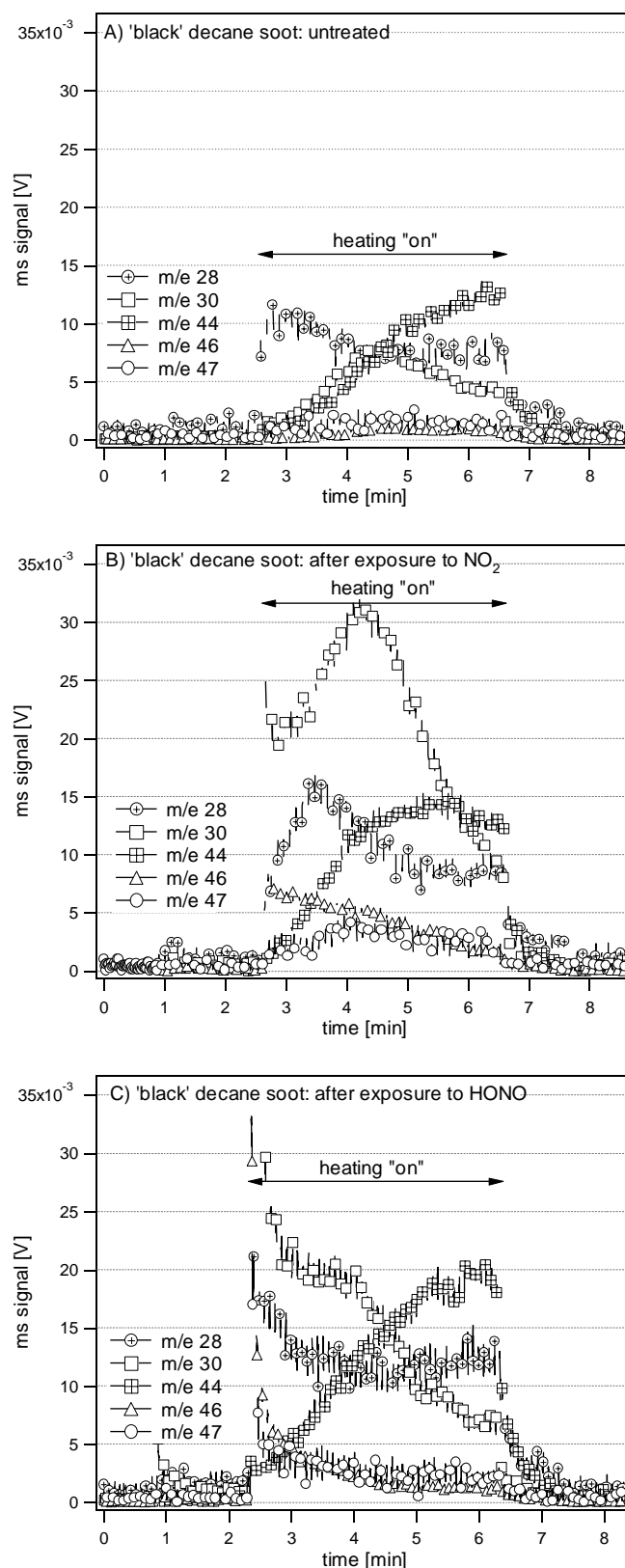


Figure 6.9.2: Heating of 'black' decane soot: A) untreated sample, mass = 10.7 mg; B) sample exposed to a NO₂ concentration of 2.26×10^{16} molecule cm⁻³ during 20 min. prior to heating, mass 10.3 mg; C) sample exposed to a HONO concentration of 1.80×10^{12} molecule cm⁻³ during 20 min. prior to heating, mass = 11.6 mg. All the heating experiments were performed using the 4 mm diameter escape orifice.

The corresponding experiments for 'black' decane soot are shown in Figure 6.9.2. For this type of soot a strong interaction with HONO has been observed and discussed in Section 6.3.2. Therefore, it is not surprising that the traces of graph C) show much higher intensities than the reference traces in graph A). All signals except m/e 44 have high initial peaks which refers to weakly bound compounds. The mass signal at m/e 30 has the property to have a second peak at $t = 4$ min. The ratio of MS signal at m/e 30/46 is too high to explain the intensity at m/e 30 solely with the desorption of NO₂.

Sample B) which has been exposed to NO₂ prior to heating has a very strong signal at m/e 30. As in the case for sample C) an initial peak and second one at $t = 4$ min may be observed. At the same time a MS signal peak is also observable at m/e 47. The ratio of both of these MS signals at $t = 4$ min approximately corresponds to the fragmentation pattern of HONO ($30/47 = 9:1$) if the corresponding reference values from graph A) are subtracted first. This suggests that the peaks at m/e 30 and 47 at $t = 4$ min are generated by the desorption of HONO, whereas the initial peak at m/e 30, on the other hand, is more probably caused by the desorption of NO₂ and NO.

We are aware that most of the statements made in this section are rather qualitative as we are not able to unambiguously identify the desorbed reactants. The use of a more specific detection method such as for instance laser induced fluorescence (LIF) would be an appropriate way in order to have more insight into the desorption processes described above. Also, a better control of the heating rate, for instance by programmable temperature desorption (PDT), would surely result in a better resolution of the desorption peaks.

6.10 Aging of 'grey' decane soot in dry synthetic air.

It is very important to know whether the soot samples produced in this study are subject to aging processes when they are exposed to air for longer spans of time. In this case the degree of saturation observed in the multiple exposure experiments (see Section 6.5) could have been increased by an ongoing oxidation of the reactive surface sites by molecular oxygen present in the sample container. Of course, this would also be important information for the evaluation of the impact of soot particles in relation to atmospheric chemistry. Arens et al. [1999] suggested that the presence of phenolic compounds in the organic fraction of soot may be responsible for the formation of HONO. We observed that a organic solution of 1,2,10-trihydroxyanthracene changed its color and was therefore probably oxidized already after one day if it was not stored under nitrogen. If such compounds are involved in the formation of HONO it cannot be excluded that soot particles are deactivated even in pure synthetic air.

Therefore, samples of 'grey' decane soot were stored in a dark container filled with dry synthetic air for different spans of time until their exposure to NO₂ in the Knudsen cell. Figure 6.10.1 clearly shows that no decrease of the reactivity is observable, even after 10 days of storage time. This statement is valid for both the uptake of NO₂ as well as for the formation of HONO. However, based on this result one cannot conclude that phenolic compounds are not involved in the formation of HONO. As will be discussed in Section 10, their reactivity strongly depends on the chemical environment.

The air of the container was purged with fresh synthetic air each time a sample has been removed. Apparently, this procedure did not lead to a loss of reactivity which could have been expected if a significant fraction of the HONO producing species had desorbed into the gas phase. The conclusion is therefore that the reactive species are rather strongly adsorbed on the soot surface.

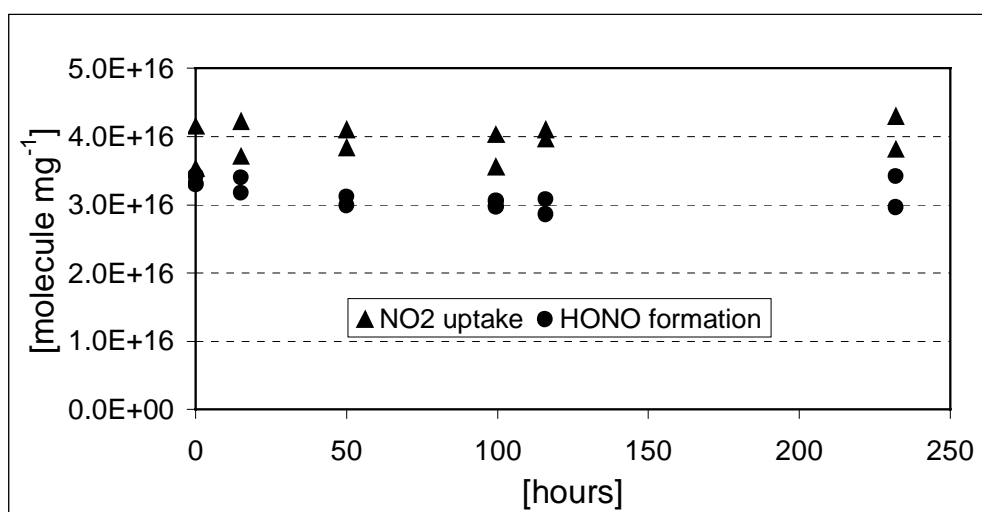


Figure 6.10.1: Reactivity of 'grey' decane soot integrated over 20 minutes after different storage times in dry synthetic air; 4 mm diameter escape orifice, mean concentration = 2.5×10^{12} molecule cm^{-3} , mean sample weight = 16.9 ± 1.5 mg.

7 The reactivity of NO₂ with hexane soot.

7.1 Products and mechanism.

Hexane is often used as a fuel in order to produce soot in the laboratory. Owing to its low boiling point it is sufficient to pour a small quantity into a beaker and ignite its vapors. Because of its simplicity this technique has been applied in several studies [Akhter et al., 1985, Chughtai et al., 1994, , Choi and Leu, 1998, Longfellow et al., 1999]. In order to establish a link to the studies cited above a series of experiments have been performed using hexane as a fuel. In the present work, however, the same co-flow system used for decane has been used in order to produce soot originating from a rich and lean flame. The appearance of the two flame types regarding the structure and emission was identical to the corresponding flames generated using decane. We therefore assume that the parameters of the decane flame indicated in Table 4.1 represent a good description for the hexane flames, as well.

Table 7.1 summarizes the results in detail. In general, it may be said that the same trends as for decane soot are noted: Hexane soot originating from a rich flame has a greyish appearance and HONO is the only product resulting from the reaction with NO₂. Hexane soot produced in a lean flame is pitch black and forms only very small amounts of HONO but important quantities of NO. Therefore, we reach the identical mechanistic conclusions as for decane soot (see R. 6.2.1.-6.2.3). In addition, the absolute amounts of NO₂ uptake and HONO generated are identical to within experimental uncertainty to those of decane soot.

An important conclusion resulting from the comparison of decane and hexane soot is that, within the group of alkane-fuels, soot properties are varying much more with the air/fuel ratio than with the type of fuel.

soot	orifice Ø [mm]	NO ₂ concentration [molec cm ⁻³]	NO ₂ uptake [molec mg ⁻¹]	HONO [molec mg ⁻¹]	HONO yield [%]	NO [molec mg ⁻¹]	NO yield [%]
hexane grey	4	8.4E12 ±3.3E11	6.1E16 ±6.4E15	4.0E16 ±1.8E15	66 ±4	n.o.	-
	14	9.9E11 ±4.0E10	3.1E16 ±1.3E15	2.6E16 ±3.3E15	83 ±7	n.o.	-
decane grey	4	7.8E12 ±4.6E11	6.0E16 ±6.0E15	4.2E16 ±4.0E15	60 ±4	n.o.	-
	14	1.1E12 ±6.0E9	2.6E16 ±2.1E15	2.5E16 ±2.6E15	84 ±6	n.o.	-
hexane black	1	1.5E14 ±3.5E12	4.8E17 ±1.1E16	n.o.	-	2.4E17 ±2.8E15	49 ±0.5
decane black	1	1.5E14 ±3.5E12	6.0E17 ±6.1E16	n.o.	-	3.0E17 ±4.5E16	50 ±2

Table 7.1: Comparison of decane and hexane soot. Uncertainties correspond to one standard deviation. n.o. refers to: no measurable amounts observed.

8 The reactivity of NO₂ and HONO with acetylene soot.

8.1 The interaction of NO₂ on acetylene soot.

Acetylene soot has been examined as a further type of soot. In this case there was no problem to produce soot of reproducible quality. In order to produce a stable flame it was sufficient to feed a commercial burner with a controlled flow of acetylene. The flame was maintained in free laboratory air which implies that the oxidant flow could not be controlled. The standard flame was fed with 135 ml/min acetylene. The results of a typical uptake experiment of NO₂ may be seen in Figure 8.1.1.

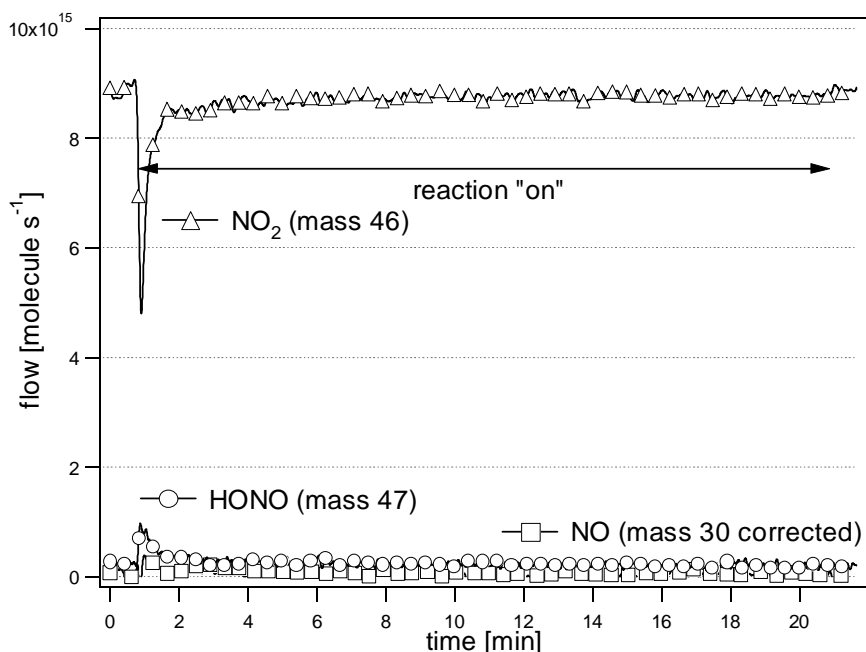


Figure 8.1.1: Uptake experiment of NO₂ on acetylene soot; sample mass = 16.2 mg, 4 mm diameter escape orifice, NO₂ concentration = 8.0×10^{12} molecule cm⁻³.

A comparison with the corresponding uptake experiments on ‘grey’ and ‘black’ decane soot (Figure 6.2.1 and 6.3.1) reveals that acetylene soot is much less reactive. The sample seems to saturate already after three minutes of exposure. Accordingly, significant amounts of HONO are released only during the first three minutes. NO could never be observed as a product. In view of the fast saturation of the samples we only considered the first 3 minutes of the uptake experiment for the data evaluation in the following.

The yields of HONO formation relative to NO₂ uptake are shown in Figure 8.1.2. It is striking that the HONO yields observed at low concentrations in the 4 mm reactor are much smaller than those observed at a similar concentration in the 14 mm reactor. In other terms,

there is not such a ‘smooth’ transition between the data obtained at 14 and 4 mm escape orifices, as it was the case for ‘grey’ decane soot (see Figure 6.2.2). The mean residence time of HONO in the reactor amounts to 0.24 and 1.8 seconds for 14 and 4 mm diameter escape orifices, respectively. This means that a HONO molecule, once desorbed, stays 7.5 times longer in the 4 mm reactor than in the 14 mm reactor. As a consequence, the probability to collide with the soot surface is also higher by a factor of 7.5 if the 4 mm reactor is compared to the 14 mm reactor. A possible explanation for the observed fall-off of the HONO yield is therefore that HONO formed in the 4 mm reactor is to a large extent destroyed by or adsorbed on the sample surface prior to its effusion into the detection chamber. We therefore performed a limited series of experiments where we exposed acetylene soot to a pure flow of HONO akin to the experiments for ‘grey’ and ‘black’ decane soot described in Sections 6.2.2 and 6.3.2.

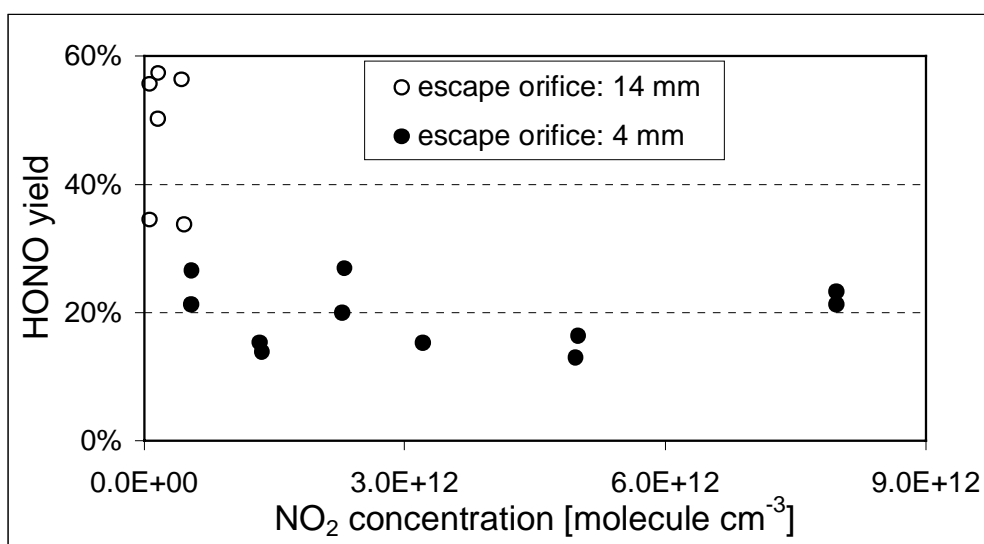


Figure 8.1.2: HONO yield relative to NO₂ taken up on acetylene soot as a function of the NO₂ concentration; yields for the first 3 minutes of interaction, mean sample mass = 16.1 ± 0.2 mg.

8.2 The interaction of HONO on acetylene soot.

HONO uptake experiments have been performed at 14, 4 and 1 mm diameter escape orifices covering a concentration range from 1.6×10^{11} to 4.1×10^{13} molecule cm⁻³ corresponding to partial pressures from 6.5 to 1685 ppb. Figure 8.2.1 shows an uptake experiment performed at 1 mm diameter escape orifice as an example. A comparison with the corresponding experiment performed on ‘black’ decane soot shown in Figure 6.3.4 suggests a close resemblance as the experimental conditions were almost identical. It may be seen that HONO undergoes a strong interaction with acetylene soot. The uptake at the beginning is not

as high as in the case of 'black' decane soot but seems to increase with ongoing time of exposure when m/e 47 (HONO⁺) is monitored.

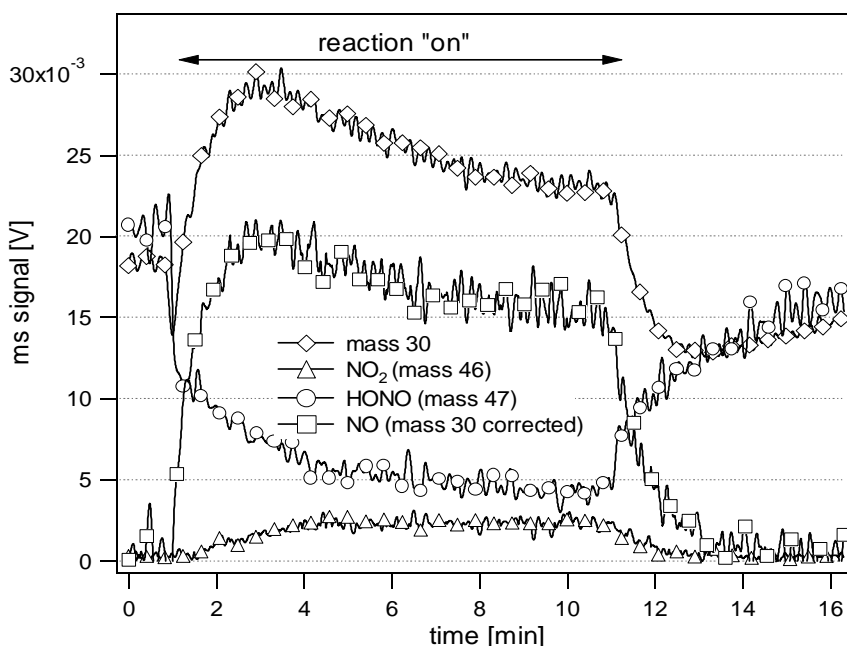


Figure 8.2.1: Uptake experiment of HONO on acetylene soot; sample mass 10.4 mg, 1 mm diameter escape orifice, initial HONO concentration = 3.57×10^{13} molecule cm^{-3} .

However, this observation may be at least partially explained by the fact that the HONO flow decreased during the experiment. There was probably also a HONO reservoir that had built up on the reactor walls. A part of this HONO reservoir desorbs into the gas phase upon the concentration drop that occurs at the beginning of the uptake experiment. The result is that the MS signal at m/e 47 decreases at a slower rate than in a clean reactor. At the end of the uptake experiment, on the other hand, the reservoir on the walls is filled up again which extends the rise time of the MS signal of HONO. That this may really be the case shows a comparison with Figure 6.3.4 where a corresponding uptake experiment has been performed for HONO on 'black' decane soot under the same conditions. In the case of 'black' decane soot the MS signal at m/e 47 attained its steady state level already approximately 2 minutes after the end of the uptake experiment. This is in good agreement with the calculated residence time of HONO in the reactor which amounts to approximately 30 seconds. In the case of the experiments with acetylene soot, on the other hand, Figure 8.2.1 reveals that it took more than 5 minutes until the HONO steady state concentration had been reestablished. The uptake experiments of HONO on 'black' decane soot were performed several weeks before those on acetylene soot. The internal surface of the reactor obviously was much more inert towards HONO at that time. However, this artifact was only observed at high HONO concentrations, i.e. in the 1 mm escape orifice reactor, and does not significantly influence the mass balance.

The observation that HONO decomposes to a large extent on acetylene soot confirms our assumption in Section 8.1 that the low HONO yields observed upon interaction with NO₂ in the 4 mm escape orifice reactor are due to fact that the probability for HONO to re-collide with the sample surface and to be decomposed is higher in the 4 mm than in the 14 mm escape orifice reactor. The fact that there was no MS signal for NO (m/e 30), the decomposition product of HONO, observed during the exposure experiments towards NO₂ is understandable because only very small amounts of NO₂ are taken up and converted to HONO. It may be seen in Figure 6.3.1 that NO produced by disproportionation of HONO only appears very slowly. The result is a very broad product peak that is hardly observable at low levels. Therefore it would be wrong to conclude from Figure 8.1.2 that the yield of 80% of nitrogen missing in the mass balance of the experiments performed in the 4 mm escape orifice reactor refers to nitrogen species that are irreversibly adsorbed on the soot surface. A large fraction of these missing 80% are probably NO and NO₂ that are desorbing at such low flow rates that they are not detectable in our system.

The differences between acetylene and ‘black’ decane soot concerning their interaction with HONO is getting obvious if the relative yields of formation of NO and NO₂ are compared. Figure 8.2.2 shows that the mass balance for acetylene soot is closed whereas in the case of ‘black’ decane soot only 50% of adsorbed nitrogen desorbed into the gas phase as NO and NO₂. Whereas the ratio of the yields of NO and NO₂ at high HONO concentrations was roughly 4:1 in the case of ‘black’ decane soot it is about 3:1 in the case of acetylene soot. Like in the case of ‘grey’ and ‘black’ decane soot it has been verified in ancillary experiments that NO does not show any interaction, neither with fresh nor with acetylene soot which has been previously exposed to NO₂.

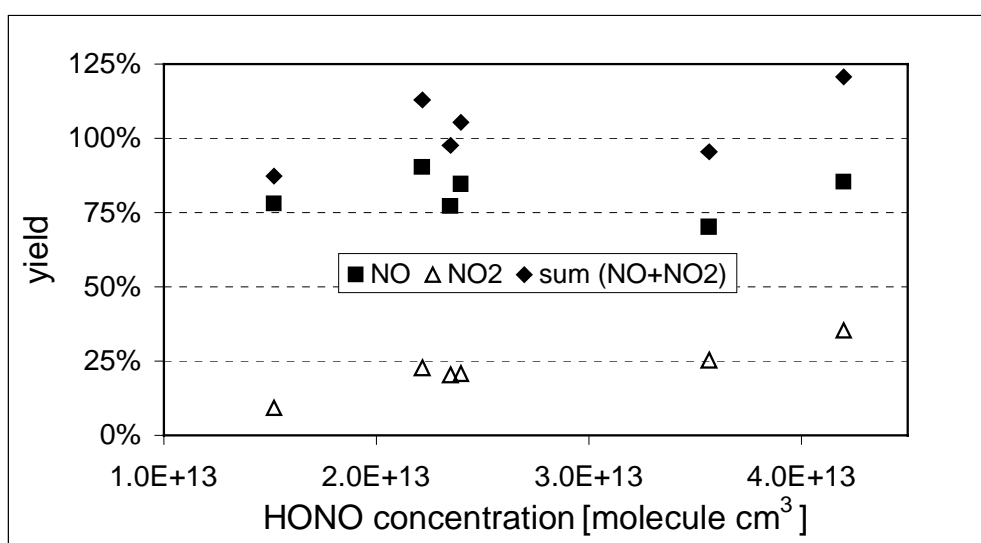


Figure 8.2.2: Relative yields of NO and NO₂ desorbed into the gas phase upon interaction of HONO on acetylene soot as a function of the HONO concentration; 1 mm diameter escape orifice, mean sample mass = 11.2 ± 1.4 mg, integrated over 3 minutes.

A possible explanation for the observed differences between acetylene and ‘black’ decane soot is that the decomposition of HONO does take place according to (R. 6.2.2b) postulated for ‘black’ decane soot but with the difference that the NO₂ fragments remain adsorbed on the surface of acetylene soot to a much smaller extent if at all, compared to ‘black’ decane soot. Therefore (R. 6.2.2b) can be modified for acetylene soot into (R. 6.2.2c):



However, some of the NO₂ that desorbs does re-adsorb again on the soot surface in reaction (R. 6.2.1). This is probably why the ratio of the yields of NO and NO₂ in the 1 mm reactor is 3:1 and not 1:1. We must take into account that NO₂ has a mean residence time of 29.4 seconds in the 1 mm reactor and therefore a high probability to collide with the surface of the soot sample where it may react according to (R. 6.2.1). This assumption is confirmed by the observation that the corresponding product ratio amounts to approximately 2:1 in the 14 mm diameter reactor where the residence time of NO₂ is only 0.24 seconds.

However, the developed reaction mechanism is of course a strong simplification and allows only qualitative conclusions. If secondary reactions or the competition between different species are becoming important the situation would be getting so complex that only computer modeling could give further insight.

8.3 Quantitative aspects of NO₂ uptake and product formation on acetylene soot.

A series of uptake measurements on varying soot masses have been performed in order to express the NO₂ uptake and the HONO release on a per mg basis. Figure 8.3.1. shows that the quantity of NO₂ taken up does not significantly increase beyond sample masses of approximately 10 mg. In addition, the difference between the uptake after 10 minutes (filled triangles) and 3 minutes (open triangles) is very small indicating that acetylene soot is to a large extent saturated already after 3 minutes. The corresponding curve for HONO formation on the other hand seems to attain constant values already at 7 to 8 milligrams. This suggests that HONO formed in deeper layers of the soot sample cannot desorb into the gas phase.

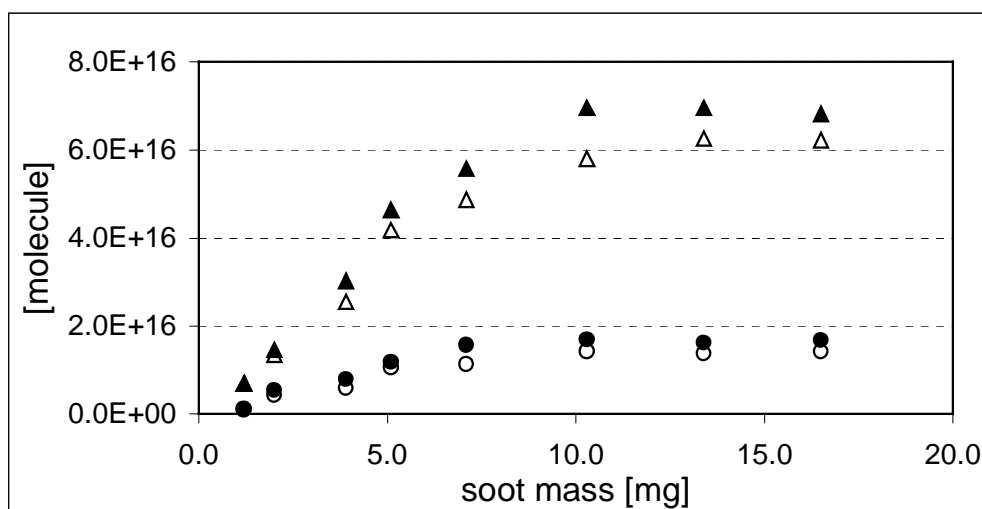


Figure 8.3.1: Mass dependence of NO₂ uptake (triangles) and formation of HONO (circles) on acetylene soot; yields were integrated over 3 minutes (open symbols) and 10 minutes (filled symbols), respectively, 4 mm diameter escape orifice, mean concentration 2.2×10^{12} molecule cm⁻³ corresponding to a partial pressure of 87 ppb.

Based on the results from Figure 8.3.1 we divide the absolute yields of our experiments by ten in order to obtain mass specific yields. Figure 8.3.2 shows that the mass specific uptake on acetylene soot is more than 10 times lower than on ‘black’ decane soot (see Figure 6.3.5). Even ‘grey’ decane soot that has an almost identical BET surface (see Table 5.1.1) has a mass specific NO₂ uptake that is roughly 6 times higher than that observed for acetylene soot (see Figure 6.2.4). On the other hand it is surprising that acetylene soot is very reactive towards HONO whereas ‘grey’ decane soot is not at all. Thus, it may be concluded that there must be different reactive sites that are responsible for the reactivity towards NO₂ and HONO, respectively.

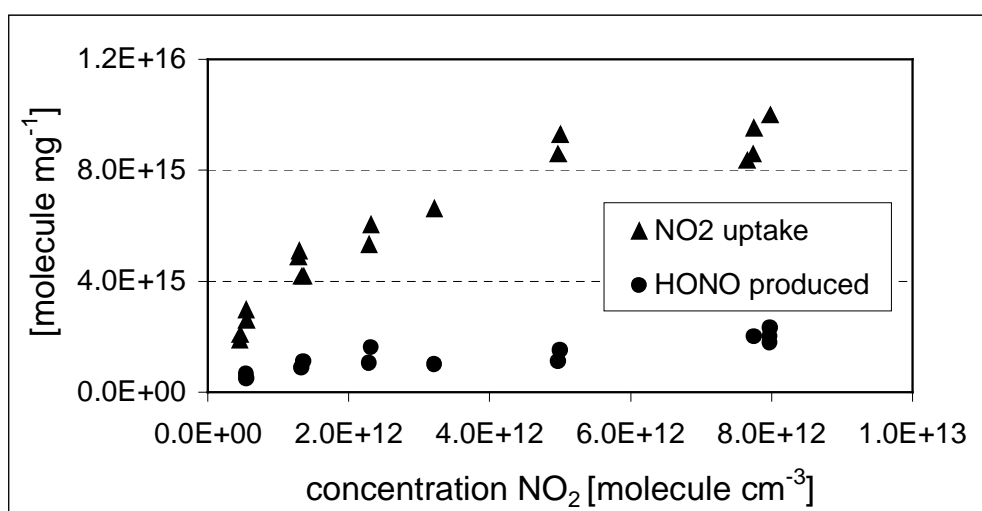


Figure 8.3.2: Mass specific NO₂ uptake and HONO formation on acetylene soot as a function of the NO₂ concentration; 4 mm diameter escape orifice, integrated over 3 minutes, all the samples had a geometric surface area of 19.6 cm²

8.4 Uptake kinetics of NO₂ and HONO on acetylene soot.

8.4.1 Uptake coefficients of NO₂ on acetylene soot.

Figure 8.4.1 shows the initial uptake coefficients (γ_0) that have been measured for NO₂ on acetylene soot. The maximum value amounts to approximately 0.09 measured for the lowest NO₂ concentration of 5.7×10^{10} molecule cm⁻³. However, γ_0 is decreasing with increasing NO₂ concentration and is only 0.012 at the maximum concentration of 7.7×10^{12} molecule cm⁻³.

A comparison with the corresponding uptake coefficients of ‘grey’ and ‘black’ decane soot as displayed in Figure 6.7.1 shows that the results for acetylene soot are not significantly different. On a first view this may be surprising as it has been noted that acetylene soot is much less reactive concerning the total amount of NO₂ taken up. The very first interaction of NO₂ on soot is according to our reaction scheme, its adsorption on surface site {S₁} (R. 6.2.1). As γ_0 considers only the very beginning of the interaction we can assume that its value mainly reflects the adsorption rate of NO₂ on {S₁}. The fact that γ_0 is almost identical for acetylene as well as for both types of decane soot means therefore that it is a rather unspecific process which is almost independent of the specific properties of the soot sample at hand. This observation has also been made by Tabor et al. [1994] who measured values for γ_0 on commercial soot types such as FW2, Printex 60 and Flame Soot 101 which did not significantly differ although these types have large differences in their BET surface areas, their elemental composition and their reactivity with NO₂.

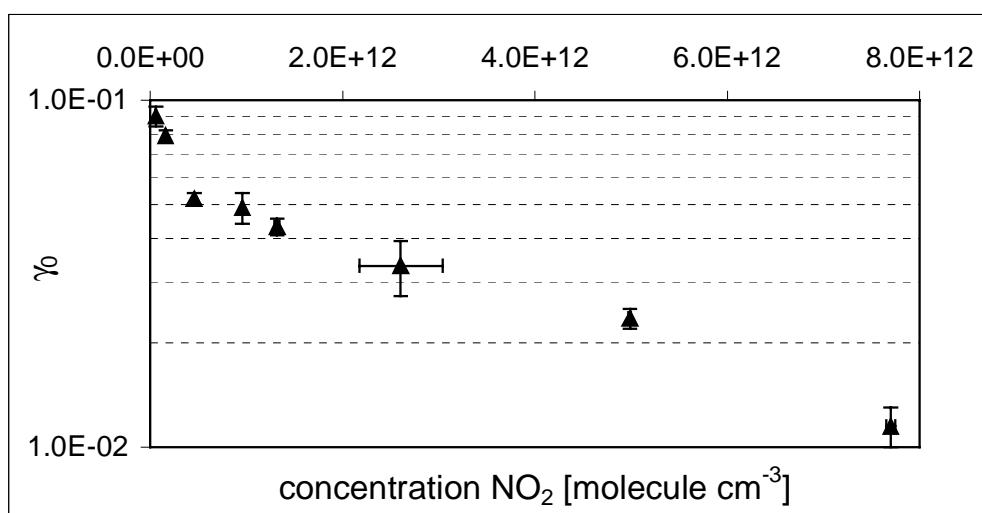


Figure 8.4.1: Initial uptake coefficient (γ_0) of NO₂ on acetylene soot as a function of the NO₂ concentration; 14 and 4 mm diameter escape orifices, mean sample weight 16.3 mg. γ_0 has been using the geometric surface area of the samples (19.6 cm²).

The uptake kinetics will, on the other, also be influenced by reactions (R. 6.2.2) and (R. 6.2.3) if one considers longer times of interaction. This is the reason why we calculated uptake coefficients based on signals observed after three minutes of interaction time. These values are related to the BET surface of acetylene soot as deeper sample layers are probed as well. It has been noted in Section 8.3 that approximately 10 milligram of the soot sample corresponding to a total surface area of 7200 cm² had been probed by NO₂ after three minutes of exposure time (see Table 5.1.1). Figure 8.4.2 shows $\gamma_{3\text{min}}$ of acetylene soot as a function of NO₂ taken up per unit surface area. A comparison with Figure 6.7.2 shows that the corresponding uptake coefficients of ‘black’ decane soot are quite similar. The difference is that the corresponding results for ‘black’ decane soot were obtained after 10 minutes of exposure time whereas an equal saturation at similar NO₂ concentrations is already observed after 3 minutes in the case of acetylene soot. This is in good agreement with the BET surface area which is smaller by a factor of three if acetylene is compared to ‘black’ decane soot.

We postulated in Section 6.2.2 that saturation effects observed in our experiments are primarily due to a temporal depletion of the adsorption site $\{S_1\}$. Figure 8.4.1 shows that initial uptake coefficients (γ_0) measured on acetylene soot have approximately the same values as those on ‘grey’ and ‘black’ decane soot. This suggests that the number of sites $\{S_1\}$ does not significantly vary among the three types of soot. If acetylene soot is nevertheless saturating much faster than decane soot then the reason may be in the fact that reactions (R. 6.2.2) and (R. 6.2.3) which convert $\{S_1 \bullet \text{NO}_2\}$ into $\{S_1\}$ are much slower on acetylene than on decane soot. Even if acetylene soot has a much slower kinetics towards NO₂ uptake than decane soot it could theoretically turn over the same absolute amounts of NO₂ as the two types of decane soot, albeit on a much longer time scale. The statement that acetylene soot is less reactive than decane soot is therefore based on its slower kinetics of NO₂ uptake.

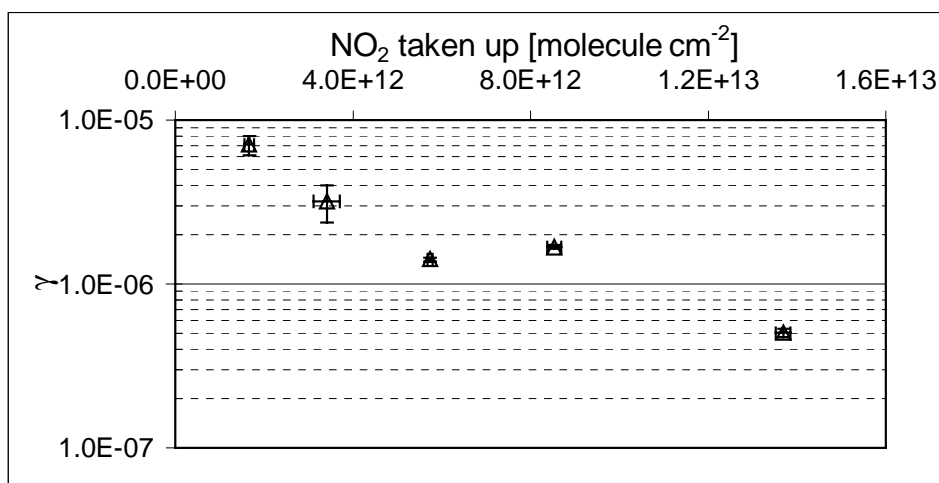


Figure 8.4.2: Uptake coefficient (γ) of NO₂ on acetylene soot depending on the amount of NO₂ taken up; 14 and 4 mm diameter escape orifices, mean sample weight 16.3 mg, time of exposure = 3 min., amount of NO₂ taken up is expressed relative to the BET surface area of the samples.

8.4.2 Uptake coefficients of HONO on acetylene soot.

The initial uptake coefficients (γ_0) of HONO on acetylene soot have the same characteristics as those measured on ‘black’ decane soot. Figure 8.4.3 shows that γ_0 obtained at low concentrations in the 14 mm escape orifice reactor is not so clearly decreasing with increasing HONO concentration as is generally observed for the uptake of NO₂ on soot. The mean value for γ_0 in the 14 mm escape orifice reactor is 0.03 and thus approximately the same as the corresponding value measured on ‘black’ decane soot. Only at higher concentrations, namely in the 4 mm escape orifice reactor, γ_0 is decreasing by a factor of two from 0.01 to 0.005 with increasing HONO

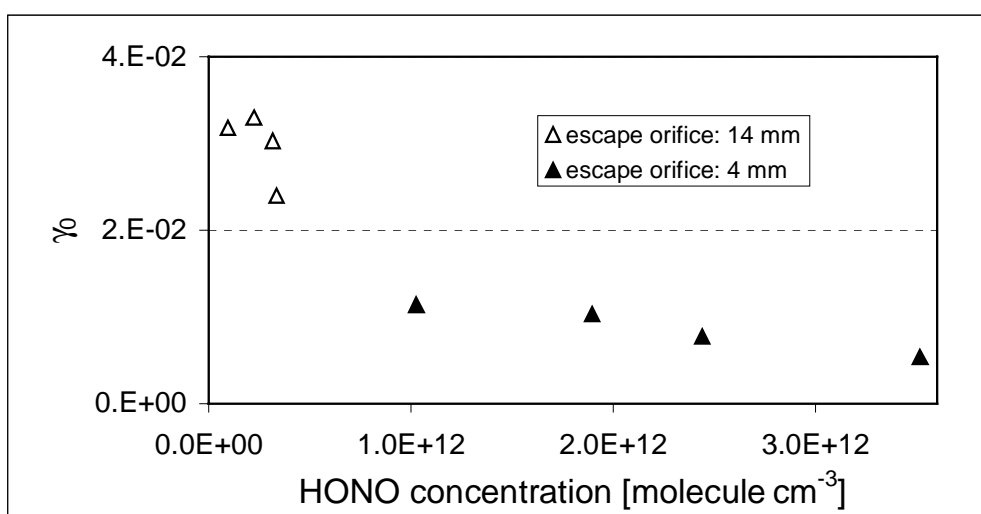


Figure 8.4.3: Initial uptake coefficient (γ_0) of HONO on acetylene soot as a function of the HONO concentration; mean sample weight 13.2 ± 2.4 mg. γ_0 has been calculated using the geometric surface area of the samples (19.6 cm²).

concentration. The corresponding values obtained in the 1 mm escape orifice reactor are ranging from 4.7×10^{-4} for a HONO concentration of 1.4×10^{17} molecule cm⁻³ down to 2.2×10^{-4} for a HONO concentration of 3.9×10^{17} molecule cm⁻³. However, one must keep in mind that γ_0 values obtained in the 1 mm escape orifice reactor are probably underestimated due to the adsorption/desorption artifact as discussed in Section 8.2. In comparison, the initial uptake coefficients of NO₂ on acetylene as well as on both types of decane soot are roughly three times higher than for the interaction of HONO with the same substrate. On the other hand, the uptake of HONO seems to saturate much slower in both cases. On ‘black’ decane soot as well as on acetylene soot it has been observed that the HONO uptake rate is approximately stable during the first 5 minutes (see Figures 6.3.4 and 8.2.1). However, because we do not know what the probing depth is after 5 minutes of interaction we make again the conservative assumption that HONO was in contact with the whole sample after five minutes. Doing the

same calculation as in the case of ‘black’ decane soot (see Section 6.8) a correction factor of roughly 500 is obtained by which γ_0 must be divided in order to get $\gamma_{5\text{min}}$. The results are of the same order of magnitude as in the case of ‘black’ decane soot and therefore the same conclusions may be reached as in Section 6.8: Acetylene soot shows stronger interactions with HONO than ‘Lamp black 101’ that has been examined by Kleffmann et al. [1999]. Therefore it is not surprising that even the lowest uptake coefficients that we have measured for acetylene soot are still roughly 20 times higher than those measured by Kleffmann et al. on ‘Lamp black 101’.

8.5 Heating of acetylene soot samples.

A limited series of experiments has been performed where samples of acetylene soot have been heated up after an exposure to NO₂ and HONO, respectively. The procedure was the same as for the corresponding experiments for ‘black’ and ‘grey’ decane soot described in Section 6.9.

The general features are shown in Figures 8.5.1 A), B) and C) and are quite similar to the corresponding traces of ‘black’ decane soot. The sample that has been exposed to NO₂ (Figure B)) clearly shows higher signals at m/e 28 and 30 at the beginning of the heating cycle compared to the reference sample at the same time. A small initial peak is observable at m/e 46 as well. It is striking that all the signals are significantly smaller than those observed for ‘black’ decane soot. However, this is not surprising as Figures 6.3.5 and 8.3.2 demonstrate that acetylene soot adsorbs much less NO₂ if it is exposed to the same concentration during the same time. A further difference is that the second peak at m/e 30 at t = 4 min is much less pronounced for acetylene than for ‘black’ decane soot. Accordingly, a peak at m/e 47 cannot be observed for acetylene soot at t = 4 min, either. In Section 6.9 we postulated that this peak at t = 4 min is caused by desorbing HONO. As acetylene soot produces only very small amounts of HONO upon interaction with NO₂ it is understandable that no corresponding signal is observed at t = 4 min. The interpretation of the initial peaks at m/e 28, 30 and 46 is the same as for ‘black’ decane soot. We attribute them to the desorption of NO (m/e 30), NO₂ (m/e 46) which originates from NO₂ that has been irreversibly adsorbed and to CO (m/e 28) which may be a product of the oxidation of some surface sites by NO₂.

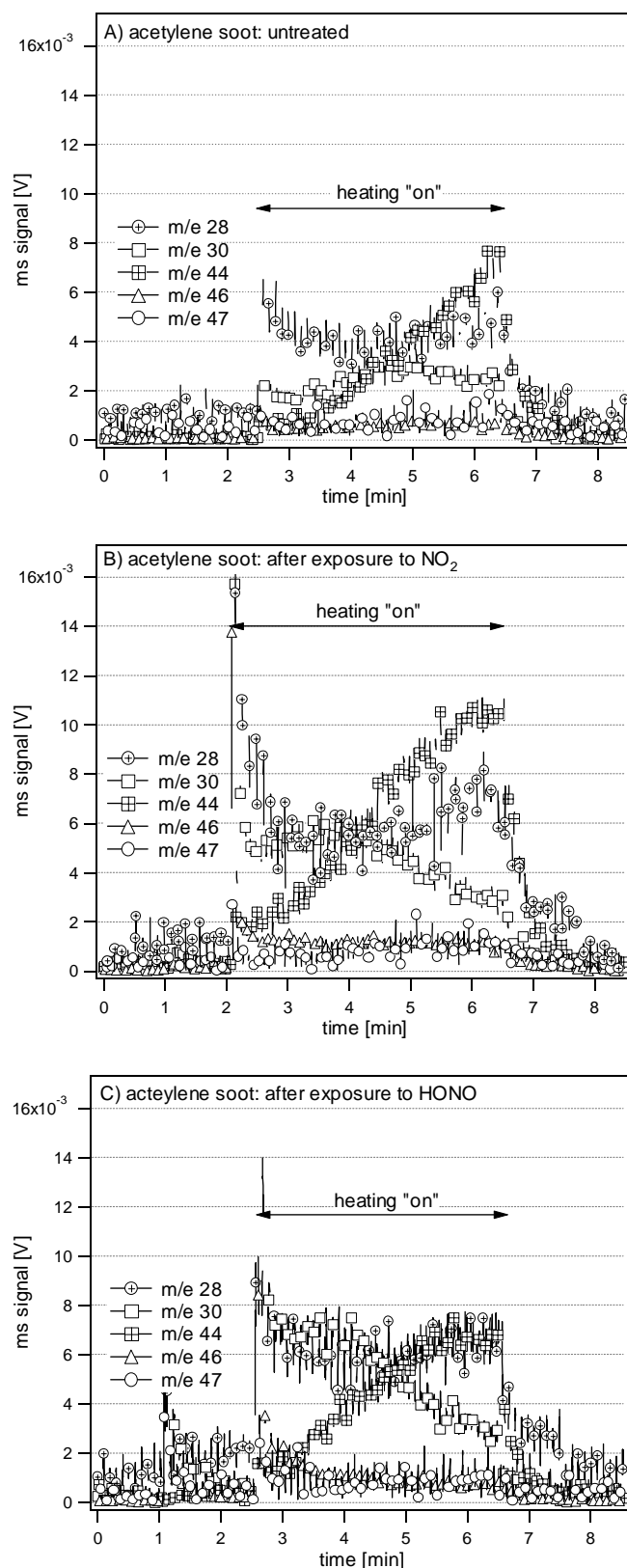


Figure 8.5.1: Heating of acetylene soot: A) untreated sample, mass = 10.7 mg; B) sample exposed to a NO₂ concentration of 2.3×10^{12} molecule cm⁻³ during 20 min. prior to heating, mass 10.4 mg; C) sample exposed to a HONO concentration of 2.2×10^{12} molecule cm⁻³ during 20 min. prior to heating, mass = 11.1 mg. All the heating experiments were performed at 4 mm diameter escape orifice.

Figure C) shows the MS signals as a function of time that are observed if acetylene soot is heated after it has been exposed to HONO. The differences to the reference sample (Figure A)) are quite small and much less pronounced than in the case of ‘black’ decane soot. This is to be expected as it has been shown in Figure 8.2.2 that approximately 100% of HONO that is adsorbed on acetylene soot may be found again in the gas phase as NO and NO₂ owing to the closed mass balance. Thus only small amounts of nitrogen are retained on the soot surface. As a consequence only a small signal at m/e 30 can be observed when acetylene is heated up in contrast to the situation in the case of ‘black’ decane. We have seen in Section 6.3.2 that only 50% of the amount of HONO that is taken up desorbs back into the gas phase as NO and NO₂. Thus, it is not surprising that in contrast to acetylene soot high amounts of NO and NO₂ are desorbed if ‘black’ decane soot is heated up after exposure to HONO (see Figure 6.9.2).

8.6 Aging of acetylene soot

Samples of acetylene soot have been stored in synthetic air for different time spans prior to their exposure to NO₂ in order to look whether deactivation of soot is occurring. The same procedure has been applied as for the corresponding experiments with ‘grey’ decane soot described in Section 6.10. Figure 8.6.1 shows that no deactivation is observable also for acetylene soot. The conclusion are therefore the same as for ‘grey’ decane soot: 1) The reactive compounds are not oxidized by molecular oxygen. 2) No significant desorption losses of the reactive compounds are occurring.

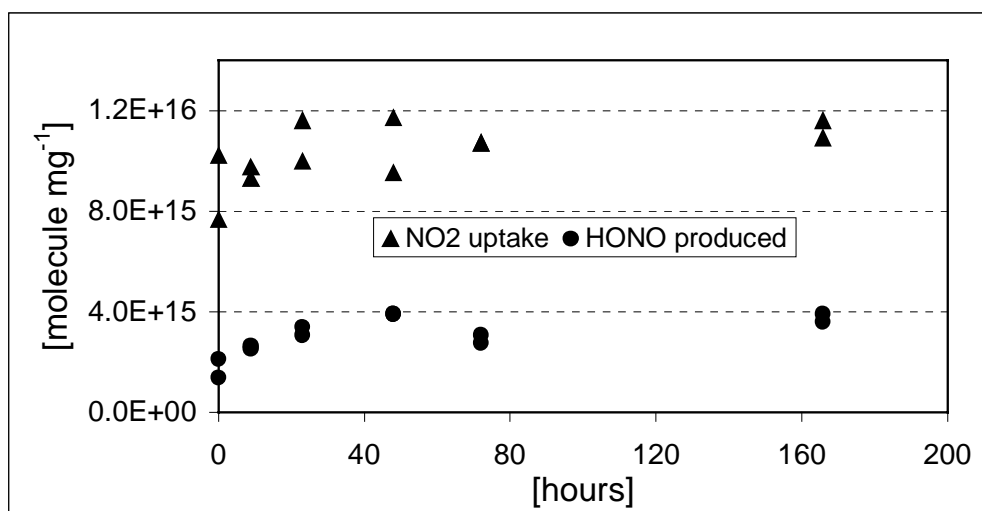


Figure 8.6.1: Reactivity of acetylene soot after different storage times in dry synthetic air integrated over 3 minutes; 4 mm diameter escape orifice, mean concentration = 8.1×10^{12} molecule cm⁻³, mean sample weight = 16.2 ± 0.2 mg.

9 Soxhlet extraction of 'grey' decane soot.

In reaction (R. 6.2.2) we postulated a reducing agent $\{C\sim H\}_{RED}$ which converts NO_2 into HONO. In order to examine whether this component is exerting its reactivity also in the absence of the three-dimensional soot skeleton Soxhlet extractions have been performed using benzene and tetrahydrofuran as solvents. The goal was to extract both the non-polar components using benzene as well as the polar components of the organic fraction of soot using THF. The dried soot residues were also examined in order to test how their reactivity has changed after the removal of a part of the organic fraction. A detailed description of the extraction can be found in Section 4.4.

Table 9.1 presents a survey of the results. The benzene-extraction is non reactive on both the polar as well as the non-polar support in a NO_2 uptake experiment. This is shown by a comparison of the values for NO_2 taken up with the corresponding values of the reference experiment where the bare sample support has been exposed. A very small NO_2 uptake is observed but no HONO has been measured when the THF-extraction is sprayed on a silica-gel support. However, Figure 9.1 shows that if the THF-extraction is sprayed on a non-polar C18 reverse phase support an instantaneous NO_2 -uptake accompanied by HONO formation is observed. The characteristics of the observed traces are very similar to those of the experiment on 'grey' decane soot shown in Figure 6.2.1: Large initial signals for NO_2 uptake and HONO desorption, respectively, are observed which subsequently slowly decrease. This decrease of the HONO signal is considerably slower in the case of the extraction compared to 'grey' decane soot. This is probably related to the properties of the three-dimensional structure of the support. The used silica-gel TLC-plates have a BET surface area of $550\text{ m}^2\text{ g}^{-1}$ which is considerably higher than the BET surface area of $72\text{ m}^2\text{ g}^{-1}$ that has been measured for 'grey' decane soot. Unfortunately there were no information available about the non-polar RP C18 plates but we assume that also these supports have a BET surface area considerably higher than the examined soot samples.

A further characteristic feature of the uptake experiments with THF-extractions is that the HONO signal does not instantaneously disappear when the sample plunger is lowered and the sample chamber sealed from the NO_2 flow. It is still observable at low intensity for an additional two to three minutes. This is in contrast to experiments performed with soot samples. The only explanation is that the reactive compounds are desorbing from the TLC-plate and adsorb on the walls of the Knudsen flow reactor where they also produce HONO until they are completely removed by pumping. The conclusion is that the reactive compounds have much weaker interactions with the C18 reverse phase coating than with the soot matrix.

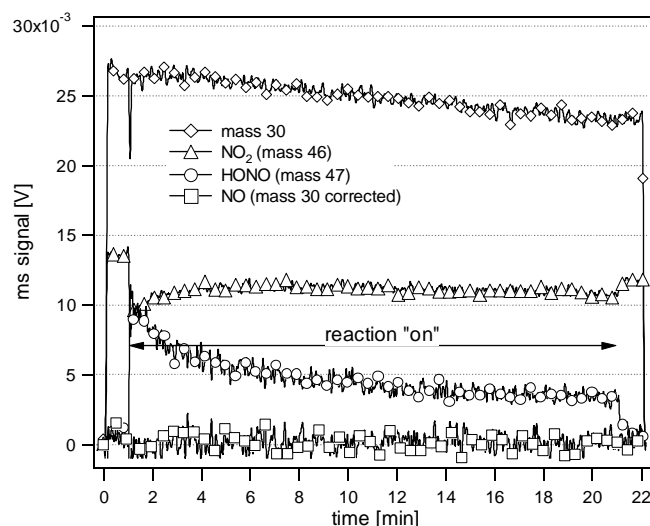


Figure 9.1: Raw data of an uptake experiment of NO_2 on the THF-extraction; sample support RP-C18, 14 mm diameter escape orifice, initial NO_2 concentration = 3.3×10^{11} molecule cm^{-3} .

Results in Table 9.1 show that the THF-extractions on the non-polar support follow the same trend as the samples of 'grey' decane soot presented Figure 6.2.2: HONO yields of 100% at low NO_2 concentrations and lower yields (50%) at higher concentrations of NO_2 . No NO has ever been observed in any uptake experiment. If we compare the amount of NO_2 taken up and HONO formed measured on a fresh sample of 'grey' decane soot with the sprayed THF-extraction we note that the reactivity is approximately the same. It therefore appears that both the adsorption site $\{S_1\}$ as well as the reducing agent $\{C\sim H\}_{\text{RED}}$ may readily be transferred using THF. This also holds for $\{S_2\}$ as up to 50% of NO_2 is irreversibly adsorbed without producing HONO at a high NO_2 concentration. Thus, the three reactants $\{S_1\}$, $\{S_2\}$ and $\{C\sim H\}_{\text{RED}}$ are rather polar species that are well soluble in THF and therefore transferable. Akhter et al. [1985] have shown in an extended extraction study that a large amount of different PAH's is present on the soot surface. On the other hand, they also showed that some functionalities such as carbonyl, ether or anhydride groups always remained in the bulk phase of soot. They stated that these groups are incorporated into the graphitic structure that is forming the 'backbone' of soot and therefore are not extractable.

	solvent	orifice Ø [mm]	support	NO ₂ concentration [molec cm ⁻³]	NO ₂ uptake [molec mg ⁻¹]	HONO [molec mg ⁻¹]	NO [molec mg ⁻¹]	HONO yield [%]	NO yield [%]
fresh	-	14	-	3.20E+11	2.30E+16	2.30E+16	n.o.	100	0
decane soot	-	4	-	2.49E+12	4.75E+16	3.60E+16	n.o.	76	-
extraction of decane soot*	benzene	14	silica gel	3.19E+11	n.o.	n.o.	n.o.	-	-
	benzene	14	RP C18	3.20E+11	8.50E+14	n.o.	n.o.	-	-
	THF	14	silica gel	1.88E+11	8.27E+14	n.o.	n.o.	-	-
	THF	14	RP C18	3.27E+11	1.84E+16	1.97E+16	n.o.	107	-
	THF	4	RP C18	2.48E+12	2.22E+16	1.14E+16	n.o.	51	-
decane soot after extraction (residue)	benzene	14	-	3.22E+11	5.97E+15	3.93E+15	4.30E+14	66	7
	benzene	4	-	2.48E+12	1.36E+16	6.54E+15	1.40E+15	48	10
	THF	14	-	3.27E+11	6.05E+15	3.90E+15	4.22E+14	64	7
	THF	4	-	2.55E+12	1.19E+16	5.04E+15	1.34E+15	42	11
reference exp.**	-	4	silica gel	1.41E+12	n.o.	n.o.	n.o.	-	-
reference exp.**	-	14	RP C18	3.19E+11	8.29E+14	n.o.	n.o.	-	-

Table 9.1: Reactivity of benzene and THF Soxhlet extractions of 'grey' decane soot and their residues, respectively.

*absolute numbers were divided by the factor $(x\text{ml}/200\text{ml}) \times 500\text{mg}$; the average volume of sprayed extraction amounted to 8 ml.

x = number of ml of the extract that have been sprayed on the sample support

200 ml = total volume of the extraction

500 mg = total soot mass that has been extracted

** absolute numbers of reference experiments were divided by 20 according the formula cited above $\{(8\text{ml}/200\text{ml}) \times 500\text{mg} = 20\text{mg}\}$

n.o. refers to: no measurable amounts observed.

The fact that the THF-extraction is only reactive on the non-polar C18 substrate as opposed to the silica-gel support is not easy to interpret. There may be interactions such as the formation of hydrogen-bonds or dipole-dipole interactions between the extracted species and the Si-OH groups of the substrate that result in the deactivation of the extracted species. If we look at the remaining reactivity on the soot after extraction using THF it became obvious that the reactive compounds had not been quantitatively extracted. Extracted soot is still forming HONO quantities that are corresponding to approximately 15% of that formed on fresh soot. In addition, it also forms NO. Therefore, the properties of 'grey' decane soot seem to approach those of 'black' decane soot after extraction. A possible interpretation of this observation is that the removal of a part of the organic fraction is setting free functionalities that are adsorbing and decomposing HONO. The residue of the benzene-extraction has almost the identical properties towards NO₂ uptake as the residue from the THF-extraction. HONO formation is reduced by a factor of 6 as well but in contrast to the extraction with THF there is no 'reactivity-transfer' to the solution as far as HONO formation is concerned. This could be explained if only part of the compounds that are contributing to HONO formation are extracted by benzene.

As discussed above it was observed that the reactive compounds in the THF-extraction are desorbing during the uptake experiment. We performed therefore a scan from m/e 40 to 300 during the sample preparation and following evacuation of a THF-extraction. Figure 9.2 shows that indeed many organic compounds are desorbing and can be detected. The signals at m/e 205 and 220 were the highest mass peaks that could be detected. However, even if we were sure that we had measurable MS signals of the HONO producing species it would be a real challenge to unambiguously identify the compound or the group of compounds in question.

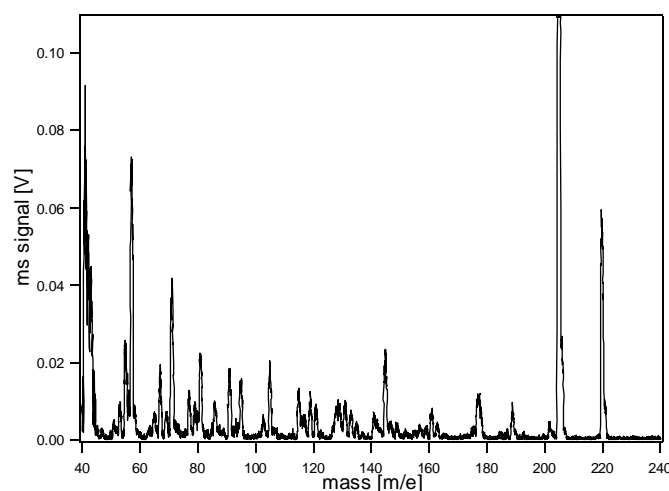


Figure 9.2: Scan of the desorbing fraction of a THF-extraction sprayed on RP C18; 14 mm diameter escape orifice.

10 A model compound: 1,2,10-trihydroxyanthracene.

10.1 1,2,10-trihydroxyanthracene condensed on thinlayer chromatography plates.

Arens et al. [1999] recently proposed phenolic compounds such as 2,7-dihydroxynaphthalene or 1,2,10-trihydroxyanthracene as possible structures responsible for the reactivity of soot concerning HONO formation. They showed that pure solid surfaces of 1,2,10-trihydroxyanthracene are converting NO_2 into HONO with reaction probabilities between 10^{-6} and 10^{-5} . Using a wetted wall flow tube reactor they were able to claim that aqueous solutions of 2,7-dihydroxynaphthalene are also reactive, the more the higher the pH. Based on this observation they postulated a reaction mechanism in which the deprotonated species, that is the phenolate ion, serves as electron donor in order to reduce NO_2 to NO_2^- . This nitrite ion subsequently reacts with a proton to form HONO.

Owing to its low vapor pressure we have chosen 1,2,10-trihydroxyanthracene (techn. 85%, Aldrich) in order to investigate how this compound behaves in our experiments. Its structure is displayed in Figure 10.1.1. Fine coatings on different types of thinlayer chromatography plates were produced by condensing 1,2,10-trihydroxyanthracene from the vapor phase. The mass of the deposited compound was not measurable using our balance and may therefore have been lower than 300 μg . A detailed description of the procedure is given in Section 4.5.

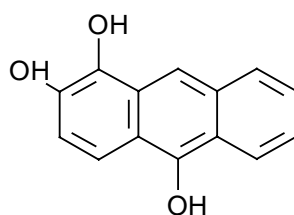


Figure 10.1.1: 1,2,10-trihydroxyanthracene.

Figure 10.1.2a shows an uptake experiment of NO_2 on 1,2,10-trihydroxyanthracene that has been deposited on a silica-gel plate. The instantaneous decrease of signals at m/e 30 and 46 after the opening of the sample chamber clearly indicates that NO_2 is taken up. γ_0 is calculated to be approximately 0.01. On the other hand, there is only a very small increase of m/e 47 which means that only very small amounts of HONO are released. The signal at m/e 30 was also recorded but did not show a significant increase upon exposure of the sample. We therefore have omitted it in the Graph. Figure 10.1.2b shows the signals that are obtained if

the sample from Figure 10.1.2a is heated up after its exposure to NO_2 . Signals at m/e 47 and 30 instantaneously appear and steadily increase. A signal of lower intensity is also recorded at m/e 46. If we assume that m/e 46 represents NO_2 and subtract its contribution to m/e 30 from the MS signal intensity then the ratio m/e 47/30 corresponds to the fragmentation pattern of HONO which is approximately 9:1. An additional verification for the observation of HONO comes from heating up an untreated sample of 1,2,10-trihydroxyanthracene. In this case no significant MS signals at m/e 30, 46 and 47 have been observed. If we evaluate the integrals of the MS signals then we see that 1.04×10^{17} molecules or 35% were desorbed as HONO upon heating in relation to 2.95×10^{17} NO_2 molecules that had been taken up. However, this yield only indicates a lower limit of HONO formation as the heating procedure was prematurely halted in order to avoid the overheating of the reactor.

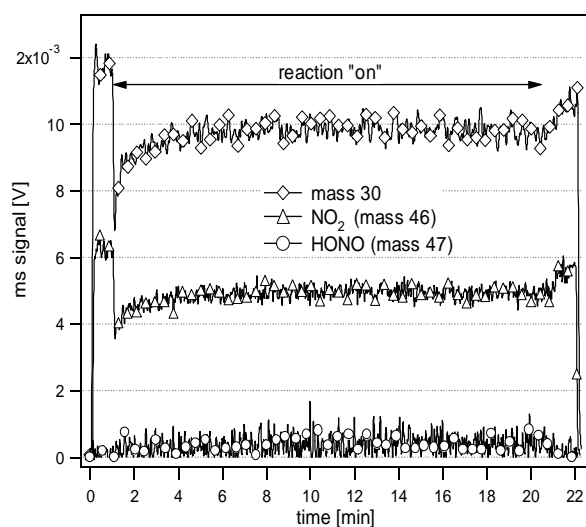


Figure 10.1.2a: Uptake of NO_2 on 1,2,10-trihydroxyanthracene condensed on silica-gel; 4mm diameter escape orifice, initial NO_2 concentration = 1.3×10^{12} molecule cm^{-3} , geometric surface area of the sample = 10.5 cm^2 .

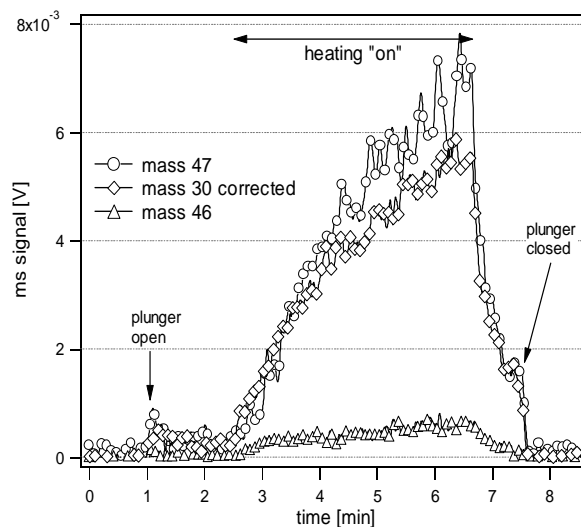


Figure 10.1.2b: Heating of the sample from Figure 10.1.2a after its exposure to NO_2 ; 14 mm diameter escape orifice, geometric surface area of the sample = 10.5 cm^2 , trace at m/e 47 is ten times amplified in relation to m/e 30.

The conclusion is that significant amounts of HONO have been formed *in situ* which however did not desorb during the experiment shown in Figure 10.1.2a. Apparently, HONO is strongly adsorbed on the polar silica gel support or on 1,2,10-trihydroxyanthracene itself. In contrast to ‘black’ decane soot where the adsorbed HONO is decomposing it does not react on

the coated silica gel support but may be desorbed upon heating. A possible explanation why HONO is not decomposing on the silica gel plate is that the high BET surface area of the support ($550 \text{ m}^2 \text{ g}^{-1}$) is leading to lower surface densities of HONO. This would slow down the second order reaction rate of the HONO disproportionation reaction according to (R. 6.2.2b).

Figure 10.1.3 presents an example for the same type of experiment as shown in Figure 10.1.2a with the only difference that 1,2,10-trihydroxyanthracene has been condensed onto a RP C18 plate. The initial uptake (γ_0) amounts to approximately 0.02 and is therefore even higher than for the 1,2,10-trihydroxyanthracene/silica-gel system. However, the fact that the sample is fast saturating results in a total uptake of NO_2 of only 4.9×10^{16} molecules which is approximately 6 times less than measured for the corresponding experiment performed on silica gel. On the other hand, a small HONO peak is observable. The conclusion is that 1,2,10-trihydroxyanthracene condensed on a RP-C18 plate has an adsorption rate for NO_2 that saturates much faster if compared to the system on silica gel. Consequently, the amount of HONO desorbed must also be lower but the small quantity that is produced already desorbs at ambient temperature.

The comparison between the depositions of 1,2,10-trihydroxyanthracene on silica-gel and RP-C18 demonstrates in an impressive way that the interaction between the reactive compound and the sample support is a key factor that influences its reactivity towards NO_2 . The fact that these interactions really change the chemical reactivity and environment of 1,2,10-trihydroxyanthracene may even be seen with the naked eye: Whereas its deposition on silica-gel leads to a red colored TLC plate the corresponding deposition on RP-C18 is yellow. First trials to examine the two types of coating using diffuse reflectance infra-red Fourier transform spectroscopy (DRIFTS) failed due to limiting sensitivity. It is therefore difficult to speculate which form of the molecule would be reactive and which one is not. Silica-gel represents a very polar surface and formation of hydrogen bonds with 1,2,10-trihydroxyanthracene are probable. It is therefore conceivable that this leads to Si-OH/1,2,10-trihydroxyanthracene-complexes with weakened hydrogen bonds with which the NO_2 could interact. On the other hand, also H_2O that is present on silica-gel in much higher amounts compared to RP-C18 may play an important role. However, these are speculations that cannot be confirmed without further spectroscopic information. In addition, one must keep in mind that the used batch of 1,2,10-trihydroxyanthracene had a purity of only 85%. Therefore, it may be conceivable that an isomer or any other contamination is responsible for the observed reactivity rather than the title compound 1,2,10-trihydroxyanthracene.

Finally, we do not want to hide that the observations discussed in this Section seem to be in contradiction with the results of the extraction study presented in Section 9 where we have seen that the THF-extraction was only reactive on the non-polar RP-C18 plates, whereas the deposition on silica-gel was almost non-reactive. However, the extraction represents a

strong perturbation of the system containing probably hundreds of different compounds. A direct comparison with the experiments presented in this Section may therefore not be possible.

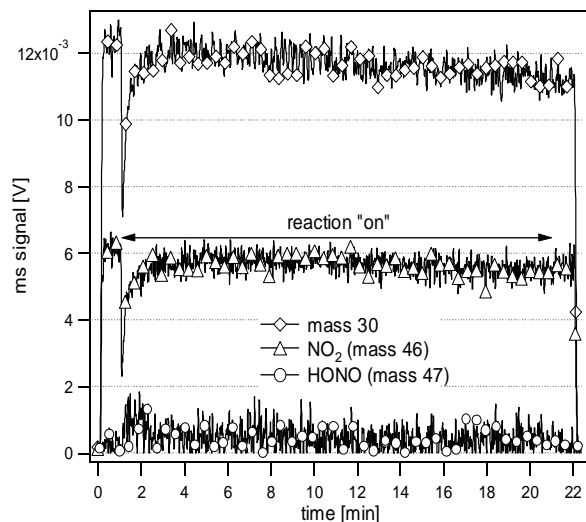


Figure 10.1.3: Uptake of NO_2 on 1,2,10-trihydroxyanthracene condensed on RP-C18; 4mm diameter escape orifice, initial NO_2 concentration = 1.3×10^{12} molecule cm^{-3} , geometric surface area of the sample 10.5 cm^2 .

10.2 1,2,10-trihydroxyanthracene condensed on soot samples.

Another series of samples has been prepared akin to Section 10.1 but with the difference that 1,2,10-trihydroxyanthracene has been deposited on both types of decane soot as well as on acetylene soot. The deposited amounts of 1,2,10-trihydroxyanthracene were not measurable using our balance and may therefore have been lower than $300 \mu\text{g}$. The goal was to examine how the chemical environment of the soot surface would influence the reactivity of 1,2,10-trihydroxyanthracene.

Figure 10.2.1a shows the uptake of NO_2 on a treated ‘black’ decane soot sample. A comparison with Figure 10.2.1b representing the corresponding reference experiment performed on a untreated ‘black’ decane soot sample demonstrates in a impressive manner the impact of the 1,2,10-trihydroxyanthracene deposition. We have seen in Section 6.3.1 that fresh ‘black’ decane soot that is exposed to NO_2 does not desorb significant amounts of HONO but leads to decomposition into NO and $\{\text{NO}_2\}$ according to (R. 6.2.2b). Figure 10.2.1a shows that the product spectrum changes dramatically after the deposition of 1,2,10-trihydroxyanthracene. 96% of NO_2 that has been taken up could be found again as HONO whereas no significant amounts of NO could be measured. If the mass specific NO_2 uptake are compared it can be stated that 5.3×10^{16} molecule mg^{-1} have been adsorbed on the treated

sample whereas only 2.7×10^{16} molecule mg^{-1} have been adsorbed on the untreated reference sample during the 20 minutes of exposure time. These numbers are based on the knowledge of Section 6.3.3 that from a sample with 19.6 cm^2 surface area only an upper layer corresponding to 12 mg is probed by NO_2 during the first 20 minutes of exposure. The treated sample had the same thickness i. e. the same mass of soot per unit of surface area but a total surface of only 10.5 cm^2 . Accordingly, the probed soot mass amounts only to 6.4 mg ($=12\text{mg} \times \{10.5\text{cm}^2/19.6\text{cm}^2\}$). This is why the absolute yields have been divided by 12 for the untreated and by 6.4 for the treated 'black' decane soot sample, respectively. Therefore we may claim that the deposition of 1,2,10-trihydroxyanthracene doubled the uptake rate of 'black' decane soot for NO_2 . Another effect of the presence of 1,2,10-trihydroxyanthracene on 'black' decane soot is that it loses its property to retain and decompose HONO according to reaction (R. 6.2.2b). One could say that 'black' decane soot was converted into 'grey' decane soot by deposition of 1,2,10-trihydroxyanthracene. The conclusion is that the chemical environment of 'black' decane soot activates the capacity of 1,2,10-trihydroxyanthracene to form HONO. It is therefore conceivable that phenolic compounds are part of the reactants of the organic fraction of soot that form HONO upon interaction with NO_2 .

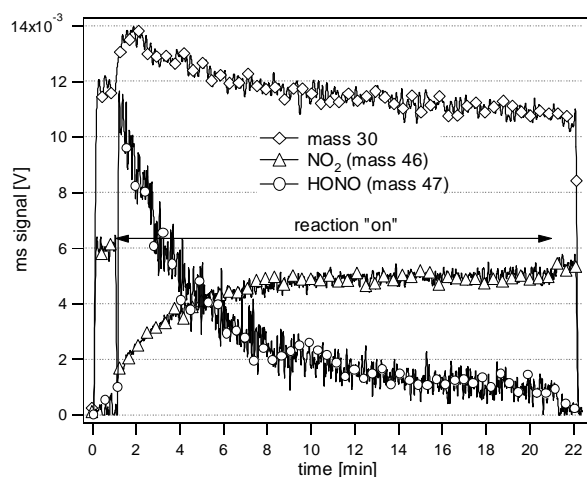


Figure 10.2.1a: Uptake of NO_2 on 'black' decane soot treated with 1,2,10-trihydroxyanthracene; 4mm diameter escape orifice, initial NO_2 concentration = 1.4×10^{12} molecule cm^{-3} , geometric surface area of the sample 10.5 cm^2 , sample mass = 10.0 mg, significant desorption of NO was not observed.

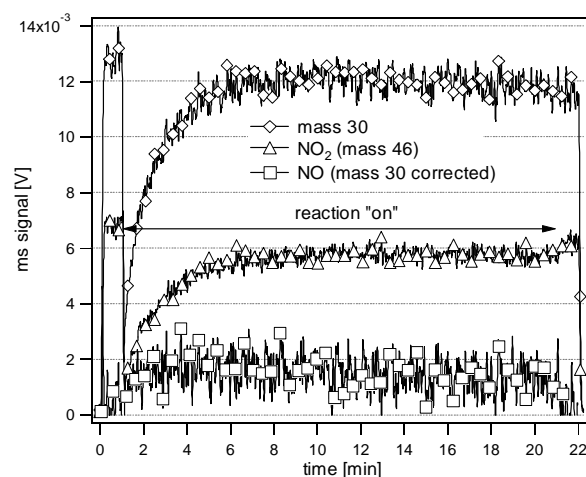


Figure 10.2.1b: Uptake of NO_2 on untreated 'black' decane soot; 4mm diameter escape orifice, initial NO_2 concentration = 1.5×10^{12} molecule cm^{-3} , geometric surface area of the sample 19.6 cm^2 , sample mass = 19.4 mg.

1,2,10-trihydroxyanthracene has also been condensed on samples of 'grey' decane and acetylene soot. All the samples had approximately a mass of 10 mg and a geometric surface area of 10.5 cm². Upon exposure to concentrations of NO₂ of 1.4×10¹² molecule cm⁻³ they revealed the same characteristics as treated 'black' decane soot shown in Figure 10.2.1a, which means increased uptake of NO₂ and a relative HONO yield of nearly 100%. The mass specific NO₂ uptake increased for 'grey' decane soot in comparison to untreated samples by a factor of approximately 1.25. This is not so much as in the case of 'black' decane soot because 'grey' decane soot already has very high uptake rates at lower concentrations of NO₂ (see Figure 6.2.4). For ten milligrams of similarly treated acetylene soot on the other hand a mass specific uptake of NO₂ of 7.7×10¹⁶ molecule mg⁻¹ has been measured after 20 minutes of exposure time which is larger by more than a factor of ten compared to an untreated sample (see Figure 8.3.2).

The conclusion is that adsorbed 1,2,10-trihydroxyanthracene may exert high reactivity concerning HONO formation on very different types on soot. This suggests that soot particles that initially do not produce HONO could subsequently be activated by condensation of phenolic or other compounds that are also present in the polluted troposphere.

11 Summary and outlook.

11.1 Summary of main results.

In the present study two different types of decane soot have been produced. It has been shown that the air/fuel ratio of the diffusion flame is a key parameter influencing the reactivity of the soot towards NO_2 . Whereas soot from a rich flame ('grey' decane soot) leads to HONO with yields up to 100% upon interaction with NO_2 , only small amounts of HONO, but significant amounts of NO are formed in the presence of soot originating from a lean flame ('black' decane soot). A reaction mechanism has been developed showing that NO_2 is initially converted to HONO by a redox reaction in a first step. HONO produced in this way is subsequently either quantitatively desorbed into the gas phase on 'grey' decane soot or it decomposes to a large extent in a disproportionation reaction on 'black' decane soot. The products of disproportionation are NO, which is instantaneously desorbed into the gas phase and NO_2 , which undergoes secondary reactions. In addition to the HONO producing pathway there is a reaction channel that leads to adsorption of NO_2 for both types of soot which is irreversible on the time scale of our standard experiments.

For 'grey' decane soot a maximum NO_2 uptake of 6×10^{16} molecule mg^{-1} has been measured at a NO_2 concentration of 8×10^{12} molecule cm^{-3} and an interaction time of 20 minutes. Under the same conditions approximately 4.2×10^{16} molecule mg^{-1} HONO have been formed which corresponds to a relative yield of 70%. The uptake of NO_2 on 'black' decane soot under the same experimental conditions is considerably higher, namely 1.2×10^{17} molecule mg^{-1} . The NO_2 taken up is converted into NO in a yield of 33%. The relative NO yield is approaching 50% at higher NO_2 concentrations. Neither the samples of 'grey' nor of 'black' decane soot completely saturated after the standard exposure time of 20 minutes.

Saturation effects that are occurring on the time scale of our experiments are primarily caused by saturation of adsorption sites and not by the depletion of the reducing agent. It seems that the fraction of NO_2 that is irreversibly adsorbed is blocking part of the surface sites where NO_2 is initially adsorbed.

Uptake coefficients γ have initial values of up to 0.1 for both types of soot. However, with increasing uptake of NO_2 γ is decreasing. After a NO_2 consumption of approximately 8×10^{13} molecule cm^{-2} , which corresponds to 13% of a formal monolayer, γ drops to values of 3×10^{-7} for 'grey' decane soot and 6×10^{-7} for 'black' decane soot, respectively. Furthermore,

our results show that the rate of initial uptake is the rate limiting step of the NO₂/soot interaction mechanism.

Experiments where 'black' decane soot has been exposed to a flow of HONO revealed that it readily decomposes into NO and NO₂. For HONO concentrations above 3.3×10^{11} molecule cm⁻³ a total product yield of 50%, whereof 40% NO and 10% NO₂, has been observed.

The initial uptake coefficient (γ_0) for HONO on 'black' decane soot did not show clear saturation effects but varied randomly in the concentration range from 1.2×10^{12} to 5.9×10^{12} molecule cm⁻³. The average value measured at these concentrations was equal to 0.027. Saturation effects occurred only at higher HONO concentrations in the 4 mm escape orifice reactor where γ_0 clearly decreased with increasing HONO concentration. A further characteristic feature of the interaction of HONO with 'black' decane soot is that the uptake rate for a given concentration remained constant during the total time of exposure, typically lasting 5 minutes. The strong interaction of HONO with 'black' decane soot shows that soot is not only a potential source, but also a potential sink of HONO. On the other hand, no significant uptake could be observed when 'grey' decane soot was exposed to HONO. This is consistent with the observation that NO₂ is converted to HONO at yields of up to 100%.

Results that have been obtained for hexane soot are qualitatively and quantitatively identical. This shows that - at least for alkane fuels - the soot properties are much more influenced by the air/fuel ratio during combustion than by the type of fuel.

Acetylene soot is an additional type of soot that has been examined. The results for the initial uptake coefficients were basically the same as for 'grey' and 'black' decane soot, that is maximum values of 0.1 which decrease with increasing concentrations of NO₂. This similarity holds only for the first few seconds of interaction because acetylene soot saturates much faster than 'grey' and 'black' decane soot with continuous exposure. The acetylene samples are generally almost completely saturated after only three minutes of exposure. This results in a maximum NO₂ uptake of approximately 9.0×10^{15} molecule mg⁻¹ which is more than a factor of ten lower than observed on 'black' decane soot. HONO yields relative to NO₂ taken up were at most 57% in the 14 mm escape orifice reactor and abruptly dropped to 20% in the 4 mm escape orifice reactor. The reason for this may be the fact that HONO, once desorbed from the soot sample, has a mean residence time of 1.8 seconds in the 4 mm escape orifice reactor which is approximately 8 times longer than in the 14 mm escape orifice reactor. The probability of HONO to collide with the surface of the soot sample and be decomposed is therefore also 8 times higher for the 4 mm diameter escape orifice compared to the 14 mm diameter escape orifice reactor. NO has not been observed as a product in the NO₂/acetylene

soot interaction probably because the flows were below the detection limit of approximately 8.0×10^{13} molecule s^{-1} .

That HONO decomposes on acetylene soot has been shown in experiments where acetylene samples were exposed to a small flow of HONO. In contrast to 'black' decane soot product yields of up to 100% have been observed in the case of HONO decomposition on acetylene soot, whereof 75% NO and 25% NO₂. One explanation for this may be that in the case of acetylene soot both fragments of the HONO disproportionation are released into the gas phase whereas 'black' decane soot only desorbs NO but retains the N(IV) species. However, not all of the observations made for acetylene soot can be explained in a satisfactory manner for the moment.

Soxhlet extractions of 'grey' decane soot that have been performed with tetrahydrofuran also produced HONO upon interaction with NO₂. This shows that the active reactants are not part of the graphitic soot backbone but are extractable, rather polar compounds of the organic fraction of soot. This assumption is supported by the observation that the corresponding benzene extraction is not reactive in relation to NO₂ uptake and HONO formation.

However, the THF-extraction was only reactive when sprayed on a non-polar RP C18 thinlayer chromatography plate. The same extraction sprayed on silica-gel almost did not interact with NO₂.

1,2,10-trihydroxyanthracene has been examined as a model compound for its potential to produce HONO upon interaction with NO₂. When deposited on silica-gel it adsorbed NO₂ in similar quantities as 'grey' and 'black' decane soot. HONO, on the other hand, was only formed and detected when the sample support was heated up subsequent to the uptake experiment. When 1,2,10-trihydroxyanthracene was deposited on RP C18 only a very small uptake of NO₂ with a small concomitant peak of HONO was observed.

11.2 Conclusions and outlook.

We think that based on the main results cited above some major conclusions may be drawn which in turn may provide the starting point for further studies:

- The combustion conditions are a key parameter influencing to a large extent the reactivity of soot particles with respect to NO₂, HONO and most probably also other gaseous pollutants. When results from laboratory studies shall be extrapolated to atmospheric conditions it is therefore absolutely necessary to establish a connection to real atmospheric

soot particles. In other terms, one has to answer the question whether laboratory generated soot samples are representative of those found in the atmosphere. A first attempt has been made in this work by comparing the obtained results with those from studies which have been performed under conditions that were closer to atmospheric conditions, for instance studies in flow reactors with suspended aerosols. In this context we claim that the data base concerning the reactivity of soot particles generated by other than Diesel engines is quite small. Corresponding data would be desirable also for soot particles generated by biomass burning or jet engines.

- Based on the experiments with ‘black’ decane soot we have postulated that HONO is produced in large amounts but decomposes to a large extent before it can leave the bulk sample and be detected. It is conceivable that the net rate of HONO formation is higher if the same soot mass were present as an aerosol in a smog chamber, because the collision rate of HONO on the aerosol particles could be smaller compared to the situation in a bulk soot sample. However, it would need computational simulation or a corresponding experiment performed in a smog chamber to test this hypothesis. This would also help to answer the question to which extent the results of bulk phase experiments are transferable to smog chamber conditions.
- The kinetic observations of our experiments suggest that saturation of the soot sample is not caused by the depletion of the reducing agent $\{C\}_{RED}$ but more probably by a depletion of the adsorption site $\{S_1\}$. This result may be very important because a reactivation of soot by the liberation of these adsorption sites is conceivable whereas a regeneration by ‘re-reduction’ of the consumed reducing sites $\{C\}_{RED}$ is not probable in an oxidative environment such as the terrestrial atmosphere. Further experiments should therefore examine whether soot may be regenerated by treatments such as UV irradiation or heating.
- Experiments performed using Soxhlet extractions showed that the HONO producing reactants are part of the organic fraction of soot. The extractions have the advantage that they can be examined by analytical techniques such as FTIR, GC-MS or HPLC. Although first attempts to characterize the extractions using DRIFTS failed due to a lack of sensitivity, further efforts will surely help to identify the HONO producing functionalities. This could be done by examining the extractions before and after exposure to NO_2 .
- Both experiments performed with Soxhlet extractions as well as with 1,2,10-trihydroxyanthracene as a model compound revealed that their potential to produce HONO strongly depends on the nature of the sample support onto which the reducing compounds are condensed. It is therefore very important to know more about the chemical interactions

with the sample support which activate or deactivate the reducing compounds. This is the reason why the DRIFTS-technique has been used in a first attempt as a characterization technique because it allows for the in situ examination of condensed films.

- The condensation of 1,2,10-trihydroxyanthracene on soot samples led to a considerable increase in HONO formation for all types of soot that have been examined. Even 'black' decane soot emitted large amounts of HONO corresponding to a yield close to 100% relative to NO₂ taken up. This observation suggests that soot and other particles may be activated with respect to HONO formation subsequent to their emission by condensation of organic pollutants that originate from other sources.
- An identification of the HONO producing functional groups also would facilitate the identification of other HONO sources. Some parallels may be drawn between the combustion processes in a diffusion flame and the formation of secondary organic aerosols. Both processes are to a large extent influenced by the reactivity of OH radicals. The atmospheric oxidation of organic compounds leading to organic aerosols may therefore be regarded as some kind of 'cold combustion' which may lead to similar functionalities as in the organic fraction of soot. Therefore, we consider an examination of secondary organic aerosols as potential HONO producing agents to be very promising.

References

- Akhter M. S., A. R. Chughtai and D. M. Smith, *Appl. Spectrosc.*, 1985, **39**, 143.
- Akhter M. S., A. R. Chughtai and D. M. Smith, *Appl. Spectrosc.*, 1985, **39**, 154.
- Allegrini, I., A. Febo and C. Perrino, in *Physico-chemical behaviour of atmospheric pollutants*, ed. G. Restelli and G. Angelletti, European Commission, Report No. EUR 15609/1, pp. 293-299, 1994.
- Allen J. O., N.M. Dookeran, K.A. Smith and A. F. Sarofim, *Environ. Sci. Technol.*, 1996, **30**, 1023.
- Ammann, M., M. Kalberer, D. T. Jost, L. Tobler, E. Rössler, D. Piguet, H. W. Gäggeler and U. Baltensperger, *Nature*, 1998, **395**, 157.
- Andrés-Hernández, M. D., J. Notholt, J. Hjorth and O. Schrems, *Atmos. Environ.*, 1996, **30**, 175.
- Appel, B. R., A. M. Winer, Y. Tokiwa and H. W. Biermann, *Atmos. Environ., Part A*, 1990, **24**, 611.
- Arens, F., M. Ammann, E. Rössler, H. W. Gäggeler and U. Baltensperger, EC/Eurotrac-2 Joint Workshop, September 20-22, 1999 Aachen, Germany.
- Aumont, B., S. Madronich, M. Ammann, M. Kalberer, U. Baltensperger, D. Hauglustaine and F. Brocheton, *J. Geophys. Res.*, 1999, **104**, 1729.
- Barnard J. A. and C. F. Cullis 1962, *Eighth Symposium on Combustion*. The Combustion Institute, Pittsburgh, PA, USA, p. 481.
- Barrie, L. A. et al., *Atmos. Environ.*, 1981, **15**, 1407.
- Baumgärtner, M., E. Bock and R. Conrad, *Chemosphere*, 1992, **24**, 1943.
- Bekki, S., *J. Geophys. Res.*, 1997, **102**, 10'751.
- Bidleman, T. F. and W. T. Foreman, in *Sources and fates of aquatic pollutants*; Eds, R. A. Hites and S. J. Eisenreich, *Advances in Chemistry* 216; American Chemical Society, Washington D.C., 1987; pp 27-56.
- Blake D. F. and K. Kato, *J. Geophys. Res.*, 1995, **100**, 7195.
- Boehm, H. P., in *Advances in catalysis and related subjects*, 1966, **16**, p 179.
- Bongartz, A., J. Kames, F. Welter and U. Schurath, *J. Phys. Chem.*, 1991, **95**, 1076.
- Bongartz, A., J. Kames, U. Schurath, C. George, P. Mirabel and J. L. Ponche, *J. Atmos. Chem.*, 1994, **18**, 149.
- Brunauer, S., *The Adsorption of Gases and Vapours*, Oxford University Press, 1944.
- Caloz, F., F. F. Fenter, K. D. Tabor and M. J. Rossi, *Rev. Sci. Instrum.*, 1997, **68**, 3172.
- Caloz, F., *Laboratory Kinetic Studies of Heterogeneous Processes Relevant to the Marine Troposphere*, Thesis n° 1628, EPFL, Lausanne, 1997.
- Calvert, J. G. and W. R. Stockwell, *Can. J. Chem.*, 1983, **61**, 983.
- Calvert, J. G., G. Yarwood and A. M. Dunker, *Res. Chem. Intermed.*, 1994, **20**, 463.

- Chaix L., H. van den Bergh and M.J. Rossi, *J. Phys. Chem.*, 1998, **102**, 10300.
- Choi, W. and M.-T. Leu, *J. Phys. Chem. A*, 1998, **102**, 7618.
- Chuan R. L. and D. C. Woods, *Geophys. Res. Lett.*, 1984, **11**, 553.
- Chughtai, A. R., S. A. Gordon and D. M. Smith, *Carbon*, 1994, **32**, 405.
- Cooke, W. F., S. G. Jennings and T. G. Spain, *J. Geophys. Res.*, 1997, **102**, 25339.
- Dollimore, D. and G. R. Heal, *J. Colloid Interface Sci.*, 1973, **42**, 233. Fabian, P., and B. Kärcher, *Phys. Chem. of the Earth*, 1997, **22**, 503.
- Farman, J. C., B. G. Gardiner and J. D. Shanklin, *Nature*, 1985, **315**, 207.
- Febo, A. and C. Perrino, *Atmos. Environ.*, 1991, **25A**, 1055.
- Febo, A., C. Perrino and I. Allegrini, *Atmos. Environ.*, 1996, **30**, 3599.
- Finlayson-Pitts, B. J. and J. N. Pitts, *Atmospheric Chemistry*, John Wiley and Sons, New York, 1986.
- Gerecke, A., A. Thielmann, L. Gutzwiller and M.J. Rossi, *Geophys. Res. Lett.*, 1998, **25**, 2453.
- Golden D. M., G. N. Spokes and S. W. Benson, *Angew. Chem.*, 1973, **14**, 602.
- Griffiths, J. F. and J. A. Barnard, *Flame and Combustion*, Blackie Academic & Professional, London, 1995.
- Haefliger O. P., T. D. Bucheli, R. Zenobi, *Analusis*, 1999, **27**, 337.
- Harling, D. F. and F. A. Heckman, *Mater. Plast. Elastomeri*, 1969, **35**, 80.
- Harrison, R. M. and A.-M. Kitto, *Atmos. Environ.*, 1994, **28**, 1089.
- Harrison, R. M., J. D. Peak and G. M. Collins, *J. Geophys. Res.*, 1996, **101**, 14429.
- Hauglustaine, D. A., B. A. Ridley, S. Solomon, P. G. Hess and S. Madronich, *Geophys. Res. Lett.*, 1996, **23**, 2609.
- Heddrich, A., thesis, Fachbereich 7: Physikalische Chemie und Chemische Technologie, Technische Hochschule Darmstadt, 1986.
- Heidenreich, R. D., W. M. Hess and L. L. Ban, *J. Appl. Cryst.*, 1968, **1**, 1.
- Herbst, G., *Brennstoff Chemie*, 1968, **44**, 217.
- Heywood, J.B., *Internal Engine Combustion Fundamentals*, McGraw-Hill, New York 1988.
- Hofmann, U. and G. Ohlerich, *Angew. Chem.*, 1950, **62**, 16.
- Homann, K. H., *Angew. Chem. Internat. Edit.*, 1968, **7**, 414.
- Homann, K. H., *Comb. and Flame*, 1967, 265.
- Intergovernmental Panel on Climate Change, (IPCC), *Climate Change 1994: Radiative Forcing of Climate Change and an Evaluation of the IPCC IS92 Emission Scenarios*. Cambridge University Press, Cambridge, UK, 1995.
- Intergovernmental Panel on Climate Change, (IPCC), *Climate change 1995: The science of climate change*, Eds. J. T. Houghton et al., Cambridge University Press, Cambridge UK, 1996.
- Jenkin, M. E., R. A. Cox and D. J. Williams, *Atmos. Environ.*, 1988, **22**, 487.

- Junkermann, W. and T. Ibusuki, *Atmos. Environ.*, 1992, **26**, 3099.
- Kalberer, M., M. Ammann, F. Arens, H. W. Gäggeler and U. Baltensperger, *J. Geophys. Res.*, 1999, **104**, 13825.
- Kalberer, M., M. Ammann, H. W. Gäggeler and U. Baltensperger, 1999, *Atmospheric Environment*, **33**, 2815.
- Kärcher, B. T., T. Peter, U. M. Biermann and U. Schumann, *J. Atmos. Sci.*, 1996, **53**, 3066.
- Kessler, C. and U. Platt, in *Physico-chemical behaviour of atmospheric pollutants*, ed. B. Versino and G. Angeletti, Dordrecht, 1984, pp 412-422.
- Killus, J. P. and G. Z. Whitten, *Int. J. Chem. Kin.*, 1990, **22**, 547.
- Kleffmann J., K. H. Becker, M. Lackhoff and P. Wiesen, *Phys. Chem. Chem. Phys.*, 1999, **1**, 5443.
- Kleffmann, J., K. H. Becker and P. Wiesen, *Atmos. Environ.*, 1998, **32**, 2721.
- Koehler, B. G., V. T. Nicholson, H. G. Roe and E. S. Whitney, *J. Geophys. Res.*, 1999, **104**, 5507.
- König, J., W. Funke, E. Balfanz, G. Grosch and F. Potts, *Atmos. Environ.*, 1980, **14**, 609.
- Kunugi, M. and H. Jinno, 1967, *Eleventh Symposium on Combustion*. The Combustion Institute, Pittsburgh, PA, USA, p. 257.
- Lammel, G. and D. Perner, *J. Aerosol Sci.*, 1988, **19**, 1199.
- Lammel, G. and J. N. Cape, *Chem. Soc. Rev.*, 1996, 361.
- Lammel, G., D. Perner and P. Warneck, in *Physico-chemical behaviour of atmospheric pollutants*, ed. G. Restelli and G. Angeletti, Dordrecht, 1990, pp 469-476.
- Larichev, M. N., J. N. Rouzaud and J. C. Petit, XXV. General Assembly, European Geophysical Society, Nice, 2000.
- Leighton, P. A., *Photochemistry of air pollution*, Academic Press, New York, 1961.
- Li, S.-M., *J. Geophys. Res.*, 1994, **99**, 25'469.
- Longfellow C. A., A. R. Ravishankara and D. R. Hanson, *J. Geophys. Res.*, 1999, **104**, 13833.
- McMillen, D. F. and D. M. Golden, *Ann. Rev. Phys. Chem.*, 1982, **33**, 493.
- Medalia, A. I. and D. Rivin, in *Characterization of powder surfaces*, ed Parfitt, G. D. and K. S. W. Sing, Academic Press, San Francisco, 1976, pp 279-351.
- Minnis, P., D. F. Young and D. P. Garber, *Geophys. Res. Lett.*, 1998, **25**, 1157.
- Nash, T., *Tellus*, 1974, **26**, 175.
- National Research Council, *Rethinking the National Ozone Problem in Urban and Regional Air Pollution*, National Academy Press, Washington, DC, 1991.
- Neftel, A., A. Blatter, R. Hesterberg and T. Staffelbach, *Atmos. Environ.*, 1996, **30**, 3017.
- Parfitt, G. D. and K. S. W. Sing, *Characterization of Powder Surfaces*, Academic Press, San Francisco, 1976.
- Penner, J. E., H. Eddleman and T. Novakov, *Atmos. Environ.*, 1993, **27**, 1277.
- Perner, D. and U. Platt, *Geophys. Res. Lett.*, 1979, **6**, 917.

- Perner, D., C. Kessler and U. Platt, in *Monitoring of gaseous pollutants by tunable diode lasers*, ed. R. Grisar, H. Preier, G. Schmidtke and G. Restelli, Dordrecht, 1987, pp. 116-119.
- Platt, U., D. Perner, G. W. Harris, A. M. Winer and J. N. Pitts Jr., *Nature*, 1980, **285**, 312.
- Pósfai, M., J. R. Anderson and P. R. Buseck, *J. Geophys. Res.*, 1999, **104**, 21685.
- Pueschel R. F., D. F. Blake, K. G. Snetsinger, A. D. A. Hansen, S. Verma and K. Kato, *Geophys. Res. Lett.*, 1992, **19**, 1659.
- Pueschel R.F., K. A. Boering, S. Verma, S. D. Howard, G. V. Ferry, J. Goodman, D. A. Allen and P. Hamill, *J. Geophys. Res.*, 1997, **102**, 13113.
- Rahn, K. A. and R. Mc Caffrey, *Ann. N.Y. Acad. Sci.*, 1980, **338**, 486.
- Rogaski, C. A., D. M. Golden and L. R. Williams, *Geophys. Res. Lett.*, 1997, **24**, 381.
- Rondón, A. and E. Sanhueza, *Tellus*, 1989, **41B**, 474.
- Rowland , F. S. and M. J. Molina, *Chemical and Engineering News*, 1994, **72**, 8.
- Sakamaki, S., S. Hatakeyama and H. Akimoto, *Int. J. Chem. Kin.*, 1983, **15**, 1013.
- Schlesinger, R. B., *Inhal. Toxicol.*, 1995, **7**, 99.
- Schuetzle D., F. S.-C. Lee, T. J. Prater and S. B. Tejada, *Int. J. Envir. Analyt. Chem.*, 1981, **9**, 93.
- Seinfeld, J. H. and S. N. Pandis, *Atmospheric chemistry and physics; from air pollution to climate change*, John Wiley & Sons, Inc., New York, 1997.
- Sheridan, P.J., R. C. Schnell, J. D. Dahl, J. F. Boatman and D. M. Garvey, *Atmos. Environ., Part A*, 1993, **27**, 1169.
- Smith, S. R. and A. S. Gordon, *J. Phys. Chem.*, 1957, **60**, 759.
- Staffelbach, T. et al., *J. Geophys. Res.*, 1997, **102**, 23'345.
- Staffelbach, T., A. Neftel and L. W. Horowitz, *J. Geophys. Res.*, 1997, **102**, 23'363.
- Strom, J. and S. Ohlsson, *J. Geophys. Res.*, 1998, 103, 11'355.
- Svensson, R., E. Ljungström and O. Lindquist, *Atmos. Environ*, 1987, **21**, 1529.
- Tabor, K., L. Gutzwiller and M. J. Rossi, *J. Phys. Chem.*, 1994, **98**, 6172.
- Ullmann, *Enzyklopädie d. techn. Chemie*, vol. 14, forth edition, Verlag Chemie, Weinheim, 1977, p 595.
- Wagner, H. G., *Soot formation in Combustion*, Bericht 22, Max-Planck-Institut für Strömungsforschung, Göttingen, 1978.
- Warnatz, J., 1984, *Twentieth Symposium on Combustion*. The Combustion Institute, Pittsburgh, PA, USA, p. 845.
- Zeldovich, Y. B., P. Y. Sadvnikov and D. A. Frank-Kamenetskii, *Oxidation of Nitrogen in Combustion*, M. Shelef, Trans., Academy of Sciences of USSR, Institute of Chemical Physics, Moscow-Leningrad 1947.

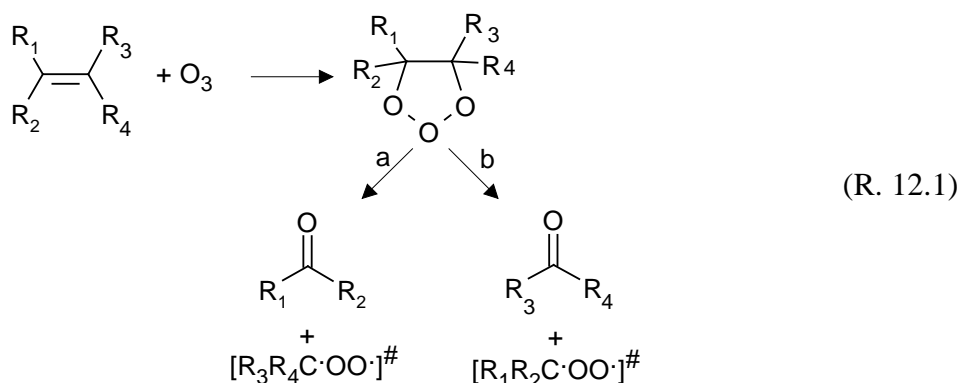
Part B

**The degradation of hydrocarbons initiated by the OH radical:
atmospheric oxidation.**

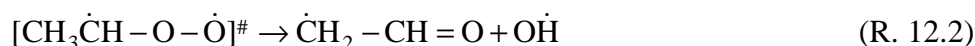
12 The OH radical in the troposphere.

12.1 Sources and concentrations of the OH radical in the troposphere.

In Section 2.2.1 it has already been mentioned that the OH radical is a key species in the day-time chemistry of the troposphere as the lifetime of most hydrocarbons depends on their reaction rate with OH. Main sources of the OH radical is the photodissociation of O₃ (R. 2.2.1-2). Additional sources are the photodissociation of HONO and formaldehyde in the presence of NO (R. 2.2.5-7) and HONO (R. 2.2.8). Recently, some attention has also been paid to the interaction of O₃ with alkenes (R. 12.1). The addition of O₃ to the olefinic double bond leads to an unstable molozonide which may decompose into two pathways in order to produce each time a carbonyl product and a Criegee biradical. Atkinson and Carter [1984] estimated that the relative importance of pathways a and b are generally comparable.



The Criegee biradical can either be collisionally stabilized or undergo different types of unimolecular decomposition. If there is a hydrogen atom in position 5 with respect to the oxygen radical then a 1,5-H shift may lead to the formation of an OH radical. (R. 12.2) shows this decomposition using the peroxyethyl biradical as an example.



Hydroxyl radicals have been observed to be formed from alkene/O₃ reactions, sometimes with close to unity yield (1 molecule of OH per 1 molecule of alkene reacted) [Atkinson and Aschmann, 1993, Rickard et al, 1999]. In contrast to the reaction mechanisms mentioned above (R. 12.1-2) may also contribute to the formation of OH radicals at night-time. In addition, it has been estimated that (R. 12.1-2) may be more important for OH production than the photolysis of O₃ at rural sites with terpene emitting coniferous forests [Paulson, et al., 1999].

The tropospheric concentrations of the OH radical show a strong diurnal variation. This is expected as most of the OH producing mechanisms are based on photodissociation reactions. Even the rates of (R. 12.1-2) are often faster at day-time as the O₃ concentration may decrease above all in urban areas with strong NO sources by up to a factor of 7 at night-time [Seinfeld and Pandis, 1997]. The resulting OH concentrations are ranging from day-time maximum concentrations of several 10⁶ molecule cm⁻³ down to concentrations of ≤ 2×10⁵ molecule cm⁻³. Since direct measurements of such small OH concentrations are still very difficult, they are often inferred from calculations based on the observed lifetimes of compounds such as methyl chloroform (CH₃CCl₃) or methane that are known to be consumed almost exclusively by the OH radical. Ehhalt et al. [1991] calculated, based on the methane oxidation cycle an OH concentration of 4.3×10⁶ molecule cm⁻³ for a rural site in Germany. Direct measurements that have been performed by Holland et al. [1995] using LIF gave very similar results for the day-time concentration of OH radicals at a rural site in the North East of Germany. Generally, the measured and calculated OH concentrations in the troposphere indicate the following ranges:

Day-time (summer)	5-10×10 ⁶ molecule cm ⁻³
Day-time (winter)	1-5×10 ⁶ molecule cm ⁻³
Night-time	≤ 2×10 ⁵ molecule cm ⁻³

12.2 The role of the OH radical in the O₃ producing photooxidation cycle.

A rough survey on the reactions producing O₃ through photooxidation has already been given in Figure 2.2.1. A more detailed scheme is shown in Figure 12.1. The most important reactions may be divided into four categories: 1) The production of the OH radical, 2) The oxidation of CO and hydrocarbons by the OH radical, 3) The ‘recycling’ of the OH radical and 4) The formation of metastable ‘reservoir’ species containing RO₂ and NO_x.

Box n° 1 contains the photodissociation reactions of O₃ as the most important day-time source of OH radicals. O(¹D) atoms are only generated at wavelengths ≤ 320 nm [DeMore et al., 1987]. Approximately 10% of these atoms react under typical tropospheric conditions with H₂O to produce two OH radicals. The mechanism consists of an insertion of the O(¹D) atom into the H₂O molecule to form a highly excited [H-O-O-H][#] intermediate which readily decomposes into two OH radicals. The remaining 90% of the O(¹D) atoms are usually quenched back by molecular oxygen or nitrogen to ground-state atomic oxygen O(³P). Most of the O(³P) atoms will then recombine with O₂ to reform O₃.

The OH radical, unlike many molecular fragments formed from carbon-containing molecules, is unreactive towards oxygen, and, as a result, it survives to react with most atmospheric trace species. These reactions are summarized in box n° 2. Carbon monoxide (CO) is the most important fuel for oxidation initiated by OH attack in unpolluted rural air. The OH/CO interaction leads to the formation of a hydroperoxyl radical (HO_2). The same product may be obtained if OH attacks a hydrocarbon (RH).

Box n° 3 reveals that HO_2 is a key species as it may react with O_3 or NO to reform an OH radical. The result is that the oxidant OH is continuously replaced as the chain carrier of the oxidation reactions. It therefore maintains the rate of degradation of the hydrocarbons and formation of ozone.

However, box n° 4 shows that there are also reactions which may stop the self sustaining photooxidation cycle. First and foremost, temperatures below 18 °C support the formation of so called reservoir species containing RO_2 and NO_x . This means that RO_2 and NO_x which are necessary for the formation of HO_2 and ozone are temporarily deactivated which makes the photooxidation cycle collapse.

Another possibility to form reservoir species is the reaction of OH with NO_2 to form nitric acid (HNO_3). This reaction mainly occurs in polluted urban areas with high NO_2 levels. Finally, at high concentrations of hydrocarbons and especially at low levels of NO_x such as in pristine areas RO_2 is forced to react with itself or with HO_2 in order to produce stable products such as acids, alcohols or hydroperoxides.

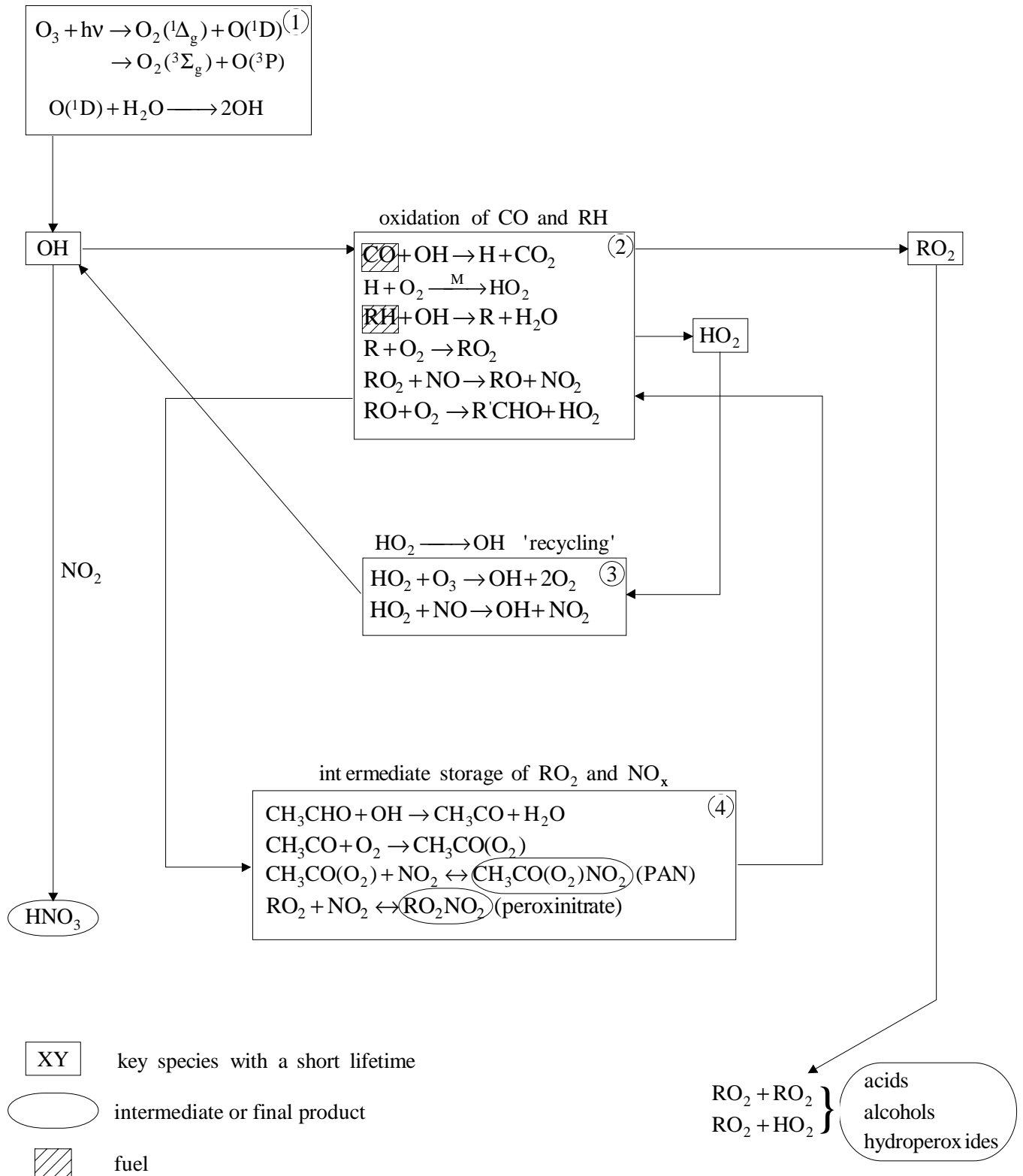


Figure 12.1: Scheme of the photooxidation cycle with OH as the key species.

possibility of thermal decomposition of the bond in α -position, especially for tertiary alkoxy radicals. The products are a carbonyl and an alkyl free radical.

Figure 12.2 shows furthermore that these reaction pathways are valid for both alkanes as well as alkenes. The difference is that the initial alkyl radical is formed by H-atom abstraction in the case of an alkane whereas OH addition is the key reaction in the case of an alkene.

OH addition is also the dominating initial step for reactions with aromatic compounds as is shown in Figure 12.3 using toluene as an example. The H-atom abstraction from the methyl group is also a possibility but approximately 9 times less probable than the OH addition. The addition can take place in all the positions relative to the methyl group but the ortho-position is energetically favored [Andino et al., 1996]. The OH adduct I may then react in two possible ways with O_2 . O_2 may abstract a H-atom to form ortho-cresol or it may undergo an addition reaction to form an unsaturated peroxy radical II. Alkyl peroxy radicals generally react with NO to form alkoxy radicals (as shown in Figure 12.2). Unsaturated peroxy radicals in contrast, are believed to cyclicize, forming bicyclic radicals such as III. After bicyclic radical formation, O_2 rapidly adds to the radical, forming a bicyclic peroxy radical IV. This radical is then expected to react with NO to form a bicyclic oxy radical V and NO_2 . Finally, repeated β -scission and further decomposition reactions occur and lead to products such as glyoxal, methylglyoxal or 1,4-butenedial etc. according to our reaction scheme. Of course, Figure 12.3 only represents one of several possible degradation pathways.

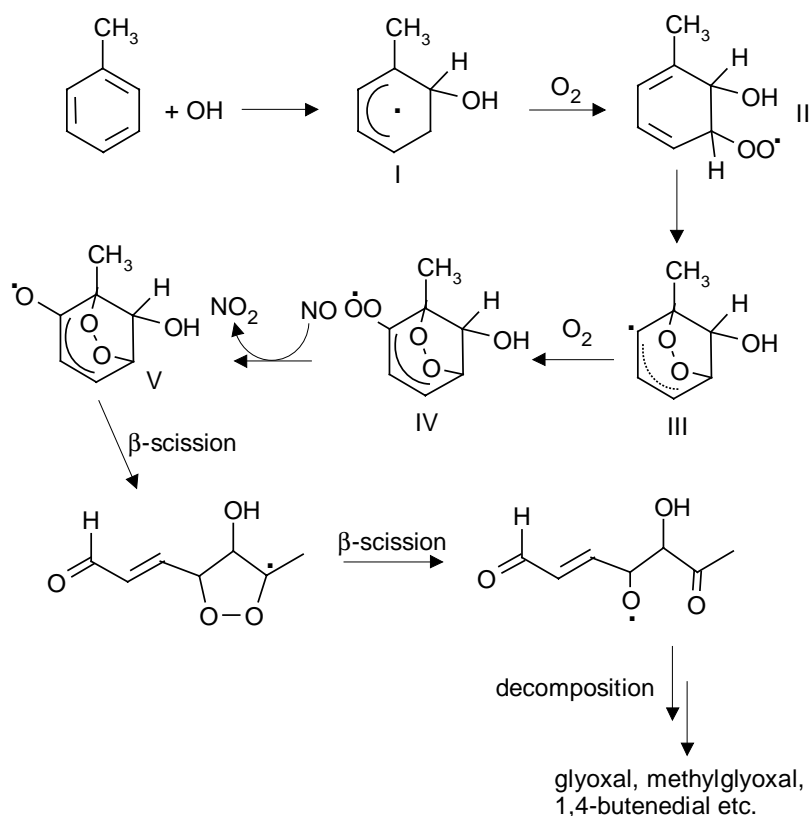


Figure 12.3: Possible degradation pathway of toluene after addition of an OH radical.

12.4 Laboratory techniques measuring the kinetics of OH radical reactions.

The experimental techniques used to study the kinetics of OH radical reactions with organics can be separated into two methods, namely, absolute and relative rate constant techniques.

12.4.1 Absolute measurement techniques.

The discharge flow system represents an absolute measurement technique. OH radicals are produced in a discharge region and flow along a tube designed to allow the addition of reactants downstream. Detection of the OH radical is typically accomplished by resonance absorption (RA), resonance fluorescence (RF), electron paramagnetic resonance (EPR), mass spectroscopy (MS), laser magnetic resonance (LMR), or laser induced fluorescence (LIF). OH concentrations between 10^9 up to 10^{14} molecule cm^{-3} are employed depending on the detection technique. The OH concentration is usually measured as a function of the reaction time with the organics which is varied using a movable injection system. The reactant concentration is often in large excess over the initial OH radical concentration which simplifies the observed decay of the OH concentration to pseudo first order kinetics.

An often used system to generate OH radicals consists of a microwave discharge of H_2 in He. The generated H-atoms react according to (R. 12.3) with NO_2 to form OH radicals.



The total pressures in such systems is generally restricted to ≤ 10 Torr in order to achieve plug-flow conditions, a special case of laminar flow. Hence, extrapolation of the results to atmospheric pressure may give rise to significant uncertainties.

A further absolute measurement technique is flash photolysis. A flash of a OH radical resonance lamp (microwave discharge of H_2O in He or Ar at approximately 1 Torr total pressure) or of a laser produces a pulse of OH radicals whose decay may be recorded measuring the absorption with a second laser set at 308 nm or using the resonance fluorescence technique. OH radicals are typically produced from the pulsed photodissociation of H_2O or HNO_3 . Other methods of producing OH radicals, such as the photolysis of $\text{N}_2\text{O}/\text{H}_2$, O_3/H_2 and NO_2/H_2 mixtures, are also used, where OH radicals are formed from the reaction of $\text{O}(^1\text{D})$ atoms with H_2 .

Slow flow systems are routinely used so that photolysis and secondary reaction products do not build up in the reaction cell. This system has also the advantage that losses of the reactants to the wall are minimized.

A major advantage of the flash or laser photolysis is that a pressure range up to atmospheric pressure or higher can be employed, making this technique of great utility for investigating atmospherically important reactions. Further details of the flash photolysis resonance fluorescence technique may be taken from a recent study that has been published by Koch et al. in 1997.

12.4.2 Relative rate techniques.

Numerous methods have been employed to obtain relative rate constant data for the reactions of OH radicals with organic compounds. The major general technique used is that of monitoring the relative rates of the disappearance of two or more organic compounds in chemical systems containing OH radicals. Clearly, in order to derive meaningful rate constant data from this experimental technique, either the organic loss processes must be solely due to reaction with the OH radical or, if another loss process (e. g. photolysis) occurs, its effect must be able to be accurately taken into account.

However, if the sole loss processes of the organic being studied (the reactant organic) and the reference organic are *via* reaction with the OH radical and dilution is negligible, then (E. 12.1) and (E. 12.2) are valid:

$$-d \ln[\text{reactant organic}]/dt = k_2[\text{OH}] \quad (\text{E. 12.1})$$

$$-d \ln[\text{reference organic}]/dt = k_1[\text{OH}] \quad (\text{E. 12.2})$$

Elimination of the OH radical concentration then leads to (E. 12.3):

$$\ln \left\{ \frac{[\text{reactant organic}]_{t_0}}{[\text{reactant organic}]_t} \right\} = \frac{k_1}{k_2} \ln \left\{ \frac{[\text{reference organic}]_{t_0}}{[\text{reference organic}]_t} \right\} \quad (\text{E. 12.3})$$

where $[\]_{t_0}$ refers to the hydrocarbon concentration at the beginning of the irradiation and $[\]_t$ to its concentration after time t of irradiation. Equation (E. 12.3) reveals the great advantage of relative rate measurements, namely that the OH concentration does not have to be known. If the assumptions that have been made for (E. 12.3) are true then the plotted data should yield a straight line with the ratio k_1/k_2 as a slope. A restriction of the relative rate technique is, on the other hand, that the quality of the obtained results largely depends on the availability of accurate data of the reference compound.

Possible sources of OH radicals are the photolysis of H_2O_2 or HONO. The technique most used in recent years is the irradiation of methyl nitrite/NO/air mixtures:



Such mixtures have been irradiated in a variety of chambers, ranging from all-Teflon chambers of ~60-6400-L volume to a 5800-L cylindrical evacuable Teflon-coated chamber with a 25-kW Xenon arc to provide for irradiation. OH concentrations of up to 3×10^8 molecule cm^{-3} were obtained in these studies. The reactant and reference organics are usually detected using gas chromatography, FTIR absorption spectroscopy or differential optical absorption spectroscopy (DOAS). For further details refer to papers from Pagani et al. [2000] or Stemmler et al. [1995].

12.5 Kinetic data for OH radical reactions obtained in laboratory studies.

Kinetic data for OH radical reactions have been published for an enormous number of different hydrocarbons. Most of the data were obtained at temperatures between 295 and 500 K. A first survey over this huge amount of data has been given by Roger Atkinson in 1986. This data collection has been updated several times since [Atkinson, 1990, 1994, 1997a, 1997b].

The simplest case is represented by alkanes as only abstraction of H-atoms occurs. As the room-temperature rate constants increase with decreasing C-H bond dissociation energy one obtains the following relation for primary, secondary, and tertiary C-H bonds:

$$k(\text{tertiary}) > k(\text{secondary}) > k(\text{primary})$$

The H-atom abstraction is exothermic, with exothermicities of 63 and 88 kJ/mole for the primary C-H bonds of methane and ethane, respectively. The exothermicities for abstraction of secondary and tertiary H atoms by OH amount to 105 and 113 kJ/mole, respectively [Benson, 1976]. For abstraction reactions are generally positive temperature dependencies of the reaction rate constant observed as shown for cyclohexane in Figure 12.4.

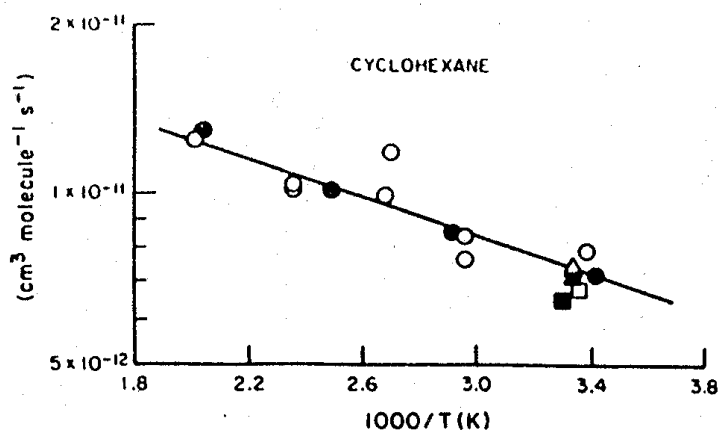


Figure 12.4: Arrhenius plot of the second-order rate constant for the reaction of OH radicals with cyclohexane [Atkinson, 1985].

An example for the temperature dependence of the rate constants measured for the interaction OH/alkenes is shown in Figure 12.5. In contrast to the interaction with alkanes, a negative temperature dependence is observed in this case. It has been shown in Figure 12.2 that the OH radicals are preferentially reacting with alkenes by addition to the double bond. The formation of the adduct is exothermic, for example by approximately 134 kJ/mole in the case of the ethene-OH adduct [Benson, 1976] as is the case for hydrogen abstraction from alkanes by OH. If the Arrhenius plot in Figure 12.5 shows a negative temperature dependence it is owing to the fact that an energetically highly excited intermediate, namely the OH adduct is formed in a first step which easily redissociates back to the reactants (see R. 12.7). The rate constant of redissociation increases faster with increasing temperature than the corresponding rate constant of the intermediate OH adduct formation which is leading to the negative temperature dependence of the overall rate constant as shown in Figure 12.5. A stable OH adduct is only obtained if the intermediate adduct can transfer its excess energy to a quenching molecule (see R. 12.8). Furthermore (R. 12.8) clearly shows that the measured rate constants strongly depend on the total pressure in the reactor.

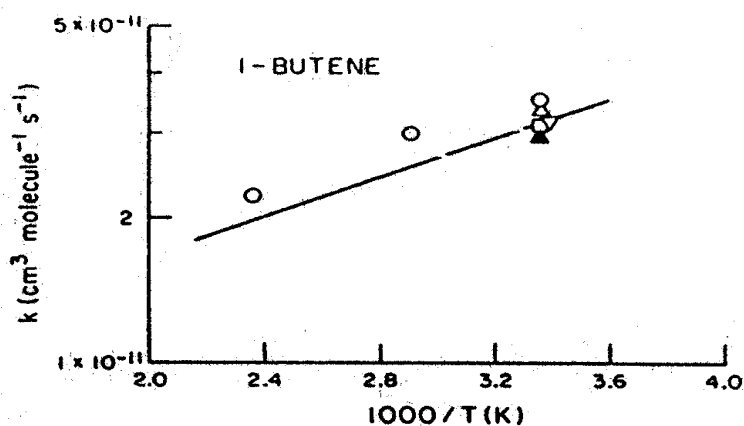
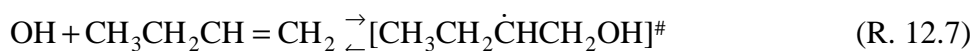


Figure 12.5: Arrhenius plot of the second-order rate constant for the reaction of OH radicals with 1-butene [Atkinson, 1985].



Negative temperature dependencies are also observed for monocyclic aromatic hydrocarbons at temperatures below ≤ 325 K. This is consistent with the observation that OH addition is the dominating reaction pathway at these temperatures. However, at temperatures higher than approximately 400-450 K H-atom abstraction starts to dominate which leads to an inversion of the temperature dependence. In the intermediate temperature range of ~ 325 -400 K non-exponential decays of OH radicals are observed. In this temperature regime any rate data obtained are a combination of the forward and reverse reaction steps and are dependent on the experimental conditions.

12.6 Estimation of OH radical rate constants.

First models to estimate reaction rate constants for alkanes consisted of summing up the contribution of each single C-H bond to the total reactivity of the molecule using a correlation of the reaction rate constants with C-H bond dissociation energies [Greiner, 1970]. This simple model can be described by (E.12.4):

$$k_{\text{total}} = N_{\text{prim}}k_{\text{prim}} + N_{\text{sec}}k_{\text{sec}} + N_{\text{tert}}k_{\text{tert}} \quad (\text{E. 12.4})$$

where N_{prim} , N_{sec} , and N_{tert} , are the numbers of primary, secondary and tertiary C-H bonds, respectively, and k_{prim} , k_{sec} , and k_{tert} are the corresponding rate constants for the reaction of OH radicals with these C-H bonds.

In the meantime kinetic data are also available for compounds containing a multitude of functional groups such as ethers, alcohols, carbonyls, aldehydes, esters, halogens etc. These data have been analyzed using nonlinear least-square fitting techniques in order to derive substituent factors which describe the influence of a certain substituent onto k_{prim} , k_{sec} , or k_{tert} , respectively. The simplistic model described in (E. 12.4) may thus be improved by the following:

$$k_{\text{total}} = \Sigma[k_{\text{prim}}^0 F(\text{X})] + \Sigma[k_{\text{sec}}^0 F(\text{X})F(\text{Y})] + \Sigma[k_{\text{tert}}^0 F(\text{X})F(\text{Y})F(\text{Z})] \quad (\text{E. 12.5})$$

where $F(\text{X})$, $F(\text{Y})$ and $F(\text{Z})$ are the substituent factors.

Corresponding structure-reactivity relationships also exist for the estimation of the rate constants for OH radical addition to aromatic rings. For this purpose Zetzsch [1982] proposed to use the excellent correlation between the OH radical rate constants and the sum of the electrophilic substituent constants, $\Sigma\sigma^+$, of Brown and Okamoto [1958]. For the reaction rate constants describing the addition of OH radicals to monocyclic aromatic rings or to biphenyl the following equation was derived:

$$\log k^{\text{add}}[\text{cm}^3 \text{ molecule}^{-1} \text{ s}^{-1}] = -11.4 - 1.39\Sigma\sigma^+ \quad (\text{E. 12.6})$$

The simplifications and assumptions made by Zetzsch were that a) steric hindrance was neglected and the electrophilic substituent constant of the ortho position was set equal to that for the para position, b) the total substituent constant $\Sigma\sigma^+$ was the sum of all substituent constants of the substituents connected to the aromatic ring, c) the OH radical adds to the position yielding the most negative value for $\Sigma\sigma^+$ (preferably a free position), and d) if all positions are occupied, the ipso position was treated as a meta position.

12.7 The degradation of compounds of low volatility in the gas phase and adsorbed on solid particles.

One of the latest extensive compilations of gas-phase chemistry relevant to the troposphere including the reactions of the OH radical has been accomplished in 1997 by Atkinson et al. Although there are a lot of data available for relatively volatile compounds only few data have been obtained for compounds with low vapor pressures, examples of which are polychlorinated-biphenyls or most pesticides in use. Among the few studies that have been performed with semivolatile compounds we want to emphasize that of Kwok et al. [1995], Brubaker and Hites [1997] and Palm et al. [1997]. Kwok et al. succeeded to measure rate constants for the gas phase reactions of the OH radical with dichlorobiphenyls and 1-chlorodibenzo-p-dioxin at ambient temperature and atmospheric pressure of air using a 7900-L smog chamber and the relative rate technique. The obtained data were used to revise a previous method for calculating the OH radical reaction rate constant based on structure-reactivity relationships.

Another technique has been chosen by Brubaker and Hites [1997] who were using a 195-mL quartz cell in order to measure the rate constants for the gas phase reactions of the OH radical with 1,2,3,4-tetrachlorodibenzo-p-dioxin at temperatures ranging from 373 up to 432 K. Instead of using a large reactor in order to minimize wall effects they performed their experiments in a very small reactor but at elevated temperatures. The results were evaluated in form of an Arrhenius plot and extrapolated to ambient temperatures.

Whereas in the two studies cited above the reactivity of the semivolatile compounds has been examined in the gas phase a completely different approach has been used by Palm et al. [1997]. They adsorbed terbuthylazine (TBA) on quartz aerosols of commercial origin of approximately 1 μm diameter and suspended them in a 2400-L smog chamber where they produced OH radicals using different precursors. The rate constants that they have measured for the degradation of adsorbed TBA are comparable with rate constants in the gas phase according to the discussion of Palm et al.

In view of the above presented state of the art we originally conceived the idea to build an experimental set-up that allows to measure rate constants for reactions of OH radicals with semivolatile compounds in the gas phase at elevated temperatures. In a second part it should have been examined how the reactivity of the semivolatile compounds changes if they are adsorbed on particulate matter at ambient temperature.

13 Experimental set-up.

13.1 Reaction cell for the measurement of the gas phase kinetics of the OH radical with organic compounds.

13.1.1 General description.

The experimental set up that has been chosen in order to measure the reaction kinetics of the OH radical with organic compounds in the gas phase is shown in Figure 13.1. It could be named a 'mini smog chamber' as the reaction cell has a volume of only 480 cm³. The small dimensions provide the advantage of simple heating and cleaning of the reaction cell and of low material costs. The major disadvantage is a high surface to volume ratio of approximately 0.9 cm⁻¹. An experimental set-up that was presented by Anderson and Hites in 1996 served as a model. They used the system to measure the reaction kinetics of the OH radical with semivolatile compounds such as biphenyl, 4,4'-dichlorobiphenyl or 2-hydroxybiphenyl [Anderson and Hites, 1996, Brubaker and Hites, 1998]. Our system essentially consists of a cylindrical reaction cell at atmospheric pressure from which a small flow of gas is continuously pumped into the closed ion source of a mass spectrometer (Prisma QMS 200, Balzers) which allows real time monitoring of organic compounds in the reactor. The reaction cell is made of Pyrex glass. A second, identical reaction cell which was used for the examination of polar compounds has been coated in our laboratory with a thin film of fluorinated ethylene-propylene polymer (Teflon® FEP 100, Dupont) in order to increase its inertness towards gas phase molecules. The cylindrical reaction cell has a diameter of 5.3 cm and a length 22 cm resulting in a volume of 480 cm³. The cylinder is equipped with a quartz window at each end (Suprasil 2, Haereus). The connection to the mass spectrometer is afforded by a quartz capillary of 30 cm length and 100 µm diameter (fused silica tubing, Supelco) which ends in the differentially pumped gas inlet system of the mass spectrometer (GEV 010, Balzers). The gas inlet system is made of stainless steel. This system has two outlets: The first is towards a needle valve that is pumped by a mechanical pump, and the second is towards a molecular leak of 10 µm diameter which is directly leading into the closed ion source of the mass spectrometer. The closed ion source basically consists of a stainless steel cylinder presenting a small orifice for the injection of the electrons. By regulating the needle valve one may control the pressure inside the gas inlet system which in turn will determine how much of the gas flow will escape through the molecular leak into the closed ion source and how much will be pumped off through the needle valve.

In order to render the technically difficult direct observation of the OH radical unnecessary a relative rate technique as described in Section 12.4.2 has been chosen. This means that the relative rates of the disappearance of two or more organic compounds in

chemical systems containing OH radicals must be monitored. In this context it is important to verify that the degradation of a hydrocarbon does not lead to products which contribute to the same MS signal at which another hydrocarbon is monitored.

In Sections 2.2.1 and 12.1 we already have presented the photodissociation of ozone which generally is considered as the main source of OH radicals in the troposphere. Owing to the simplicity of the reaction system it has been chosen as the radical source for our experimental technique:



The light source for the photodissociation of O_3 consists of a 150 W Hg/Xe high pressure short arc lamp (XBO 150 W/S UV, Osram) placed in lamp housing equipped with a parabolic reflector. The light beam emitted by the lamp has a diameter of approximately 7 cm and is therefore sufficiently large to illuminate the total cross section of the reaction cell.

Reactions (R. 2.2.1-2) show that the OH radical is not the only oxidant present in the reaction cell. We must therefore be sure that O_3 , $\text{O}({}^1\text{D})$ and $\text{O}({}^3\text{P})$ do not have significant reaction rates with the organic compounds.

Whether O_3 is degrading the organic compound of interest can directly be controlled by monitoring a O_3 /hydrocarbon mixture without irradiation of the reaction cell.

The contributions of $\text{O}({}^1\text{D})$ and $\text{O}({}^3\text{P})$ on the other hand can only be estimated. Most of the $\text{O}({}^1\text{D})$ atoms will be quenched by N_2 or O_2 in order to form $\text{O}({}^3\text{P})$. The few $\text{O}({}^1\text{D})$ atoms that are surviving can either react with H_2O or with the organic compounds. The rate constant of $\text{O}({}^1\text{D})$ for the reaction with H_2O is known to be $2.2 \times 10^{-10} \text{ cm}^3 \text{ molecule}^{-1} \text{ s}^{-1}$ [DeMore, 1992]. Even if $\text{O}({}^1\text{D})$ has a rate constant for the reaction with hydrocarbons of the same order of magnitude its contribution to the degradation of the hydrocarbon will be minimal as we have approximately 500 times more H_2O than hydrocarbons in the system (see Table 14.1).

The $\text{O}({}^3\text{P})$ atom reacts with O_2 approximately 10 times slower in order to reform O_3 than with organic compounds such as cyclohexane or toluene [Herron, 1988; Cvetanovic, 1987]. However, even those reactions will not have significant rates as we have always approximately 4000 times more oxygen in the reaction cell than hydrocarbons. In addition, it has been demonstrated by Anderson and Hites [1996] that a variation of the oxygen concentration from 0.4% to 95% did not systematically influence the measured rate constants.

13 Experimental set-up

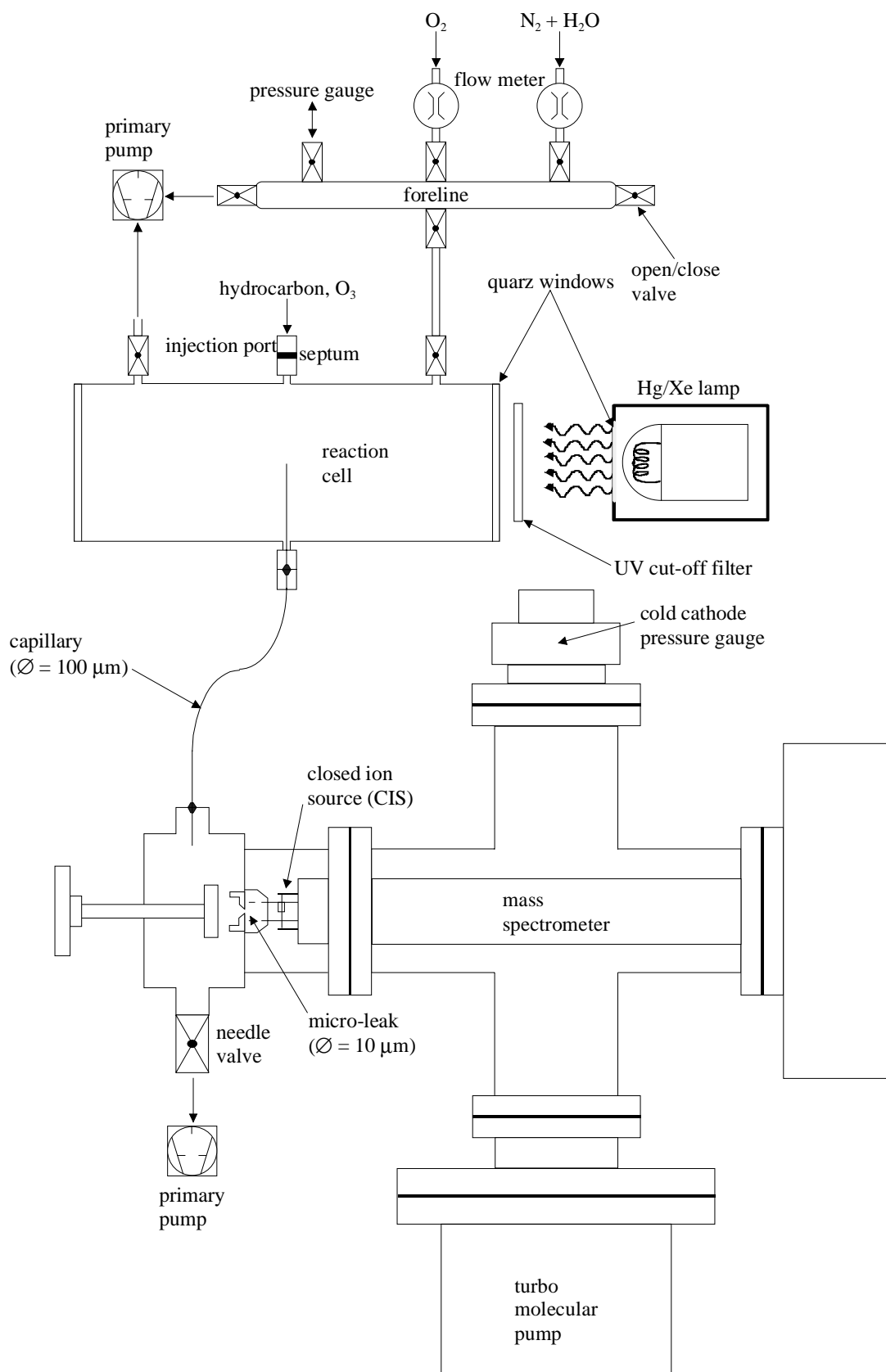


Figure 13.1: Experimental set-up for the measurement of the rate constants for the reaction of OH radicals with organic compounds using a relative rate technique.

13.1.2 Preparation of a reactive gas mixture in the reaction cell.

At the beginning of an experiment the reaction cell was pumped down to a pressure below 10^{-3} mbar. Subsequently, the cell was refilled introducing N_2 and O_2 (both Carbagas). The flows of N_2 and O_2 were separately adjusted using flow meters in order to obtain a mixing ratio of 4:1 corresponding to the tropospheric composition of air. When the pressure in the system attained 200 mbar the gas flow was additionally led through a bubbler containing distilled water until atmospheric pressure was attained. In this way mixtures of synthetic air with a relative humidity of approximately 75% were obtained.

In a first period the organic reactant and the reference compound, respectively, were injected into the reactor as solutions in CCl_4 . CCl_4 has been chosen due to its high vapor pressure (122 mbar at $20^\circ C$) and its inertness towards the OH radical. However, the presence of CCl_4 was leading to some artifacts as will be shown in Section 14.1. This is the reason why the organic reactants have been introduced directly in gaseous form later on. Therefore, some microliters of the pure compound were injected into a glass storage vessel equipped with a septum and containing synthetic air. After evaporation of the compounds some milliliters of the headspace were transferred from the balloon into the reaction cell using a gas-tight syringe. In the case of semivolatile compounds such as for example biphenyl the glass storage vessel, the syringe and the reaction cell were heated up. The transfer capillary, the gas inlet system and the detection chamber were generally heated up to temperatures that were at least 20 K higher than that of the reaction cell.

Ozone has been generated in a discharge generator (ozone generator 502, Fischer Technology) and condensed at $-75^\circ C$ on silica-gel. The silica-gel trap was equipped with a septum which enabled the transfer of some milliliters of headspace into the reaction cell. The volatile organic compounds were calibrated by injecting different volumes of the pure liquid into the reaction cell using a microliter syringe and by monitoring the corresponding MS response after equilibration of the signal. For less volatile compounds which are solid at ambient temperature solutions in CCl_4 or other solvent has been prepared and injected. The general detection limit of the mass spectrometer for organic compounds such as cyclohexane or toluene amounted to roughly 0.5-1.0 ppm.

The calibration of ozone could not be performed using the mass spectrometer as no measurable signal at m/e 48 was obtained. We do not know whether the ozone was decomposed during its passage through the capillary or whether the fragmentation in the closed ion source produces no measurable amounts of the molecular ion. The signal at m/e 32 could not be used as it was interfering with the high background concentration of O_2 . Therefore, we measured the concentration of O_3 by measuring its absorption in the UV using a 30 W Hg lamp (Carl Zeiss) as the light source and a CCD camera (TCCD-576, SI Spectroscopy Instruments) equipped with a Spectrograph (SpectraPro-150, SI Spectroscopy Instruments) as detector. Such measurements have been performed in order to measure the O_3

concentration in the O_3/O_2 mixture of the headspace of the silica-gel trap as a function of its cooling temperature. The goal was to find an appropriate temperature which allowed to obtain O_3 concentrations between $4\text{-}9 \times 10^{-2}$ mbar by transferring 5-10 ml of the headspace into the reaction cell. The corresponding temperature was revealed to be approximately -45 °C. This procedure yielded quite reproducible O_3 concentrations in the reaction cell wherefore we did forego to control its concentration in the degradation experiments later on.

13.1.3 The photochemical production of OH radicals in the reaction cell.

Reactions (R. 2.2.1 and 2.2.2) show that one needs photons of wavelengths shorter than 320 nm in order to produce OH radicals. The reason for this can be seen in Figure 13.2. According to DeMore et al. [1987] the quantum yield for the production of $O(^1D)$ atoms by photodissociation of O_3 almost drops to zero at wavelengths around 315 nm.

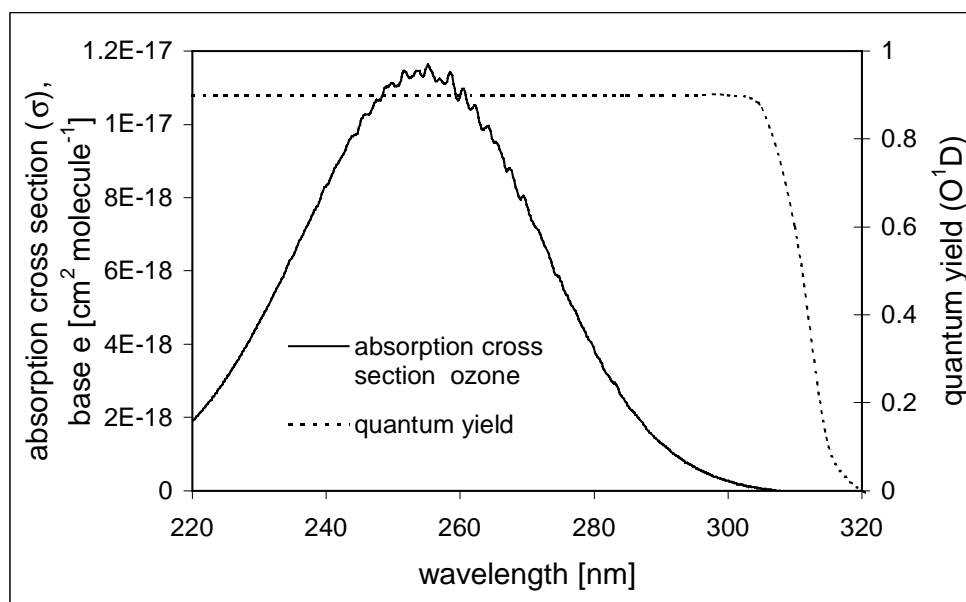


Figure 13.2: Absorption spectrum of O_3 measured at a concentration of 2×10^{-2} mbar and scaled with literature data from Finlayson-Pitts and Pitts [1986]. The dashed line represents the quantum yield for the production of $O(^1D)$ by photodissociation of O_3 according to data from DeMore et al. [1987].

On the other hand, the presence of photons of too high energies must be avoided too, in order to prevent the direct photolysis of the organic compounds. We have observed that cyclohexane that has often served as the reference compound undergoes fast photolysis if the reaction cell is irradiated with photons from the 150 W Hg/Xe lamp without UV cut-off filter. Significant rates of photolysis of cyclohexane and most other organic compounds examined in this study have been avoided by using a UV cut-off filter of three millimeter thickness

which presented a transmission of 50% at 280 nm (WG 280, Schott). Both the raw spectra as well as the spectra that is obtained using the UV cut-off filter is shown in Figure 13.3.

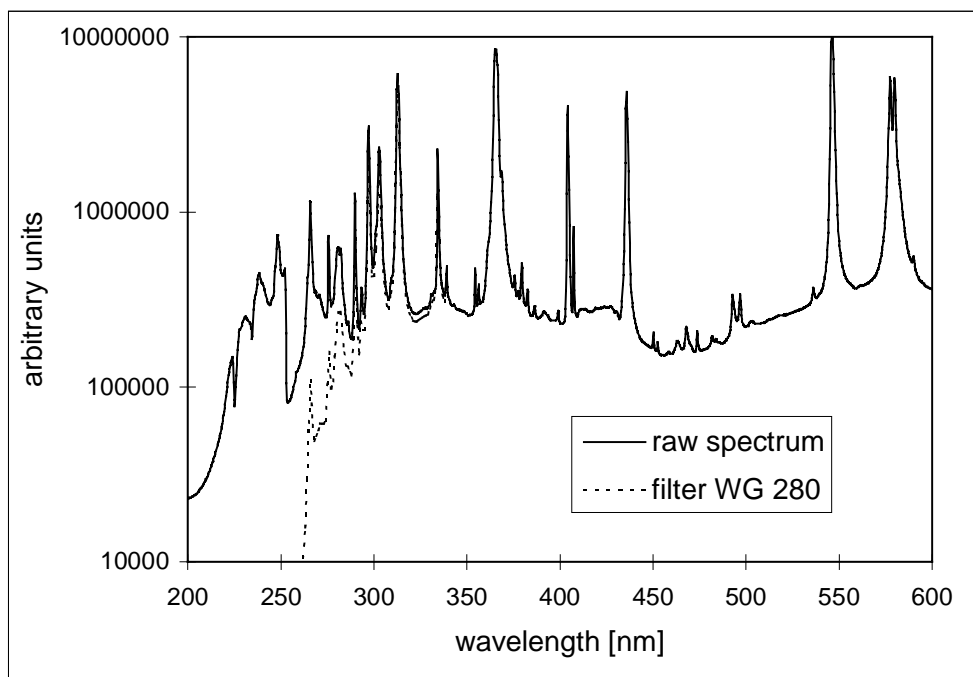


Figure 13.3: Emission spectrum of the XBO 150 W Hg/Xe high pressure short arc lamp: raw spectrum (full line) and spectrum obtained using the UV cut-off filter WG 280 from Schott.

By multiplication of the actinic flux of the lamp presented in Figure 13.3 with the absorption cross section of O_3 and the quantum yield for the formation of $O(^1D)$ we obtain the action spectrum which indicates the relative importance of the different wavelengths with respect to the formation of $O(^1D)$ atoms. The result shown in Figure 13.4 reveals that a narrow band of wavelengths ranging from 260 to 300 nm is responsible for the main production of $O(^1D)$ atoms in our reaction cell. This range belongs to the Hartley bands of ozone which are ranging from 200-300 nm. The Huggins bands, on the other hand, in the range from 300-370 nm, contribute only to a minor extent to the $O(^1D)$ production because both the absorption cross section of O_3 as well as its quantum yield for $O(^1D)$ formation have only very low values in this region. The lower limit of $O(^1D)$ formation at approximately 260 nm is given by the cut-off of the UV filter. The peaks in the action spectrum reflect the emission bands of mercury.

The formation of secondary organic aerosols could be observed with the naked eye when a mixture of O_3 /hydrocarbon was irradiated. This was above all the case when toluene had been injected in the reaction cell. However, the formation of secondary organic aerosols did not seem to interfere with the hydrocarbons in the gas phase. This may be concluded by the observation that the MS signals of the hydrocarbons instantaneously stabilized on a constant level at the end of the irradiation. That means that no losses to the aerosol surface occurred.

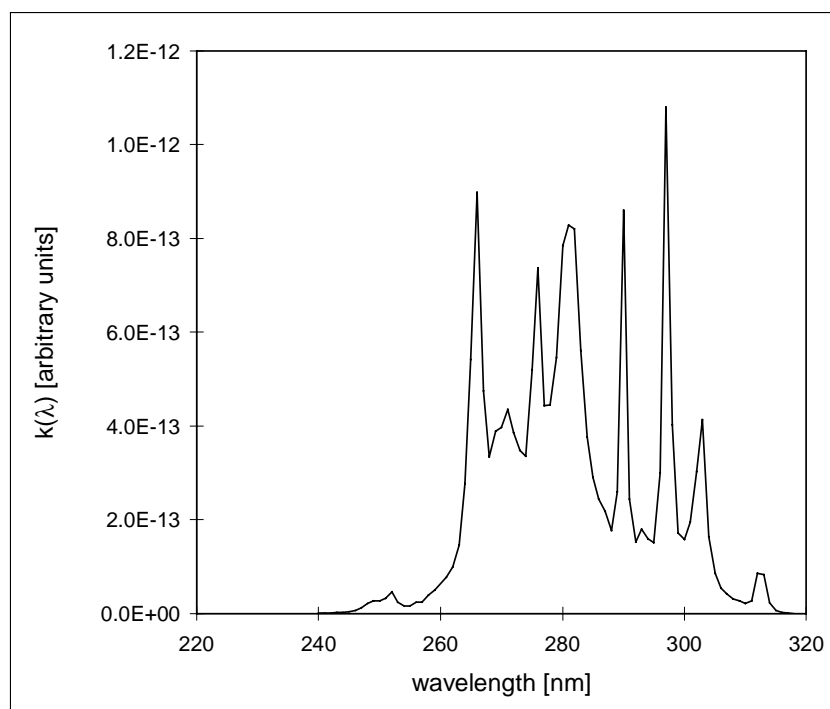


Figure 13.4: Relative rates of $O(^1D)$ formation in the reaction cell as a function of the wavelength.

13.1.4 Flow conditions in the experimental set-up.

It has been mentioned in Section 12.5 that the reaction rate of the addition of OH radicals to double bonds or aromatic systems strongly depends on the total pressure in the reactor. It is therefore preferable to work at atmospheric pressure in order to obtain results relevant for tropospheric conditions. On the other hand, we use a mass spectrometer in order to monitor the concentrations of the organic reactants in the reaction cell. The mass spectrometer works only up to maximum pressures of 1×10^{-4} mbar (closed ion source) and 5×10^{-6} mbar (secondary ion multiplier, SEM), respectively. In order to establish the required pressure gradient between the reaction cell and the detection chamber a differentially pumped system is used. Figure 13.1 shows that the connection between the reaction cell and the mass spectrometer is afforded by a quartz capillary of 30 cm length and 100 μm diameter. This capillary ends in a gas inlet system that is pumped by a mechanical pump. The pumping speed of this pump can be controlled by means of a needle valve. We have measured that owing to this regulation the pressure can be adjusted in the gas inlet system between 0.7 and 2.6 mbar corresponding to pressures between 6×10^{-7} and 2×10^{-6} mbar, respectively, in the detection chamber. Most of the gas flow is pumped off across the needle valve. Only a small fraction of the gas flow effuses through a second orifice of 10 μm diameter into the closed ion source of the mass spectrometer which is housed in the detection chamber. The pressure gradient in the detection chamber is maintained by a turbo-molecular pump.

A preliminary characterization of the flow conditions in the experimental set-up has been performed by recording the pressure drop in the reaction cell that is caused by the continuous flow of gas which is pumped across the into the gas inlet system of the mass spectrometer. Figure 13.5 shows the observed pressure drop when the reaction cell was filled with 1 atmosphere of dry synthetic air. As expected, the pressure decrease obeys first order kinetics. If the resulting value of the slope, namely $-0.00105 \text{ min}^{-1}$, is multiplied with the initial pressure in the reaction cell of 1000 mbar it may be seen that the pressure drop amounts to approximately 1 mbar min^{-1} . This corresponds to a gas volume of approximately 0.5 ml min^{-1} at atmospheric pressure. This rate remains almost constant even for long pumping times as the total pressure is only decreasing by 6% within one hour. This observation justifies the assumption that the pressure drop during a photooxidation experiment which normally only takes 15 minutes will not significantly influence the observed reaction kinetics.

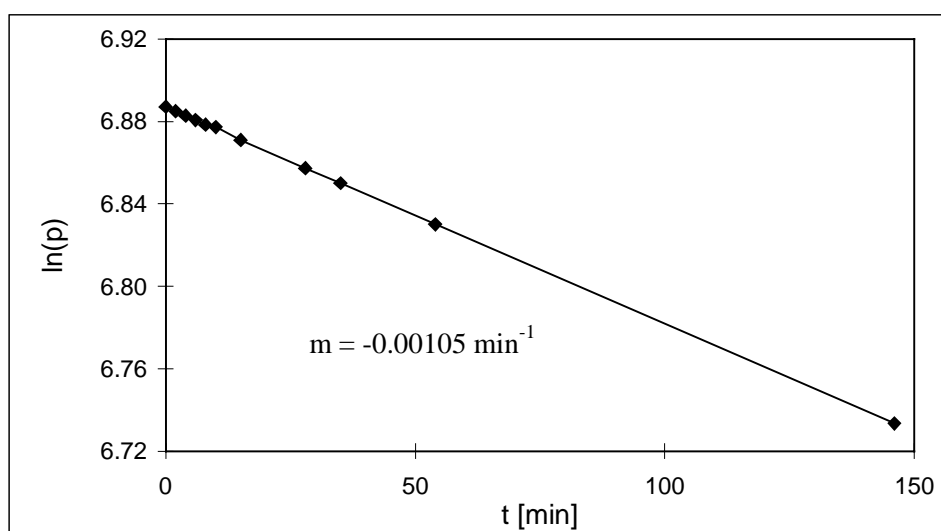


Figure 13.5: Pressure drop in the reaction cell filled with synthetic dry air due to the sampling of gas into the differential pumped gas inlet system of the mass spectrometer.

An additional observation indicated that the pumping rate was linearly decreasing with increasing length of the capillary and that the pumping rate of pure nitrogen was approximately 17% higher than that of pure oxygen. Finally, it could be observed that the pumping rate of the reaction cell did not significantly change when the pressure in the gas inlet system i. e. at the outlet of the capillary was varied between 0.7 and 2.6 mbar. All these observations are understandable if one assumes viscous flow conditions to hold in the capillary. In this case the Poiseuille equation (E. 13.1) can be applied which describes the gas flow (Q) through a straight tube:

$$Q = \frac{\pi d^4}{128 \eta l} \frac{(P_1 + P_2)}{2} (P_1 - P_2) \quad (\text{E. 13.1})$$

where d is the diameter of the tube, P_1 and P_2 the pressures at the inlet and the outlet of the tube, respectively, η the viscosity of the gas and l the length of the tube. Oxygen has a viscosity that is higher by 14% than that of nitrogen at room temperature which is in good correspondence with the observation that its pumping rate through the capillary was slower by approximately 17%.

The gas flow of 0.5 ml min^{-1} originating from the reaction cell is split up in the differentially pumped gas inlet system. Whereas most of the gas is pumped off by the primary pump only a small fraction effuses through the molecular leak of $10 \text{ }\mu\text{m}$ diameter into the closed ion source of the mass spectrometer. The highest pressure in the detection chamber (P_{DC}) at which the mass spectrometer generally was operated amounted to 2×10^{-6} mbar. As we know the conductance of the closed ion source ($C = 1 \text{ l s}^{-1}$) and the pumping speed of the turbo-molecular pump ($S = 50 \text{ l s}^{-1}$) we can estimate the pressure in the closed ion source (P_{CIS}) by (E. 13.2):

$$P_{\text{CIS}} = P_{\text{DC}} S / C \quad (\text{E. 13.2})$$

According to this calculation the maximum pressure that was attained in the closed ion source during the photooxidation experiments amounted to 1.0×10^{-4} mbar. This value corresponds to the maximum operating pressure of 1×10^{-4} mbar which is recommended by the manufacturer.

In order to obtain a linear response of the mass spectrometer for molecules of different weight and size it is necessary to avoid demixing effects. Such effects would occur if the pressure in the gas inlet system was too high. In this case it could occur that the flow through the molecular leak into the closed ion source were in the viscous regime whereas the flow leaving the closed ion source would be in the molecular regime. The result would be a relative enrichment of heavy compounds in the closed ion source leading to a non linear response with respect to the mixing ratios in the reaction cell. In order to be sure that demixing effects do not falsify the kinetics of the degradation experiments a simple test has been performed. Two gases, namely SF_6 (M_r 146 g mole^{-1}) and Ne (M_r 20 g mole^{-1}), have been injected into the reaction cell in order to be diluted with a constant flow of 66 ml min^{-1} of synthetic air. This flow rate was chosen because it approximately corresponds to the degradation rates of the organic compounds observed during the photooxidation experiments. The raw data of the dilution experiment are shown in Figure 13.6. The ratio of the concentrations of the two gases in the reaction cell is the same at any moment during the experiment as both gases are subjected to the same rate constant of dilution. The same is true for the concentrations in the closed ion source if no demixing effects are occurring. Therefore, in the absence of demixing effects a straight line with a slope equal to one should result if the raw data are evaluated

according to (E. 12.3). Figure 13.7 shows that this was indeed the case. The dilution experiment has been performed at a pressure of 5×10^{-6} mbar in the detection chamber. As this pressure was higher by a factor of 2.5 than the highest pressure used in the photooxidation experiments and the mass difference between SF_6 and neon was higher than for every pair of reference and reactant compound used we assume that no significant demixing ever occurred during our photooxidation experiments.

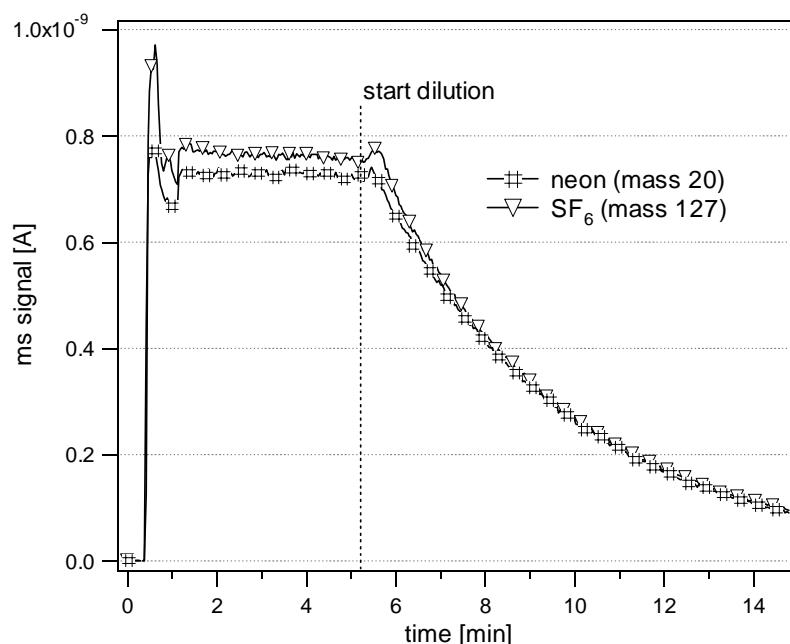


Figure 13.6: Dilution experiment of neon and SF_6 at a flow of 66 ml min^{-1} of synthetic air. The pressure in the detection chamber was 5×10^{-6} mbar.

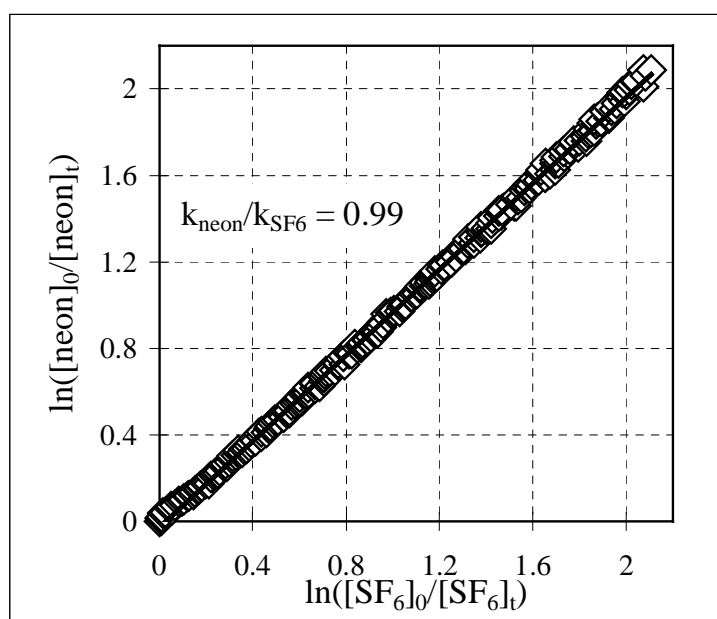


Figure 13.7: Data evaluation of the dilution experiment shown in Figure 13.6 according to (E. 12.3). A slope close to one indicates that no significant demixing effects occurred in the closed ion source of the mass spectrometer.

14 Results of the photooxidation experiments.

14.1 Validation of the system using cyclohexane and toluene.

In a first attempt we wanted to make sure that the degradation rates of organic compounds measured in our system are solely due to the attack of OH radicals. We therefore examined the interaction of the OH radical with toluene and cyclohexane for which large number of reference data are available in the literature. For cyclohexane reaction rate constants have been measured by Greiner [1970], Atkinson et al. [1982, 1983], Tuazon et al. [1983] and Tully [1985]. All this data are in good agreement although very different techniques such as flash photolysis combined with resonance absorption, relative rate techniques in smog chambers or laser photolysis combined with resonance fluorescence have been used. Atkinson [1985] analyzed these data and derived the following Arrhenius expression (E. 14.1) valid for temperatures ranging from 263 up to 555 K:

$$k(\text{cyclohexane}) = (2.73_{-0.74}^{+1.03}) \times 10^{-11} e^{-(390 \pm 81)/T} \text{ cm}^3 \text{ molecule}^{-1} \text{ s}^{-1} \quad (\text{E. 14.1})$$

where the error limits are two least-squares standard deviations. The calculated rate constant at 298 K amounts to (E. 14.2):

$$k(\text{cyclohexane}; 298 \text{ K}) = 7.38 \times 10^{-12} \text{ cm}^3 \text{ molecule}^{-1} \text{ s}^{-1} \quad (\text{E.14.2})$$

with an estimated overall uncertainty at 298 K of $\pm 20\%$.

Atkinson [1985] derived a corresponding Arrhenius expression (E.14.3) also for toluene. In this case data from Hansen et al. [1975], Perry et al. [1977] and Tully et al. [1981] who all worked using flash photolysis were considered. The equation is valid for temperatures below 325 K where the formation of the OH adduct dominates:

$$\begin{aligned} k(\text{toluene}, T \leq 325 \text{ K}) \\ = (2.10_{-0.90}^{+1.59}) \times 10^{-12} e^{(322 \pm 149)/T} \text{ cm}^3 \text{ molecule}^{-1} \text{ s}^{-1} \end{aligned} \quad (\text{E. 14.3})$$

where the error limits are two least-squares standard deviations. The calculated rate constant at 298 K amounts to (E. 14.4):

$$k(\text{toluene}; 298 \text{ K}) = 6.19 \times 10^{-12} \text{ cm}^3 \text{ molecule}^{-1} \text{ s}^{-1} \quad (\text{E.14.4})$$

with an estimated overall uncertainty at 298 K of $\pm 20\%$.

In addition to the well-founded data base, cyclohexane and toluene also have the advantage that owing to their high vapor pressure no significant adsorption losses to the walls are expected to occur.

Figure 14.1 shows raw data from a typical photooxidation experiment performed using cyclohexane and toluene. Both compounds were injected in gaseous form into the reactor containing synthetic air of approximately 75% rh at $t \approx 1$ min. The response of the mass spectrometer at m/e 56 (cyclohexane) and 91 (toluene) follows instantaneously. A signal peak of the mass spectrometer immediately after the injection was always observed as the compounds were injected close to the capillary which pumps the gases into the closed ion source of the mass spectrometer. Some milliliters of the ozone containing headspace of the silica-gel trap were injected at $t \approx 2$ min. In so doing, some milliliters of the content of the reaction cell were sucked back into the syringe and re-injected into the cell several times. This procedure served to accelerate the mixing of the gases in the reactor. Finally, the irradiation of the reactor was started at $t \approx 7.25$ min. An instantaneous decrease of both compounds, cyclohexane as well as toluene, could be observed. At $t \approx 12$ min, when approximately 86% of the cyclohexane and 76% of toluene had been degraded by the OH radicals the experiment was halted.

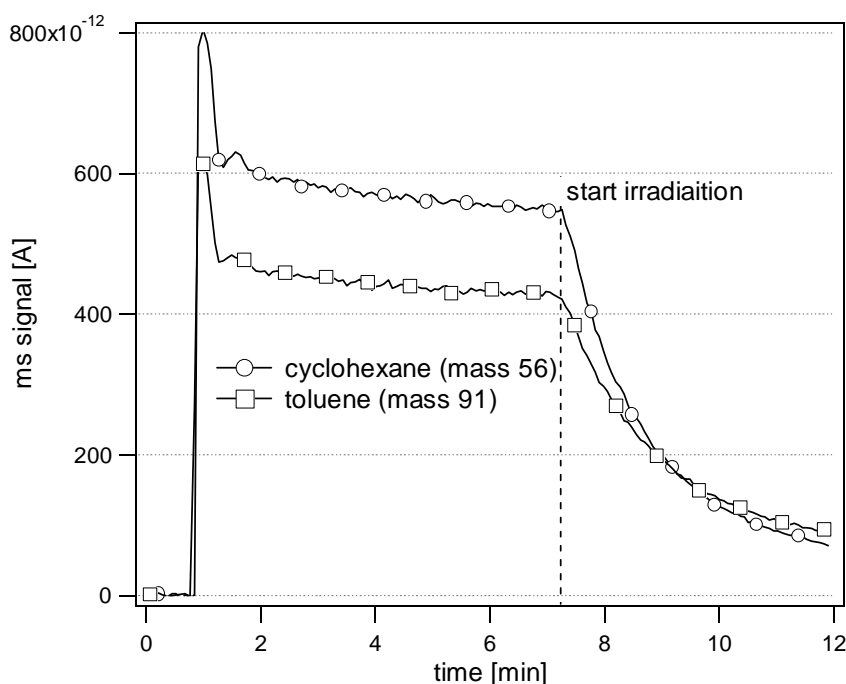


Figure 14.1: Degradation of toluene and cyclohexane by OH radicals at 298 K. The concentrations were 18 ppm for toluene, 16 ppm for cyclohexane and approximately 90 ppm for ozone.

The evaluation of the raw data from Figure 14.1 according to (E. 12.3) is shown in Figure 14.2. As can be seen a straight line with a slope of 0.76 is resulting which should correspond to the ratio of the reaction rate constants of toluene and cyclohexane, respectively. The ratio that is calculated according to the recommendations of Atkinson (E. 14.1 and 14.3) for a temperature of 298 K amounts to 0.84 and is therefore in good agreement with our result.

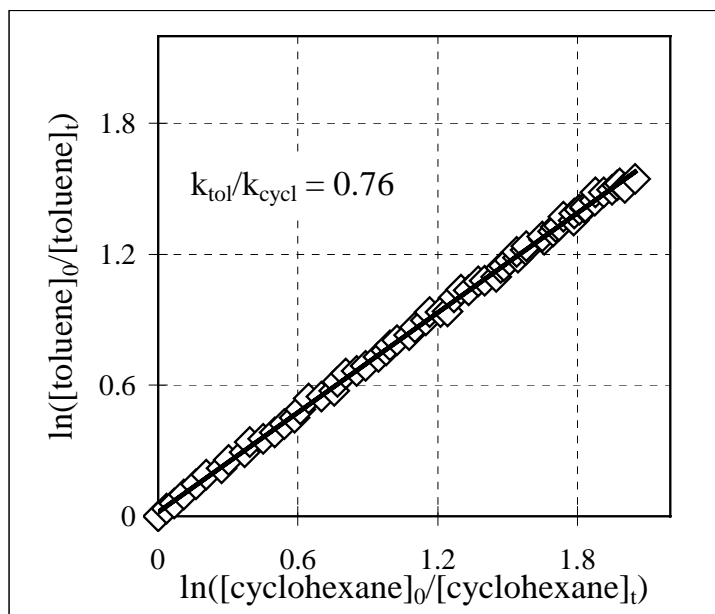


Figure 14.2: Evaluation of the raw data shown in Figure 14.1 according to equation (E. 12.3).

Additional measurements have been performed at different temperatures by varying the concentrations of both the organic compounds as well as ozone. For experiments at higher temperatures the reactor has been wrapped with an aluminum foil and a heating wire. The aluminum foil served to a better distribute the heat. The temperature control was afforded by a thermocouple/PID system. The results are summarized in Figure 14.3. whereas the conditions of the measurements may be found in Table 14.1. Figure 14.3 shows that the ratios of $k(\text{toluene})/k(\text{cyclohexane})$ are slightly smaller than the recommendations of Atkinson [1985] over the whole temperature range. Nevertheless, excellent agreement may be stated. An even better agreement is observed when the results of the present work are compared to those of Anderson and Hites [1996]. Table 14.1 shows that varying concentrations of cyclohexane, toluene and ozone did not systematically affect the results. This makes us confident that oxidants other than OH radical did not significantly contribute to the degradation of the organic compounds.

Absolute degradation rates in experiments 2 and 6 where the concentration ratio $[\text{O}_3]/[\text{organics}]$ was rather low were clearly slower than in the other experiments.

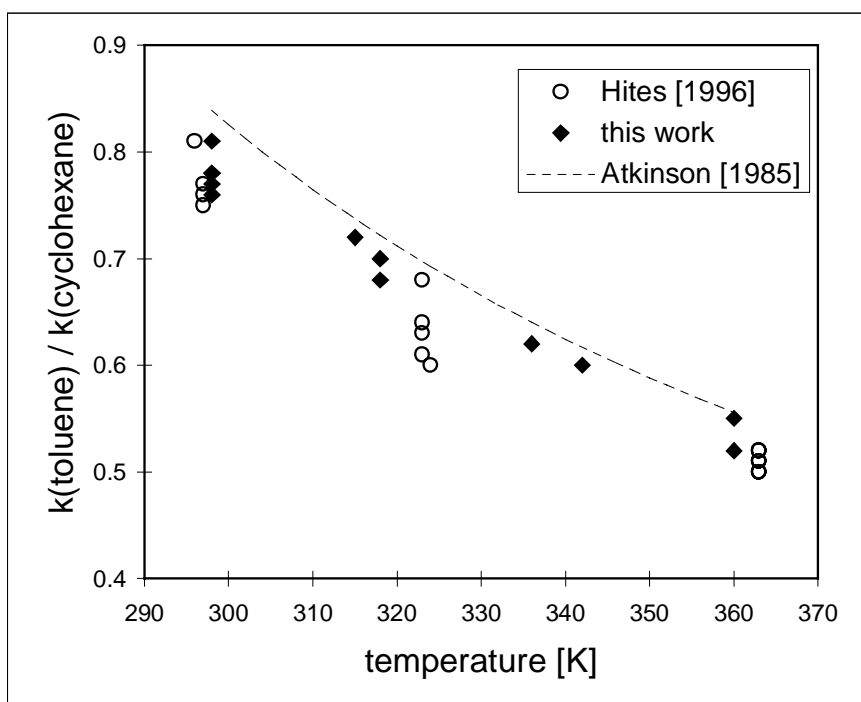


Figure 14.3: Ratios of $k(\text{toluene})/k(\text{cyclohexane})$ measured at different reactant concentrations as a function of temperature. Details may be taken from Table 14.1.

meas. n ^o	temperature [K]	O ₃ [mbar] [ppm]	[tol] / [cyclo] [ppm]	[H ₂ O] [ppm]	k(tol) / k(cyclo)
1	298	~90 ppm	18 / 16	~25'000	0.76
2	298	~45 ppm	15 / 15	~25'000	0.81
3	298	~90 ppm	28 / 14	~25'000	0.78
4	315	~90 ppm	26 / 15	~25'000	0.72
5	318	~90 ppm	32 / 15	~25'000	0.68
6	318	~45 ppm	22 / 19	~25'000	0.70
7	336	~90 ppm	30 / 17	~25'000	0.62
8	342	~70 ppm	14 / 16	~25'000	0.60
9	360	~90 ppm	35 / 18	~25'000	0.52
10	360	~90 ppm	31 / 17	~25'000	0.52
11	298	~70 ppm	12 / 14	~25'000	0.78
12	298	~70 ppm	15 / 12	~25'000	0.77

Table 14.1: Results and conditions of the measurements shown in Figure 14.3. The concentrations of O₃ and H₂O were estimated according to the procedure on the filling of the reactor and the preparation of the gas mixtures (see Section 13.1.2).

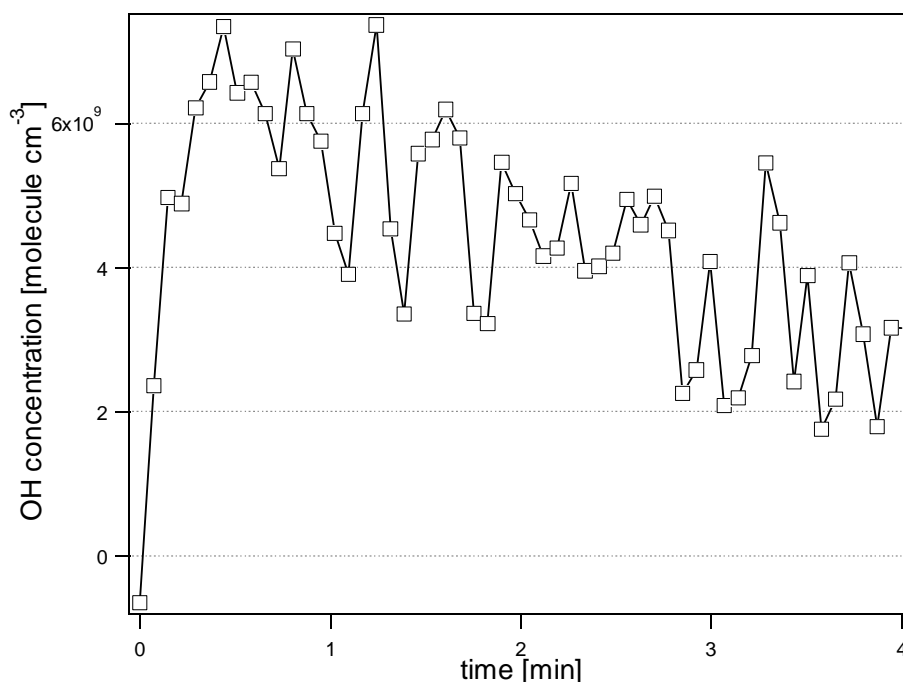


Figure 14.4: Calculated OH concentrations during the experiment shown in Figure 14.1 The OH concentrations have been calculated using the decay trace of cyclohexane and assuming $k(\text{cyclohexane}; 298 \text{ K})$ to be $7.38 \times 10^{-12} \text{ cm}^3 \text{ molecule}^{-1} \text{ s}^{-1}$. $t = 0 \text{ min}$ refers to the start of the irradiation.

Because the rate constants for the reaction of OH radicals are known in the case of cyclohexane and toluene one may use the experimental decay traces of the organic compounds to deduce the OH radical concentration during an experiment. This has been done using the cyclohexane trace shown in Figure 14.1. Assuming the reaction rate constant $k(\text{cyclohexane}; 298 \text{ K})$ to be $7.38 \times 10^{-12} \text{ cm}^3 \text{ molecule}^{-1} \text{ s}^{-1}$ one obtains calculated OH concentrations for the experiment as shown in Figure 14.4. According to this trace a maximum concentration of approximately $7 \times 10^9 \text{ molecule cm}^{-3}$ is attained 20 to 30 seconds after the start of the irradiation. The concentration subsequently decreases continuously in order to attain values of approximately $2.5 \times 10^9 \text{ molecule cm}^{-3}$. The OH radical concentrations in our reactor are therefore more than 10 times higher during the whole experiment compared to smog chamber experiments where using (R. 12.4-6) typical concentrations of approximately $2\text{-}3 \times 10^8 \text{ molecule cm}^{-3}$ are attained. The advantage of higher OH radical concentrations are significantly reduced elapsed times for experiments.

It has been mentioned in Section 13.1.2 that we initially injected the organic compounds into the reactor as a solution in CCl_4 . The injected volume of CCl_4 typically amounted to $6 \mu\text{l}$ leading to concentrations in the reactor of approximately 3200 ppm. The ratios of $k(\text{toluene})/k(\text{cyclohexane})$ that have been measured in the presence of CCl_4 were systematically too low showing a mean value of 0.62 at 298 K. Thus, the rate constant of

cyclohexane is overestimated with respect to the rate constant of toluene or the one for toluene underestimated, accordingly. The data evaluation of such an experiment according to (E. 12.3) involving CCl_4 as a solvent for the hydrocarbons is shown in Figure 14.5. It may be seen that these experiments led to perfectly straight lines. This indicates that the absence of curvature is not a sufficient criterion in order to state that the reaction rate constants of OH radicals have been correctly measured.

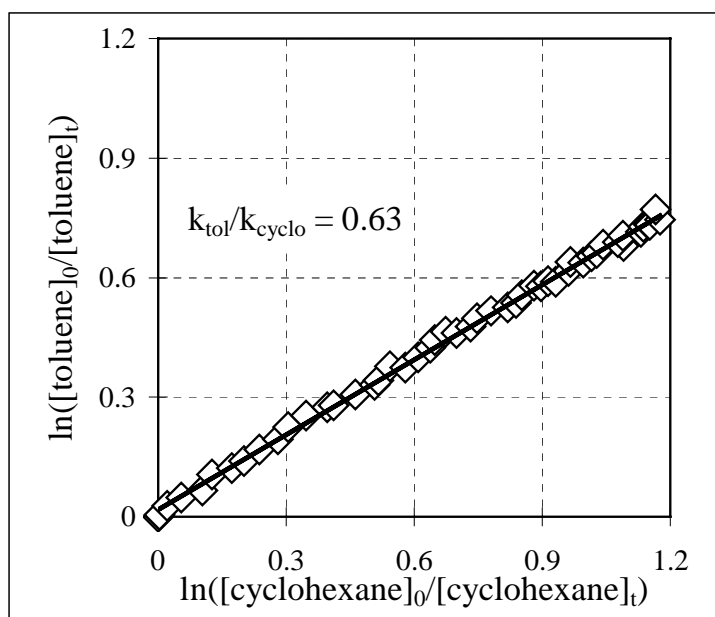


Figure 14.5: Results of a degradation experiment of toluene and cyclohexane by OH radicals at 298 K performed in the presence of CCl_4 . The concentration was 22 ppm for toluene, 24 ppm for cyclohexane, 3200 ppm for CCl_4 and approximately 70 ppm for ozone.

An error in the measured values would be understandable if CCl_4 would be photolyzed in order to produce Cl radicals. The reaction rate constant of Cl with toluene is 5.9×10^{-11} molecule $\text{cm}^{-3} \text{s}^{-1}$ (Shi and Bernhard, 1997) which is considerably lower than the corresponding value for the reaction with alkanes such as n-hexane (3.4×10^{-10} molecule $\text{cm}^{-3} \text{s}^{-1}$) or n-heptane (3.9×10^{-10} molecule $\text{cm}^{-3} \text{s}^{-1}$) (Atkinson, 1997). Thus, the presence of Cl radicals in the reactor would most probably lead to decreased ratios of $k(\text{toluene})/k(\text{cyclohexane})$. The fact that the MS signal of CCl_4 at m/e 117 did not change when the irradiation was started is not a sufficient argument to exclude a significant production of Cl radicals by photolysis. Due to the high reactivity of Cl radicals very low i. e. not measurable concentrations would be sufficient to disturb the system. Finally, we found that even dilution experiments which were performed in the absence of light but in the presence of CCl_4 did not have a slope of 1.0 for the ratio $k(\text{dilution, toluene})/k(\text{dilution, cyclohexane})$ but slopes between 0.7 and 0.8 when data were evaluated according to (E. 12.3). This would mean that cyclohexane is diluted faster than toluene which is physically not understandable. The only explanation we have is that the presence of CCl_4 was leading to

secondary reactions in the closed ion source of the mass spectrometer. However, when CCl_4 was not present in the reaction cell then both the dilution as well as the OH experiments yielded correct results.

14.2 1,3,5-trimethylbenzene (mesitylene).

The actual goal was to measure rate constants for the reaction of OH radicals with semivolatile compounds. The plan was to proceed stepwise by examining compounds with continuously decreasing vapor pressures. After toluene with a boiling point of 110°C we examined therefore 1,3,5-trimethylbenzene (mesitylene) which has a boiling point of 164°C .

A problem observed for mesitylene was the fact that dilution experiments together with cyclohexane as reference compound resulted in values of 1.14 to 1.24 instead of 1.0 for the ratio of $k(\text{dilution, mesitylene})/k(\text{dilution, cyclohexane})$. This is quite surprising because rather the opposite could be expected: Compounds with lower vapor pressures have larger reservoirs of molecules which are adsorbed on the walls of the reactor. When the concentration of the molecule in the gas phase is decreasing for instance due to dilution then part of the molecules of the wall reservoir will desorb into the gas phase in order to maintain the adsorption/ desorption equilibrium. The result would be a rate of dilution that is slowed down, i. e. a ratio of $k(\text{dilution, mesitylene})/k(\text{dilution, cyclohexane})$ that is smaller than 1. However, in the present case the opposite has been observed. Varying the reactor temperatures between 323 K and 363 K did not affect this observation. The decrease of the pressure in the detection chamber down to 9×10^{-7} mbar did not change the measured dilution rate constants, either. Also trials using different reference compounds such as acetone or hexane or using a FEP-coated reactor instead of a glass reactor did not improve the results. Whatever has been attempted, the measured ratios of $k(\text{dilution, mesitylene})/k(\text{dilution, cyclohexane})$ remained unchanged.

Some degradation experiments have nevertheless been performed as the error of the dilution experiment was rather small. Figure 14.6 shows an example performed at a temperature of 58°C . The measured ratio of $k(\text{mesitylene})/k(\text{cyclohexane})$ amounts to 6.53. The rate constant of cyclohexane at a temperature of 331 K is calculated according to (E. 14.1) to be $8.4 \times 10^{-12} \text{ cm}^3 \text{ molecule}^{-1} \text{ s}^{-1}$. If we multiply this value with the measured slope of 6.53 we obtain for $k(\text{mesitylene, 331 K})$ a value of $5.49 \times 10^{-11} \text{ cm}^3 \text{ molecule}^{-1} \text{ s}^{-1}$.

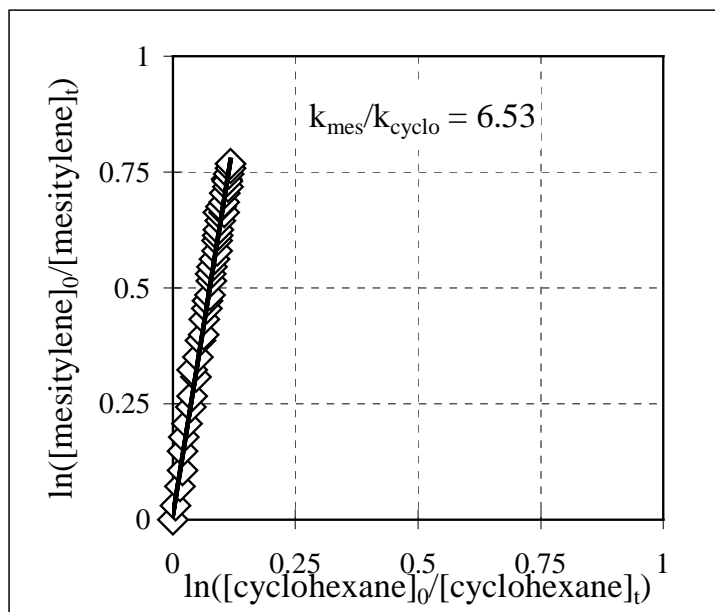


Figure 14.6: Data evaluation of a mesitylene degradation experiment performed at 331 K according to equation (E. 12.3). The concentrations were 15 ppm for cyclohexane, approximately 23 ppm for mesitylene and 90 ppm for ozone.

Only few experiments have been performed with mesitylene as the organic reactant. Figure 14.7 reveals that no significant difference could be observed between the results obtained at 331 K and those obtained at 340 K wherefore we reach $5.7 \times 10^{-11} \text{ cm}^3 \text{ molecule}^{-1} \text{ s}^{-1}$ as a mean value of the reaction rate constant for the total temperature range of 331 to 340 K examined. However, these rate constants are probably overestimated as we have seen above that mesitylene disappears in a dilution experiment at a rate that is faster by 10 to 20% compared to that of the reference compound. In the simplest case the reaction rate constants may therefore be divided by a factor of 1.1 to 1.2. Only few reference data could be found in the literature where the rate constant of the reaction of mesitylene with the OH radical has been measured at a similar temperature. The values of Perry et al. [1977] which were obtained in a smog chamber study show a decreasing trend with increasing temperature and are generally in good agreement with our results. Based on later data Atkinson [1994] recommended a reaction rate constant of $5.75 \times 10^{-12} \text{ molecule cm}^{-3} \text{ s}^{-1}$ at 298 K. The observed temperature trend is consistent with the assumption that the formation of an OH adduct is the dominating reaction pathway at these lower temperatures. Perry et al. [1977] presented also rate constants for 1,2,3- and 1,2,4-trimethylbenzene which show the same trend but with absolute values that are lower by a factor of approximately 1.5 for 1,2,4-trimethylbenzene and by a factor of 2 for 1,2,3-trimethylbenzene.

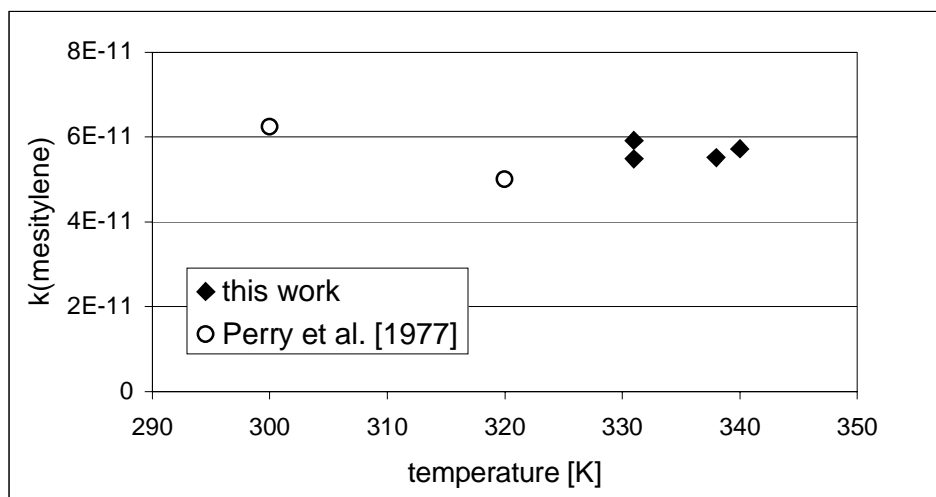


Figure 14.7: Comparison of $k(\text{mesitylene})$ measured in the present study with those of Perry et al. [1977].

14.3 Biphenyl.

Biphenyl was the compound with the lowest volatility ($T_{\text{boil}} = 529 \text{ K}$) that could be examined under acceptable conditions in our experimental set-up. Figure 14.8 shows a dilution experiment with cyclohexane as reference compound performed at 323 K. The measured slope of less than 1.0 reveals that a significant part of biphenyl had adsorbed on the reactor walls from where it desorbed into the gas phase upon dilution. The dilution rate of biphenyl was significantly slowed down in this case. Other dilution experiments, on the other hand, gave results for $k(\text{dilution, biphenyl})/k(\text{dilution, cyclohexane})$ that were larger than 1.0 with maximum values of up to 1.2. Thus, it was very difficult to state when the walls represented a net sink and when they represented a net source of biphenyl. Also, a regular cleaning of the reaction cell would not improve reproducibility. A correction for wall effects could therefore not be made.

However, we considered this artifact to be acceptable all the more as it appeared to be significant above all at the end of the dilution experiment when the biphenyl concentrations were small. In the degradation experiments we evaluated therefore only the beginning of the decay traces neglecting data points obtained at very low concentrations of biphenyl.

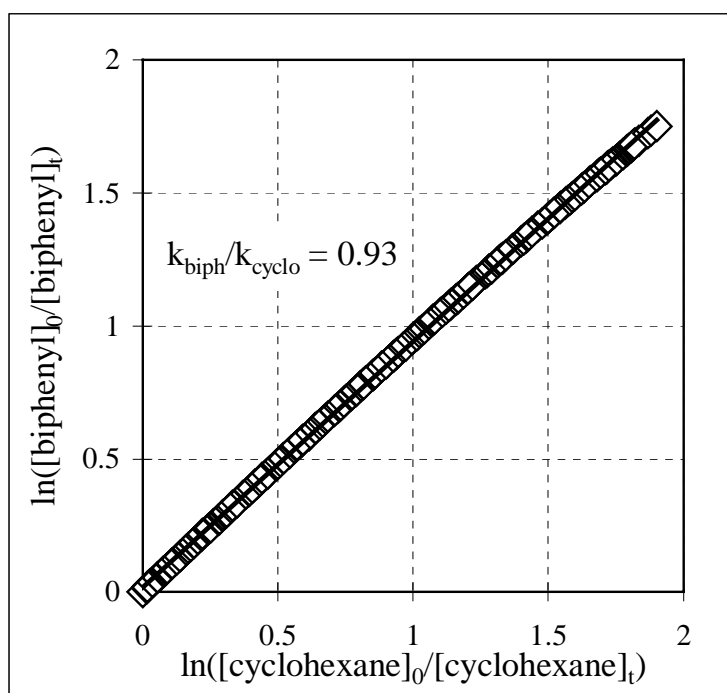


Figure 14.8: Data evaluation of a dilution experiment according to (E. 12.3). The slope of 0.93 indicates that the dilution rate of biphenyl is slowed down by biphenyl molecules that are desorbing from the walls into the gas phase. The reaction cell was heated up to 323 K.

Figure 14.9 shows raw data from a degradation experiment which has been performed at 50 °C. It may be seen that the biphenyl signal is slightly but continuously decreasing prior to reaction which indicates that biphenyl was indeed adsorbing on the walls of the reactor. A small perturbation of the biphenyl trace at $t = 3$ min reflects the injection of O_3 . The fact that the biphenyl trace does not show an accelerated decrease after $t = 3$ min indicates that O_3 shows no significant reaction rate with biphenyl. This was expected as the rate constant of the reaction of O_3 with biphenyl is $< 2.0 \times 10^{-19}$ molecule $cm^{-3} s^{-1}$ at room temperature [Atkinson, 1994]. By multiplying this constant with an estimated O_3 concentration of 90 ppm one gets a reaction rate of only $4.4 \times 10^{-4} s^{-1}$ compared to the rate of OH reaction of approximately $3 \times 10^{-2} s^{-1}$. The irradiation was started at $t = 4.8$ min and lasts for two minutes. The traces of both compounds, biphenyl as well as cyclohexane are instantaneously stabilized after the end of the irradiation at $t = 6.8$ min. This suggests that the two compounds did not significantly adsorb onto the surfaces that have been created by the photochemical production of secondary organic aerosols.

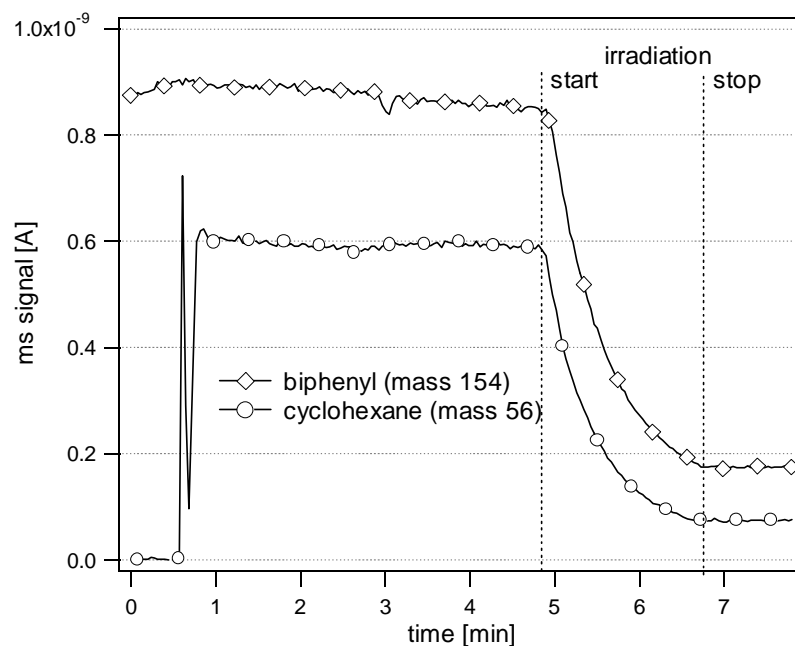


Figure 14.9: Degradation of biphenyl and cyclohexane by OH radicals at 333 K. The concentrations were approximately 20 ppm for biphenyl, 17.5 ppm for cyclohexane and approximately 90 ppm for ozone.

The results of all the experiments performed with biphenyl are summarized in Figure 14.10. Literature data for the same temperature range has not been found. A comparison with rate constants measured at room temperature shows that these values are similar to those that were obtained at 323 K in the present work. Our values may therefore be slightly overestimated as one expects a negative temperature dependence of the rate constant.

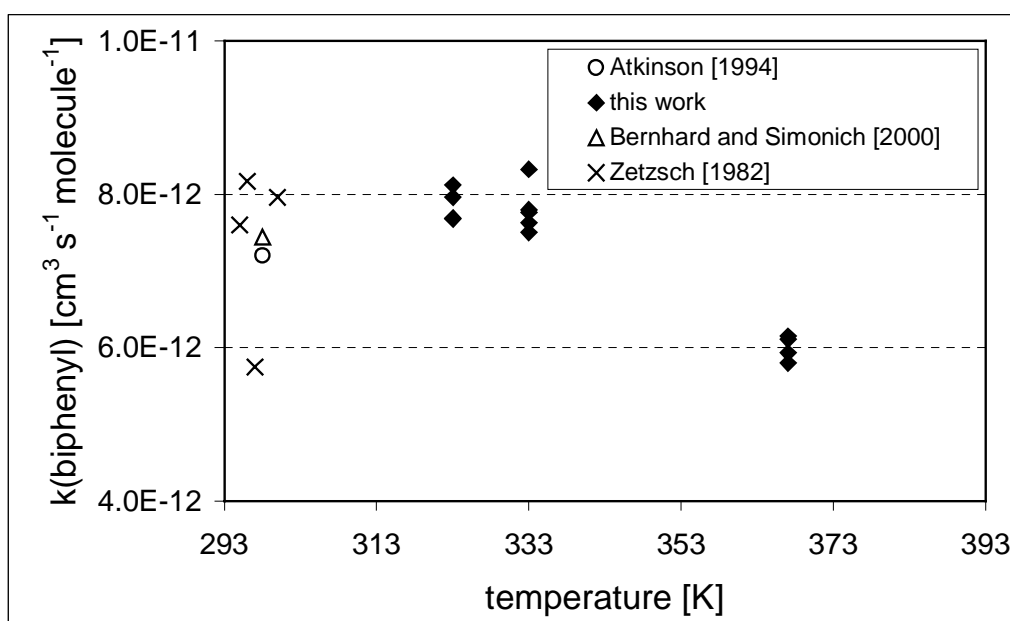


Figure 14.10: Comparison of $k(\text{biphenyl})$ measured in the present study with literature data.

Biphenyl certainly represents a critical case for our experimental set-up due to the mentioned problems of interactions with the walls. The obtained results imply a high degree of uncertainty and cannot be accepted without reservations. That these problems become more important when compounds with even lower vapor pressures or polar groups were examined is not surprising and will be discussed in the next Section.

14.4 Semivolatile and polar compounds.

Whereas for biphenyl more or less acceptable conditions of measurement could be attained the experimental set-up revealed to be completely unsuitable for even less volatile compounds such as phenanthrene or anthracene. Even at 373 K a measurable MS signal for these two compounds could only be observed when the absolute amount that had been injected as solution in toluene exceeded 1 μmol . If this amount would have been completely evaporated then a theoretical concentration of 50 ppm would have resulted. A dynamic range sufficiently high to perform a dilution experiment could only be obtained when one additional μmole was injected. An example of such a dilution experiment performed in the glass reactor is shown in Figure 14.11. The strong curvature of the trace clearly shows that during the dilution significant amounts of phenanthrene were desorbing from the walls of the reactor into the gas phase. Attempts that have been performed in the Teflon reactor led to even less convincing results.

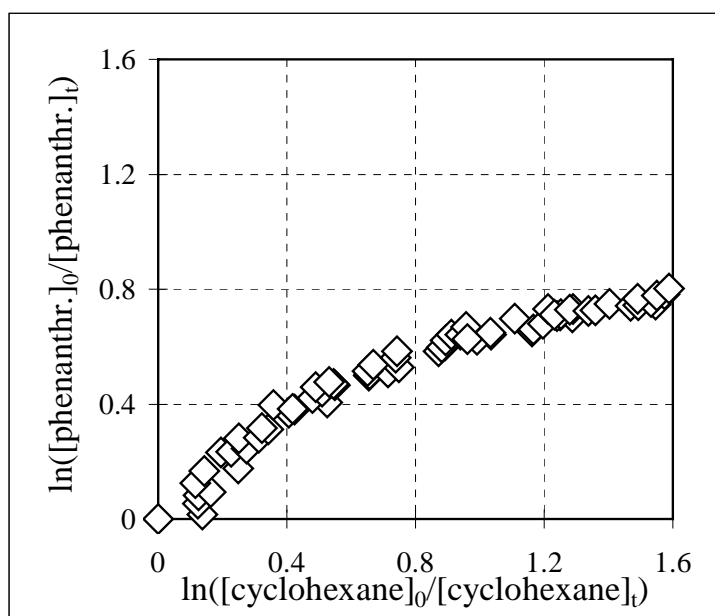


Figure 14.11: Data evaluation of a dilution experiment according to (E. 12.3). The strong curvature indicates that significant amounts of phenanthrene were desorbing from the walls into the gas phase. The experiment was performed in the glass reactor at a temperature of 371 K.

Compounds containing polar functionalities such as phenol ($T_{\text{boil}} = 455 \text{ K}$), or aniline ($T_{\text{boil}} = 457 \text{ K}$) led to the same problems as phenanthrene and anthracene despite of their relatively high vapor pressures. Also in this case amounts between 1 and 2 μmole had to be injected in order to obtain measurable MS signals and dilution experiments with a volatile reference compound led to similar traces as that shown in Figure 14.11. The results in the Teflon reactor were slightly better but nevertheless not acceptable.

In addition, for other compounds such as 1,4-dichlorobenzene or dioctylether problems of highly unstable MS signals appeared which we attribute to secondary reactions in the closed ion source. It already has been discussed in Section 14.1 that the presence of CCl_4 was leading to artifacts in the closed ion source. A nonlinear response of the MS signal has been observed for mesitylene even in the absence of CCl_4 (see Section 14.2). In the case of 1,4-dichlorobenzene and dioctylether the MS response was sometimes varying by up to a factor of 4 within only 30 seconds. This phenomenon decreased when the standard pressure in the detection chamber of $2 \times 10^{-6} \text{ mbar}$ was reduced. This observation suggests that secondary reactions in the closed ion source were responsible for the unstable MS response. However, a reduction of the pressure in the detection chamber is also decreasing the sensitivity of the mass spectrometer and therefore does not represent a solution of the problem.

The conclusion of these observations is that both the coating of the reactor as well as the detection system need considerable improvements if semivolatile compounds are to be examined.

15 Conclusions and outlook.

An experimental set-up has been built which allowed the measurement of the rate constants of the reaction of volatile organic compounds with the OH radical in the gas phase using a relative rate technique. The system could be called a 'mini smog chamber' in relation to the fact that the reaction cell had a volume of only 480 cm³. The photodissociation of O₃ has been chosen as the source of OH radicals and mass spectrometry was used for the online monitoring of the organic compounds in the reaction cell. The sensitivity of the mass spectrometer afforded a typical initial minimum concentration of the organic compounds in the reaction cell of approximately 10 ppm.

The system was validated by measuring the relative rate constants of the reactant pair cyclohexane/toluene. These measurements have been performed for temperatures ranging from 300 to 360 K and gave results which were in excellent agreement with literature data. In addition, it has been clarified whether the results changed with changing concentration ratios of the organic reactants and of O₃, respectively. As this was not the case, we concluded that the obtained values correctly reproduced the rate constants of the interaction between the OH radical and our test compounds.

A major advantage of the experimental set-up was the short duration of an experiment owing to OH radical concentrations of up to 7×10^9 molecule cm⁻³. The time span between the injection of the organic compounds and the end of the irradiation normally ranged between 10 and 20 minutes. A further advantage consisted in the easy handling of the system owing to the achieved miniaturization.

However, it became apparent that the experimental set-up also had some important limitations. The high surface to volume ratio of approximately 0.9 cm⁻¹ was a decisive obstacle for the measurement involving semivolatile compounds. Biphenyl which has a boiling point of 529 K was the compound with the lowest volatility that could be examined in our reaction cell whereas other compounds such as anthracene or phenanthrene adsorbed to a large extent on the glass walls of the reaction cell even at temperatures of up to 373 K. Attempts that have been performed in a Teflon coated reactor did not lead to an improvement of the situation. Compounds containing polar groups such as phenol ($T_{\text{boil}} = 455$ K), or aniline ($T_{\text{boil}} = 457$ K) presented even more problems despite of their relatively high vapor pressure which suggests that specific interactions with the Teflon coated surface occurred.

Additional problems were found in the closed ion source of the mass spectrometer. At the beginning it was observed that the presence of CCl₄ was causing artifacts in the kinetics of even simple dilution experiments. The only explanation we have is that CCl₄ decomposes in the closed ion source in order to form highly reactive fragments, such as for example Cl atoms, which in turn are responsible for secondary reactions with the organic reactants.

However, the occurrence of non linear and unstable MS signals could be observed for other molecules such as mesitylene or dioctylether, even in the absence of CCl_4 . The observation that the importance of these problems slightly decreased when the pressure in the detection chamber was decreased also indicates that these phenomena were most probably caused by secondary reactions in the closed ion source. However, a decrease of the pressure is always accompanied by a considerable loss of sensitivity and therefore does not represent the solution of the present problem.

The original goal, namely to measure rate constants of the reaction of semivolatile compounds with the OH radical at first in the gas phase and subsequently with the organic compounds condensed on solid particles was clearly not attained in view of the technical problems listed above. The heterogeneous part of the project could therefore never be considered. Further attempts to resolve the technical problems bear the risk to be very expensive, both in time as well as in financial resources. Nevertheless, some summary considerations shall be given in the following:

- In order to extend the group of compounds that can be examined in the 'mini smog chamber' it obviously is necessary to improve the inertness of the walls of the reaction cell. Whereas glass is generally considered to be an appropriate environment for non polar compounds, Teflon or fluorinated ethylene propylene (FEP) is the material of choice in the case of polar molecules. Both materials have been used in the present study. The coating of glass with thin FEP films certainly is not routine work. In the context of Knudsen cell studies where FEP coatings are also used we became aware that the quality of the coatings strongly depends on the temperature program of the thermal treatment during the curing process. A reproducible procedure leading to coatings of optimal quality has not yet been found and will need further investigation.

On the other hand, it is probably easier to improve the heating of the cell. Wrapping a heating wire around the reaction cell involves the risk to have cold spots where the semivolatile compounds preferentially will condense. This problem could be resolved by placing the complete reaction cell into an oven.

- The second field where improvements must be achieved is detection. In our system where we worked with a closed ion source problems of non linear and unstable signals occurred, probably owing to fast secondary reactions. It is questionable whether a breakthrough will be achieved using the present apparatus. The only way to avoid secondary reactions is to lower the pressure but this results in a considerable loss of sensitivity. The consequence is that the mass spectrometer must be exchanged for a model with a better performance allowing to have the same sensitivity at lower pressures.

References

- Anderson, P. N. and R. A. Hites, *Environ. Sci. Technol.*, 1996, **30**, 301.
- Andino, J. M., J. N. Smith, R. C. Flagan, W. A. Goddard and J. H. Seinfeld, *J. Phys. Chem.*, 1996, **100**, 10967.
- Atkinson, R., *Atmos. Environ.*, 1990, **24**,1.
- Atkinson, R., D. L. Baulch, R. A. Cox, R. F. Hampson, J. A. Kerr, M. J. Rossi and J. Troe, *J. Phys. Chem. Ref. Data*, 1997b, **26**, 521.
- Atkinson, R. and S. M. Aschmann, *Environ. Sci. Technol.*, 1993, **27**, 1357.
- Atkinson, R. and W. P. L. Carter, *Chem. Rev.*, 1984, **84**, 437.
- Atkinson, R., D. L. Baulch, R. A. Cox, R. F. Hampson Jr., J. A. Kerr and J. Troe, *J. Phys. Chem. Ref. Data*, 1997a, **21**, 1125.
- Atkinson, R., *J. Phys. Chem. Ref. Data, Monogr. No. 2*, 1994, **11**, 216.
- Atkinson, R., S. M. Aschmann and J. N. Pitts, *Int. J. Chem. Kinet.*, 1983, **15**, 75.
- Atkinson, R., S. M. Aschmann, A. M. Winer and J. N. Pitts, *Int. J. Chem. Kinet.*, 1982, **14**, 507.
- Benson, S. W., *Thermochemical Kinetics, 2nd edition*, John Wiley & Sons, New York, 1976.
- Bernhard, M. J. and S. L. Simonich, *Environ. Tox. Chem.*, 2000, **19**, 1705.
- Brubaker, W. W. and R. A. Hites, *Environ. Sci. Technol.*, 1998, **32**, 3913.
- Cvetanovic, R. J., *J. Phys. Chem. Ref. Data*, 1987, **16**, 261.
- DeMore, W. B., S. P. Sanders, D. M. Golden, R. F. Hampson, M. J. Kurylo, C. J. Howard, A. R. Ravishankara, C. E. Kolb and M. J. Molina, *Chemical Kinetics and Photochemical Data for use in Stratospheric Modeling*, JPL Publication 92-20, Jet Propulsion Lab, Pasadena, CA, 1992.
- DeMore, W. B., M. J. Molina, S. P. Sanders, D. M. Golden, R. F. Hampson, M. J. Kurylo, C. J. Howard and A. R. Ravishankara, *Chemical Kinetics and Photochemical Data for use in Stratospheric Modeling*, JPL Publication 87-41, Jet Propulsion Lab, Pasadena, CA, 1987.
- Ehhalt, D. H., H.-P. Dorn and D. Poppe, *Proc. R. Soc. Edinb. B*, 1991, **97**, 17.
- Finlayson-Pitts, B. J. and J. N. Pitts, *Atmospheric Chemistry: Fundamentals and Experimental techniques*, John Wiley & Sons, New York, 1986.
- Greiner, N. R., *J. Chem. Phys.*, 1970, 53, 1070.
- Hansen, D. A., Atkinson, R. and J. N. Pitts, *J. Phys. Chem.*, 1975, **79**, 1763.
- Herron, J. T., *J. Phys. Chem. Ref. Data*, 1988, **17**, 967.
- Holland, F., M. Hessling and A. Hofzumahaus, *J. Atmos. Sciences*, 1995, **52**, 3393.
- Koch, R., W. U. Palm and C. Zetzsch, *Int. J. Chem. Kinet.*, 1997, **29**, 81.
- Kwok, E. S. C. and R. Atkinson, *Environ. Sci. Technol.*, 1995, **29**, 1591.
- Michelsen, H. A., R. J. Salawitch, P. O. Wennberg and J. G. Anderson, *Geophys. Res. Lett.*, 1994, **21**, 2227.

- Pagani, C., J. Arey and R. Atkinson, *Int. J. Chem. Kin.*, 2000, **32**, 79.
- Palm, W.-U., M. Elend, H.-U. Krueger and C. Zetzsch, *Environ. Sci. Technol.*, 1997, **31**, 3389.
- Paulson, S. E., M. Y. Chung and A. S. Hasson, *J. Phys. Chem.*, 1999, **103**, 8125.
- Perry, R. A., Atkinson, R. and J. N. Pitts, *J. Phys. Chem.*, 1977, **81**, 296.
- Rickard, A. R., D. Johnson, C. D. McGill and G. Marston, *J. Phys. Chem.*, 1999, **103**, 7656.
- Shi, J. C. and M. J. Bernhard, *Int. J. Chem. Kinet.*, 1997, **29**, 349.
- Stemmler, K., D. J. Kinnison and J. A. Kerr, *J. Atmos. Chem.*, 1996, **100**, 2114.
- Tuazon, E. C., W. P. L. Carter, R. Atkinson and J. N. Pitts, *Int. J. Chem. Kinet.*, 1983, **15**, 619.
- Tully, F. P., A. R. Ravishankara, R. L. Thompson, J. M. Nicovich, R. C. Shah, N. M. Kreutter and P. H. Wine, *J. Phys. Chem.*, 1981, **85**, 2262.
- Zetzsch, C., *15th International Conference on Photochemistry*, Stanford, CA, June 27-July 1, 1982.

Remerciements

Je remercie le Professeur H. van den Bergh pour l'accueil qu'il m'a réservé dans son laboratoire ainsi que pour l'intérêt qu'il a porté à mon travail. En outre, il a pris les bonnes décisions dans les moments cruciaux ce qui m'a permis de mener ma thèse à bon terme.

Je tiens également à remercier le Dr. M. J. Rossi pour son assistance scientifique et technique durant toute la durée de ma thèse. D'innombrables problèmes et questions nous ont conduit à des discussions 'marathons', d'autant plus intéressantes lorsque nos points de vue divergeaient.

Je remercie tous les membres (actuels et anciens) du groupe "Chimie Hétérogène" avec lesquels j'ai vécu des moments privilégiés. Je citerai en particulier (par ancienneté) Andres Thöny, Lukas Gutzwiller, Sabine Seisel, Thomas Koch, François Caloz, Benoît Flückiger, Arnaud Aguzzi, Carine Jornod-Alcala, Christian Santschi, Christoph Delval et Bernadett Tóth. J'ai spécialement apprécié la présence des "special guests" Michihiro Mochida, Norimichi Takenaka et Trevor Brown qui m'ont permis de faire connaissance avec des cultures encore plus exotiques que la culture romande.

J'adresse encore mes remerciements à toutes les personnes qui ont lu et corrigé le texte ainsi qu'aux personnes dont les critiques m'ont été d'un grand apport.

Meinen Eltern danke ich herzlich dafür, dass sie all meine Entscheidungen mitgetragen und mich stets unterstützt haben.

E finalmente ma soprattutto vorrei ringraziare a te, Marilou, perché mi hai mostrato che ci sono anche altre cose che le scienze naturali.

Curriculum Vitae

Name: Dominik STADLER

Address: Ch. des Vignes-d'Argent 1
1004 Lausanne
Tel: +41 21 625 08 64

Place, Date of Birth: Basel, February 15, 1970

Nationality: Swiss

Education

1989 Swiss Leaving Certificate (Maturität, Type B).

1989-1994: Studies of Environmental Sciences, at the Swiss Federal Institute of Technology in Zurich.
Undergraduate Thesis on liposome/water systems as a model for cell membranes in toxicological studies.

1994-1996: Practical studies at Ciba-Geigy and Novartis, Basel.

1996-2000: Ph.D. Thesis "A Laboratory Study of Heterogeneous Reactions Relevant to the Atmospheric Boundary Layer: Soot as a Reactive Substrate" at the Laboratory for Air and Soil Pollution of the Swiss Federal Institute of Technology in Lausanne.

Languages:

German: mother tongue
French: fluent
English: very good knowledge
Italian: basic knowledge